Balance maintenance of a humanoid robot using the hip-ankle strategy

S. Kiemel

Master of Science Thesis

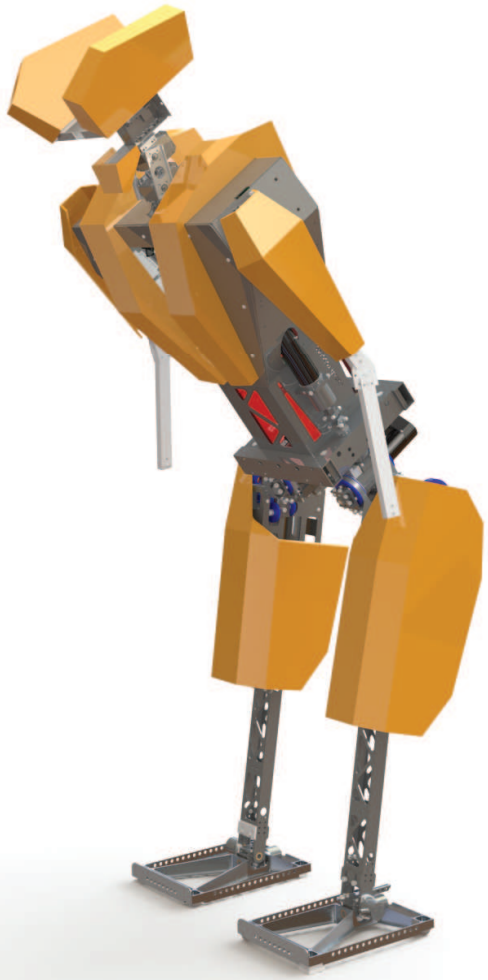

TU Delft Delft University of Technology

Faculty of Mechanical, Maritime and Materials Engineering

Balance maintenance of a humanoid robot using the hip-ankle strategy

Master of Science Thesis

For the degree of Master of Science in Mechanical Engineering at Delft University of Technology

S. Kiemel

May 15, 2012

Faculty of Mechanical, Maritime and Materials Engineering · Delft University of Technology

Delft University of Technology
Department of
BioMechanical Design

The undersigned hereby certify that they have read and recommend to the Faculty of Mechanical, Maritime and Materials Engineering for acceptance a thesis entitled

Balance maintenance of a humanoid robot using the hip-ankle strategy

by

S. Kiemel

in partial fulfillment of the requirements for the degree of

Master of Science Mechanical Engineering

Dated: May 15, 2012

Supervisor(s):

dr.ir.M. Wisse

Reader(s):

Prof. Dr. F.C.T. van der Helm

Dr. Ir. A.L. Schwab

Abstract

Prevention of falling is of major importance in the practical application of humanoid robots. This thesis focuses on the hip-ankle strategy as a method to maintain balance when subjected to a large disturbance. This strategy is characterised by a large rotation of the hip joint which repositions the Centre of Mass (CoM). The hip-ankle strategy is compared to the ankle strategy which locks the hip joint and compensates for a disturbance by applying ankle torque.

Various hip-ankle strategy controllers have been presented in literature of which three implementations on humanoid robots are known. However, none of the research provided experimental evidence that a humanoid robot can withstand larger disturbances by using the hip-ankle strategy compared to the ankle strategy. The goal of this research was therefore to *provide experimental evidence that a humanoid robot can maintain balance for larger disturbances by using the hip-ankle strategy than solely using the ankle strategy.*

First, simple models were used to investigate the theoretical maximum allowable disturbance for the humanoid robot TUlip. The Inverted Pendulum Model (IPM) was used to simulate the ankle strategy where ankle torque was the only control input. The hip-ankle strategy was simulated using the Inverted Pendulum plus Flywheel Model (IPFM) where flywheel torque served as an additional control input. The hip-ankle strategy was implemented by using bang-bang control input profile on the flywheel. Disturbances were applied in horizontal direction to the CoM of the model and measured in terms of applied impulse. In these simulations the hip-ankle strategy was able to maintain balance for disturbances 33.6% larger than the ankle strategy.

Next, a control algorithm was developed for the humanoid robot TUlip. In the control algorithm, the hip-ankle strategy was implemented by the application of virtual forces and torques on the trunk of the robot. These virtual forces were then transfered to joint torques by means of Virtual Model Control (VMC). The Instantaneous Capture Point (ICP) of the robot was controlled to a desired location by modulating the Centre of Pressure (CoP) of the robot. If the CoP is sufficient to keep the ICP within the foot, the control algorithm will lock the hip joint and balance using solely the ankle torque. In case the ICP crosses the edge of

the foot, a large virtual torque on the upper body is applied in the direction of the ICP which results in a rotational acceleration of the upper body. The ICP will then be pushed back into the foot and the application of ankle torque will then be sufficient again to maintain balance.

In order to evaluate if it is physically possible for the humanoid robot TUlip to maintain balance using the hip-ankle strategy control algorithm, a simulation was performed. The Double Inverted Pendulum Model (DIPM) was used as a model for TUlip and constraints in terms of maximum joint torque and range of motion were included. The ankle strategy and the hip-ankle strategy were then subjected to horizontal impulsive disturbances to the back of the upper body of the robot and measured in terms of impulse. The hip-ankle strategy was able to withstand 16.6 % larger pushes than the ankle strategy.

Finally the hip-ankle strategy was experimentally evaluated on the humanoid robot TUlip. Disturbances were created by swinging a weight at the end of a pendulum to the back of the upper body of the robot. The applied impulse was measured by measuring the disturbance force over time by using a load cell. Experimental results showed that the hip-ankle strategy implemented on the humanoid robot can maintain balance for disturbances 19.3 % larger than solely using the ankle strategy.

The main conclusion of this thesis is that the hip-ankle strategy can be used to improve the balance maintenance on a humanoid robot. This thesis provided the first experimental evidence that a humanoid robot can maintain balance for larger disturbances by using the hip-ankle strategy than using the ankle strategy.

Table of Contents

List of Figures

List of Tables

Nomenclature

List of Acronyms

CoP	Centre of Pressure
CoM	Centre of Mass
ICP	Instantaneous Capture Point
DBFC	Dynamic Balance Force Control
VMC	Virtual Model Control
DIPM	Double Inverted Pendulum Model
LIPM	Linear Inverted Pendulum Model
LIPFM	Linear Inverted Pendulum plus Flywheel Model
IPM	Inverted Pendulum Model
IPFM	Inverted Pendulum plus Flywheel Model
DoF	Degree of Freedom
IMU	Inertial Measurement Unit
VTP	Virtual Toe Point
SEA	Series Elastic Actuation

List of Symbols

$\boldsymbol{\tau}$	Vector of joint torques
$\boldsymbol{C}$	Vector of Coriolis and centrifugal terms
$\boldsymbol{F}_g$	Vector with gravitational forces
$\boldsymbol{M}$	Mass matrix
$\boldsymbol{W}$	Wrench on trunk
$\mathcal{T}$	Kinetic energy
$\mathcal{V}$	Potential energy
τ_a	Ankle torque
$\tau_a^{max,+}$	Maximum positive ankle torque
$\tau_a^{max,-}$	Maximum negative ankle torque
τ_f	Flywheel torque
τ_{max}	Maximum flywheel torque
τ_{tr_y}	Virtual torque on trunk
θ_{max}	Maximum flywheel angle
φ_a	Ankle angle
φ_h	Hip angle
f_x	Virtual horizontal force on trunk
f_z	Virtual vertical force on trunk
g	Gravitational constant
l_f	Front edge of the foot
l_r	Rear edge of the foot
m	Total mass of the robot
x_G	CoM position in x-direction
$x_{CoP_f}^{max}$	Maximum CoP position at the front of the foot
$x_{CoP_r}^{max}$	Maximum CoP position at the rear of the foot
x_{CoP}^{des}	Desired CoP location in x-direction
x_{ICP}	ICP location in x-direction
x_{ICP}^{des}	Desired ICP location in x-direction
z_{G_c}	Constant height of the LIPM mass
φ	Joint angle

Acknowledgements

I would like to thank my supervisor, Martijn Wisse, for his guidance throughout the process of this thesis. You were a true inspirator and motivated me to make the best out of it. I would also like to thank you for the many great opportunities you have given me in the Delft Biorobotics Laboratory. It has been a fantastic time and it truly was a valuable experience.

Secondly, I would like to thank Tomas de Boer for helping me to select this research topic, being my supervisor for the first few months and for the great cycling sessions we had. I would also like to thank my colleagues at the Delft Biorobotics Laboratory. Together we had many nice discussions and the delicious lunches. For all the mechanical help and advise I would like to thank Jan van Frankenhuyzen and the guys from the mechanical workshop. For software related issues Eelko van Breda and Gijs van der Hoorn were always ready to provide their help. Guus Liqui Lung helped solving many issues regarding the electronics of the robot, your help was of great value. Special thanks to my direct colleagues working on TUlip, Bart Vissers, Riewert van Doesburgh, Tim van der Ven and Jesper Smith. We had many interesting discussions and you were truly of great help at many times. I am very grateful to the people proofreading parts of this thesis, Bart Vissers, Riewert van Doesburgh, Tim van der Ven, Sander van Weperen and Rogier de Jong. Your valuable contribution is much appreciated.

In my years at Delft University of Technology I had the opportunity to cooperate with many students but I would like to give a special thanks to, Sander van Weperen, Jurren Pen, Pieter Pluimers, Niels van der Geld, Eric Kievit, Tim van Wageningen and Bart Fugers. We have shared our knowledge, many coffees and wonderful experiences.

Finally I would like to thank my family, my girlfriend and my friends for their continuing encouragement, support and helping me to take my mind off my study when needed.

Delft, University of Technology — S. Kiemel
May 15, 2012

Chapter 1

Introduction

Research in the field of humanoid robotics is of great importance as it can potentially be used in the development of prosthetics, exoskeletons, and rehabilitation devices. These devices can support elderly or handicapped people in regaining their walking ability. A major bottleneck in humanoid robotics research is balance maintenance; the ability to prevent a fall. Prevention of falling is of great importance in the practical application of humanoid robots. A fall should be prevented as it can be energetically costly and possibly harmful to the robot and environment.

To prevent falling, a humanoid should be able to withstand unexpected external disturbances such as a push to the upper body of the robot. Such a disturbance can destabilize the system; it will be unable to return to a statically stable configuration and a fall will be inevitable. The ability to withstand an external perturbation and maintain balance can also be referred to as push recovery [1, 2].

1-1 Balance maintenance strategies

A humanoid can recover from a push by applying an appropriate combination of balance maintenance strategies. This thesis investigates humanoid robot balance maintenance in an upright standing posture and when making a step is undesirable. Two balance maintenance strategies can be distinguished for this situation:

1. In case of a small disturbance, the humanoid robot (or human) can maintain its balance by locking the knee and hip joints and applying a torque on the ankles. This is comparable to the classic inverted pendulum control task and is also referred to as the "ankle strategy".

2. For larger disturbances angular momentum around the Centre of Mass (CoM) can be generated which forces the CoM backwards to its desired position. For example, after

a large push in the back, the humanoid should quickly bend its upper body forward. This strategy is indicated by the "hip strategy"[1].

1-2 Related work

The vast majority of the balancing algorithms implemented on humanoid robots solely use the ankle strategy to maintain balance [3–8]. However, research has shown that using an appropriate combination of hip and ankle strategy (from now on referred to as hip-ankle strategy) results in better performance than solely using the ankle strategy [1, 2, 9–18]. Performance is hereby measured as the largest possible unexpected external perturbation the robot is able to withstand until a fall occurs.

Various hip-ankle strategy controllers have been presented in literature and demonstrated to outperform the ankle strategy controllers in simulation. Although better performance can be obtained using the hip-ankle strategy, only three algorithms using the hip-ankle strategy have been implemented on a physical humanoid robot so far. Nenchev and Nishio (2008) [19] applied the hip-ankle strategy to a small size robot (of 0.239 m in height) by the application of virtual spring-dampers and calculating joint torques with the Reaction Null-Space method. Jalgha et al. (2009) [20] demonstrated the hip-ankle strategy on the Bioloid kit by Robotis. By defining a desired linear and angular momentum the joint velocities were obtained using Resolved Momentum Control [21]. Stephens (2011) [11, 22] demonstrated the hip-ankle strategy on the SARCOS robot using the Dynamic Balance Force Control (DBFC) algorithm [23]. This algorithm computes contact forces based on the Inverted Pendulum Model (IPM) dynamics and uses these to obtain the joint torques. [18]

1-3 Problem definition

The robots using these algorithms show hip-strategy-like lunging behaviour of the upper body as observed by humans. However, none of the research provided experimental evidence that the robot can withstand larger disturbances using the hip-ankle strategy instead of solely using the ankle strategy.

1-4 Research goal

The goal of this thesis is therefore to *provide experimental evidence that a humanoid robot can maintain balance for larger disturbances by using the hip-ankle strategy than solely using the ankle strategy.*

1-5 Approach

To achieve this goal, experiments will be performed on the humanoid robot TUlip [24]. These experiments will focus on balance maintenance in the sagittal plane in forward direction. In

[1] For humans this behaviour is also indicated by term lunging.

the experiments, the humanoid is restricted to double support upright standing and is not allowed to make a step. By applying a disturbance to the back of the robot at the upper body, the robot will be forced to a state where the ankle strategy will be unable to maintain balance. A forward lunge is then required to maintain balance for this situation. A control algorithm using the hip-ankle strategy will be implemented on the robot in order to achieve this. This control algorithm will be compared with an ankle strategy control algorithm. In order to get more theoretical insight, the ankle and hip-ankle strategy controllers are first compared by implementing them on a double inverted pendulum model in Matlab and simulating the disturbances.

1-6 Thesis outline

The structure of this thesis is as follows:

Chapter 2 introduces the humanoid robot TUlip which is the robot used to implement the hip-ankle strategy and perform the experiments.

Chapter 3 introduces the key principles of humanoid robot balance maintenance. This information is required for the analysis and synthesis of the hip-ankle strategy on the humanoid robot.

Chapter 4 selects a measure for the disturbance applied to the robot that will be used in simulation and experiments on the physical humanoid robot.

Chapter 5 presents a theoretical analysis on the benefits of using the hip-ankle strategy by using simple inverted pendulum models to simulate the ankle and the hip-ankle strategy. This results in the theoretical largest allowable disturbance for the humanoid robot for both strategies.

Chapter 6 introduces the hip-ankle strategy control algorithm that is used on the humanoid robot.

Chapter 7 presents a simulation of the hip-ankle strategy control algorithm in order to evaluate if the humanoid robot TUlip is able to maintain balance using this algorithm.

Chapter 8 introduces the experimental setup used in the experiments on the real robot with hip-ankle strategy controller.

Chapter 9 presents the results obtained from the experiments on the humanoid robot.

Chapter 10 presents a discussion on the results and the methods used. Next to the points of discussion also opportunities for future research are presented in this chapter.

Chapter 11 presents the conclusions that can be drawn on this research.

Chapter 2

Description of humanoid robot TUlip

The hip-strategy control algorithm will be implemented on the humanoid robot TUlip [25]. The performance of a control algorithm is dependent on the platform it is applied to. The goal of this chapter is therefore to *describe the design of the humanoid robot TUlip in terms of mechanics, electronics and software.*

Section 2-1 introduces some background of the humanoid robot TUlip. Section 2-2 discusses its mechanics. The electronics are discussed in section 2-3. Section 2-4 presents the software used on the robot.

2-1 Background

The humanoid robot TUlip, depicted in figure 2-1(a), was originally designed for the application of Limit Cycle Walking as a successor of the humanoid robot Flame [24]. TUlip was designed to be more versatile than its predecessor which required additional Degree of Freedom (DoF). The requirement for versatility also led to a different control approach; capturability-based control [27]. Up to now TUlip has not been able to demonstrate successful walking. In order to walk and show versatile behaviour it is essential to be able to maintain balance in a variety of situations and withstand large disturbances. The hip-ankle strategy introduced in this thesis can have a contribution to this.

2-2 Mechanics

As shown in figure 2-1(b) each leg consists of six DoF; two Dof in each ankle, one DoF in each knee joint and three DoF in each hip.

2-2-1 Dimensions

As this research will focus on the sagittal plane an illustration of TUlip in this plane is given in figure 2-2(a). The corresponding mechanical properties are presented in table 2-1. Note

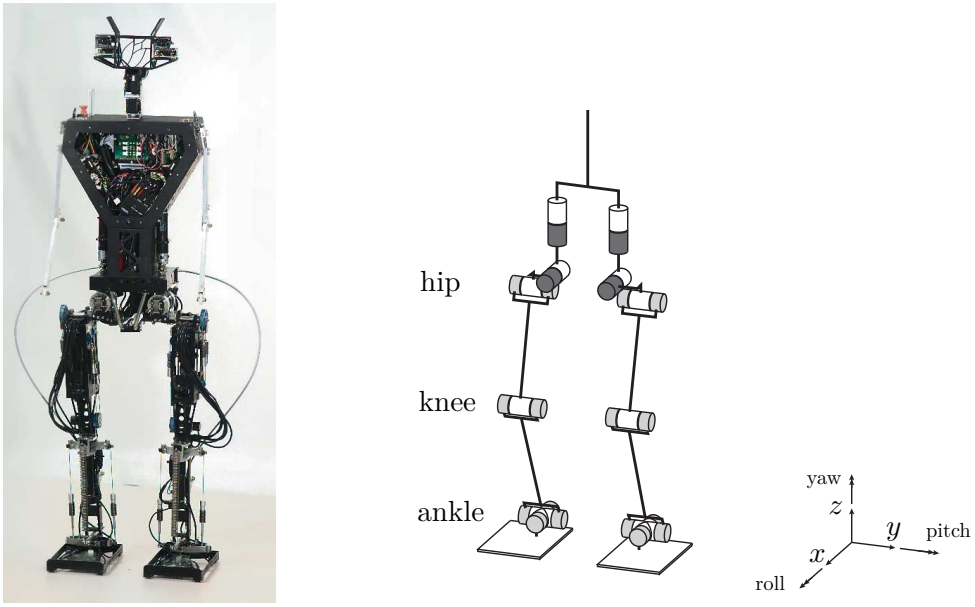

(a) Humanoid robot TUlip. (b) Model of humanoid robot TUlip.

Figure 2-1: (a) photograph of humanoid robot TUlip. During the experiments the head and arms are not used and removed from the robot. (b) a full 3D body model of the twelve DoF humanoid robot TUlip. Each leg consists of an ankle with a pitch and roll joint, a knee with a pitch joint and a hip which can perform pitch, roll and yaw rotation. Figure adapted from [26].

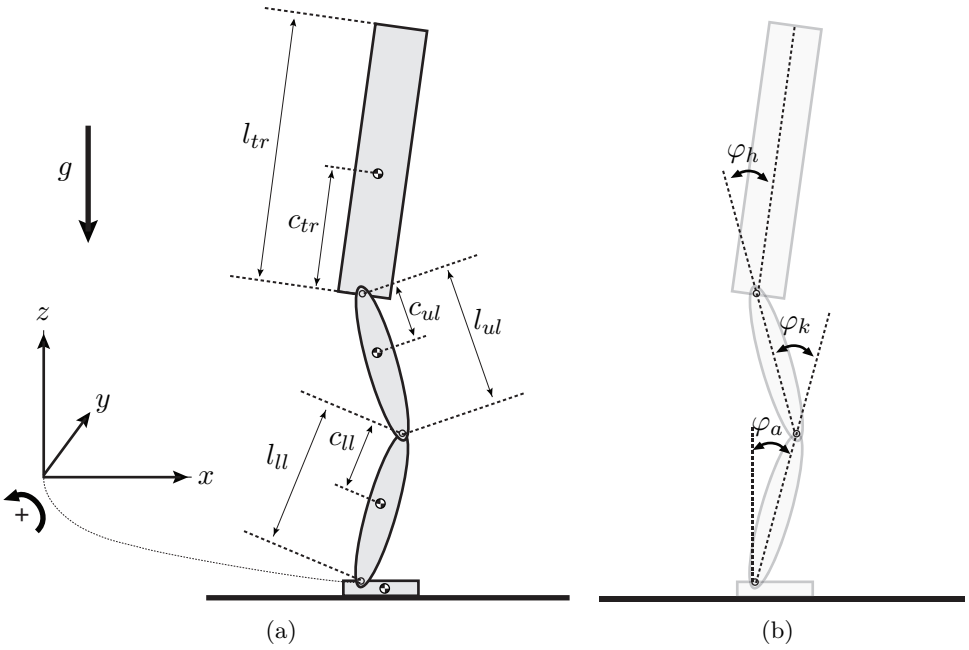

Figure 2-2: Side view of humanoid robot TUlip. (a) shows the model parameters of TUlip. In (b) the degrees of freedom for the sagittal plane are given.

that the mass of the foot in this research is neglected. The total length of TUlip in the current setup is 1.094 m, the total mass is 17.94 kg. Additionally, the front edge of the foot is at a distance of 0.138 m from the ankle joint in x-direction while the rear edge is located -0.048 m in x-direction from the ankle joint.

Table 2-1: Mechanical properties of the humanoid robot TUlip for the trunk, the upper leg and lower leg. The mass and inertia of the feet of the robot are neglected. The properties correspond to figure 2-2(a).

Body	Length l_i [m]	Mass m_i [kg]	CoM offset c_i [m]	Inertia $I_{yy,i}$ $[kgm^2]$
Trunk tr	0.499	11.46	0.225	0.20518
Upper leg ul	0.275	2×2.14	0.097	0.01133
Lower leg ll	0.320	2×1.10	0.15	0.00368
Total	1.094	17.94	-	-

2-2-2 Actuation

The DoF of interest are the hip, knee and ankle pitch joints, shown in figure 2-2(b). The corresponding range of motion is presented in table 2-2.

Table 2-2: The range of motion and transmission reduction for the three DoF of interest. The corresponding Degrees of Freedom are depicted in figure 2-2(b). The transmission reduction is the gearbox reduction plus the pulley ratio.

Body	Range of motion [rad]	Transmission reduction
Hip pitch φ_h	$-\frac{1}{3}\pi$ to $\frac{1}{3}\pi$	1:222
Knee pitch φ_k	0 to $\frac{5}{6}\pi$	1:155
Ankle pitch φ_a	$-\frac{1}{3}\pi$ to $\frac{1}{3}\pi$	1:325

The ankle, knee and hip pitch joints are actuated by means of Series Elastic Actuation (SEA) [28, 29]. This actuation principle connects a motor with a joint through an elastic element. On TUlip this elastic element is a tension spring. The elongation of this spring can be measured which is proportionally related to the applied force. The benefits of SEA are the ability to accurately control the joint torque and the compliance in the system can absorbe large impacts which prevents gearbox damage. The major downside of this actuation principle is the relatively low control bandwidth. For large torques motor saturation occurs due to the high speed required for the large spring elongations. For TUlip the torque control bandwidth was measured to be 10-15 Hz for torques of to 5 Nm and approximately 5-10 Hz for torques between 5-12 Nm [26].

2-3 Electronics

TUlip has a single onboard computer which is a 1 GHz Diamond Systems Poseidon board with 512 MB RAM. Two FPGA's are dedicated to count the encoder pulses and communicate this with the Elmo Whistle amplifiers which power the motors.

On the motors of Tulip Maxon are HEDS 5540 encoders mounted with 500 counts per revolution. The SEA joints have a second encoder mounted at the joint side in order to measure the joint angle and the elongation of the elastic element. These are Scancon 2RMHF incremental encoders with 7500 counts per revolution.

The upper body contains an XSens MTi Inertial Measurement Unit (IMU) which consists of accelerometers, gyroscopes and magnetometers in order to measure orientation and acceleration in 3D.

Each foot has four pressure sensors (Tekscan Flexiforce) on the corners of the foot, these sensors are used as contact sensors [24, 26].

The power supply is divided in a motor and a computer part. Both parts can be powered by an external power supply or by using battery packs.

2-4 Software

The computer of TUlip runs Debian Linux with the real-time framework Xenomai. The software architecture is based on RoboFrame and written in C++. The architecture consists of a hardware abstraction layer and a motion control layer. The hardware abstraction layer provides communication between the hardware of the robot and the motion control layer. The motion control layer runs in a real-time loop of 1 kHz and contains all the control algorithms for the motion of the robot.

A special graphical user interface has been designed that allows for online controller tuning and can also be used to log data of experiments.

2-5 Summary

The humanoid robot TUlip will be used in the experiments to compare the ankle and hip-ankle strategy. The robot consists of two legs with six Degrees of Freedom each. The ankle, knee and hip pitch joints are force controlled by means of Series Elastic Actuation (SEA). An important quantity for this research is the maximal pitch angle of the hip joint. This joint is limited to $\frac{1}{3}\pi$ rad in forward and backward rotation.

The next chapter introduces the key principles of maintaining balance on a humanoid robot.

Chapter 3

Humanoid robot balance control

To properly build up the argument that the hip-ankle strategy outperforms the ankle strategy, the introduction of various key concepts is required. Therefore, this chapter further elaborates on the ankle and hip-ankle strategy in section 3-1. Additionally, it gives an explanation why the hip strategy should be used at all. Section 3-2 introduces the Instantaneous Capture Point (ICP) as an important point on the ground that can be used to maintain balance on a humanoid robot. This point will later be of great value in the analysis and synthesis of the balance control algorithm.

3-1 Strategies to maintain balance

Two strategies can be distinguised to maintain balance; the ankle strategy and the hip-ankle strategy. This section introduces both strategies and explains why the hip-ankle strategy should be used at all.

3-1-1 Ankle strategy

As explained by Horak & Nasher (1986) [30], humans tend to use the ankle strategy in case of relative small disturbances. An example of this strategy is given in figure 3-1(a) where a disturbance pushes the CoM from its desired state. The ankle strategy is a relatively simple strategy and many applications of this strategy on humanoid robots are known [2, 4, 5, 31, 32]. The hip joint is locked and ankle torque is used to bring back the CoM to its desired position. If we consider the hip joint as locked, the system in figure 3-1(a) can be considered to have one Degree of Freedom (DoF) with the ankle torque as commanded quantity. The contact between the foot and floor is a unilateral constraint since no attractive forces exists between the two. If the (required) ankle torque will become too large the foot will start to rotate. This should be prevented at all times because the system then becomes underactuated. The limitation of this strategy is therefore the amount of ankle torque that can be applied without foot rotation to occur.

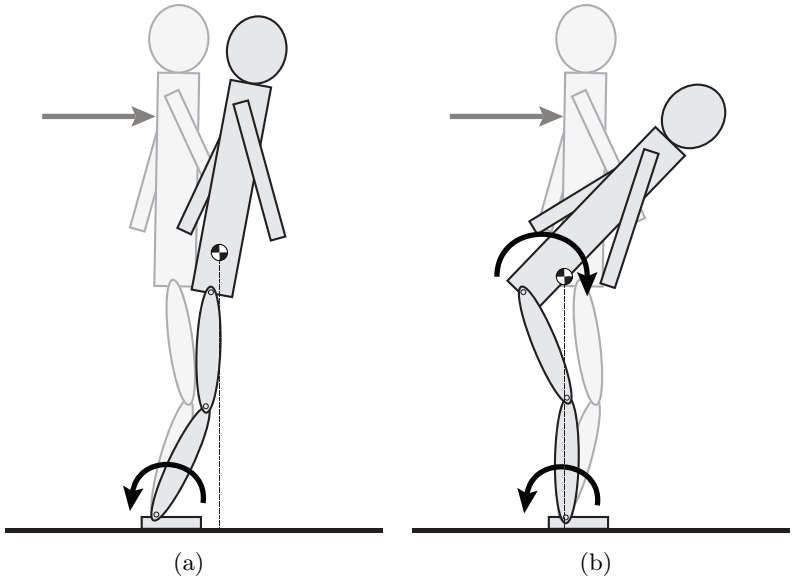

Figure 3-1: The ankle strategy and the combination of the hip and ankle strategy (hip-ankle strategy). In case of the ankle strategy (a), the hip joint is stiff and an ankle torque is applied to bring the CoM back to its desired position. In case of the hip-ankle strategy (a), a large torque on the hip joint is applied which creates forward angular accelerationof the upper body. This angular acceleration creates a large deflection at the hips and shifts the CoM backwards over the feet.

3-1-2 Hip-ankle strategy

In case of a too large disturbance the ankle strategy will not be sufficient to prevent a fall. Angular acceleration of the upper body can be generated in the direction of the disturbance by applying a torque on the hip joint as depicted in figure 3-1(b); the hip-ankle strategy. In this figure a horizontal disturbance force is applied to the back of the robot, as a response a large torque is applied on the hip joint and the upper body bends forward. This forward torque in combination with ankle torque results in a backward motion of the CoM to its desired position [1, 2, 27, 33, 34]. Limitations of this strategy are the amount of hip torque that can be applied, the range of motion of the joint that is accelerated and the inertia of the segment which is accelerated.

Why using the hip-ankle strategy?

As introduced above, the hip-ankle strategy can be applied in case the ankle strategy is not sufficient. Another option would be to make a step, however, several situations might occur where stepping is not possible or where using the hip-ankle strategy is more beneficial. In this situation the robot is thus fully dependent on the hip-ankle strategy in order to prevent a fall. Three examples of these situations are illustrated by figure 3-2 and explained below:

1. Stumble recovery See figure 3-2(a). A situation where the hip strategy is useful is when the swing foot hits the ground while walking. A sudden stop of the robot is required

while the CoM might have large forward velocity. By lunging forward in combination with applying ankle torque the robot might still be able to maintain balance. A similar situation occurs when the robot intentionally makes the transition from walking to stopping. To stop the robot the step length can be adjusted and a the CoM can be accelerated backwards by lunging forward. Using this strategy results in the robot having to take less steps in order to come to a stop.

2. Requirement of a cross step See figure 3-2(b). Another situation that can occur is when the robot should take a step to maintain balance but the weight of the robot is incorrectly distributed. The CoM of the robot is situated such that a cross step is required. For example if the robot balances on the left leg and a disturbance is applied to the left, the desired foot position for the right foot is on the left side of the stance foot. It is physically not possible to place the foot at that position and a lunge in that direction might prevent a fall [8].

3. Occurrence of an obstacle See fig 3-2(c). The final example where a step is not possible is the occurence of an obstacle. In case of a large disturbance, when an obstacle is situated in the direction of that disturbance, a step cannot be taken but the hip strategy can be used to prevent a fall.

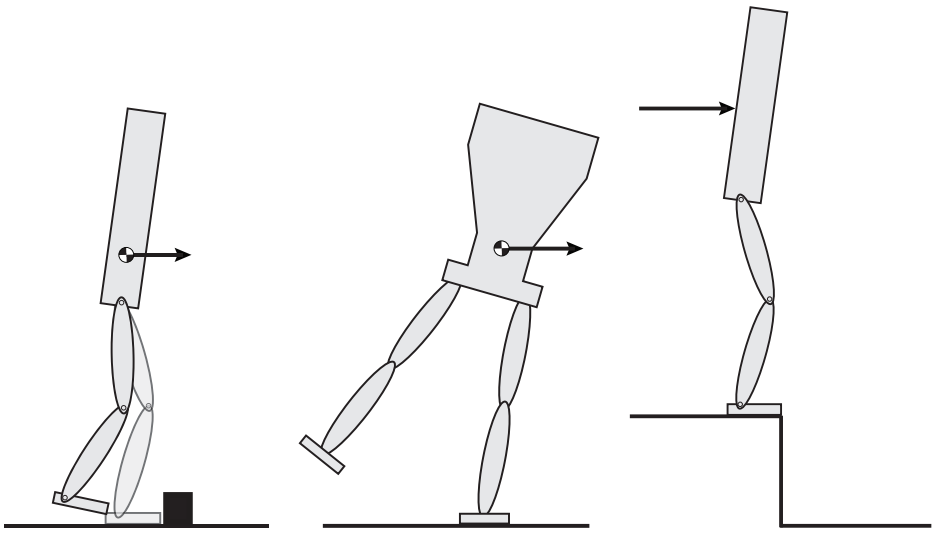

Figure 3-2: Situations in which using the hip strategy can be beneficial in order to maintain balance. In (a), the robot hits the floor or an obstacle while walking. By lunging forward, the forward CoM velocity of the robot can be compensated. Figure (b) shows a front view of the robot, it has a sidewards CoM velocity or a disturbance in the direction of the arrow. In order to regain balance a step in the direction of the disturbance is required. However, this requires a cross step; the right leg should place its foot on the other side of the stance foot. This is physically not possible on the robot, the hip-ankle strategy will be of great value because it can still regain balance. In (c) a large disturbance is applied to the back of the robot. Because of an obstacle the robot can not make a step. However the hip-ankle strategy can still prevent a fall by lunging forward.

For a humanoid robot, the hip strategy will thus be useful in a variety of situations. This thesis will focus on balance maintenance in the sagittal plane with disturbances applied to the back of the robot (as shown in figure 3-2(c)).

3-2 Analysis and control using the Instantaneous Capture Point

As mentioned in section 3-1 a humanoid robot can maintain balance using the ankle strategy and in case of large disturbances the hip-ankle strategy can be used. In order to maintain balance on a humanoid robot it is therefore crucial to measure how close the system is to falling. Because a humanoid robot is a system with complex dynamics it is useful to approximate this dynamics by a simple model. The simple model used in this research is the Linear Inverted Pendulum Model (LIPM) [4, 27], introduced in section 3-2-1. It is used to analyse the CoM motion of the robot and calculate the Instantaneous Capture Point (ICP). The ICP, introduced in section 3-2-3, is a point on the ground which indicates how close the system is to falling and can be used to control the balance of a humanoid robot. The location of the ICP can be modulated by another another point on the ground; the Centre of Pressure (CoP). This point is introduced in section 3-2-2.

3-2-1 Linear Inverted Pendulum Model

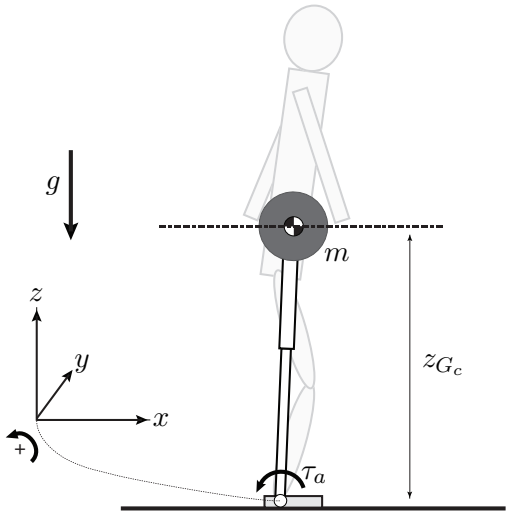

Figure 3-3: The LIPM consists of a point mass m and a massless telescopic leg. Ankle torque τ_a can be applied at the base of the pendulum. The equation of motion of this model is linearised by constraining the CoM to fixed height z_{G_c}. The LIPM therefore simplifies the dynamics of the humanoid robot and can be used to derive an analytical solution for the ICP. The CoP is a point on the ground that indicates the amount of ankle torque applied. This point can be used to control the location of the ICP.

The LIPM, depicted in figure 3-3, can be used to analyse and control a humanoid robot in order to prevent a fall. This model consists of a point mass and a massless telescopic leg. The point mass is situated at the CoM of the robot and has the same mass (m) as the robot. The

telescopic leg is the dynamical equivalence of the force excerted by the legs of the robot on its CoM. On the LIPM of figure 3-3 torques τ_a can be applied at the base of the pendulum. The equations of motion for this model are linearised by constraining the CoM to a fixed height ($\ddot{z}_G = 0$). This results in

$$\tau_a = - m\ddot{x}_G z_{G_c} + mgx_G \tag{3-1a}$$

$$\ddot{x}_G = \frac{g}{z_{G_c}}(x_G - \frac{\tau_a}{mg}) \tag{3-1b}$$

$$\ddot{x}_G = \omega_0^2(x_G - \frac{\tau_a}{mg}) \tag{3-1c}$$

with x_G the CoM position in x-direction, m is the total mass of the robot, τ_a is the ankle torque, $\omega_0 = \sqrt{\frac{g}{z_{G_c}}}$ is the reciprocal of the time constant of a single pendulum where z_{G_c} is the constant height and g the gravitational constant [27]. Equation (3-1c) shows that the system is equivalent to a mass-spring system with negative spring stiffness, the farther away the location of the CoM from the origin, the larger the force which pushes it away. The LIPM simplifies dynamics of the actual robot for a great deal as it reduces the number of Degrees of Freedom (DoF) compared to the actual robot and linearises the equations of motion. For the humanoid robot TUlip this means a reduction from twelve to one DoF. Moreover, because (3-1c) is a second order linear differential equation it can be solved analytically.

3-2-2 Centre of Pressure

The derived equation of motion (3-1c) gives theoretical insight in the dynamical behaviour of a humanoid robot. A crucial feature in the maintenance of balance is the application of ankle torque. The CoP is the point on the ground that indicates the amount of ankle torque applied. Equation (3-1c) can be rewritten as

$$\ddot{x}_G = \omega_0^2(x_G - x_{CoP}) \tag{3-2}$$

The parameter x_{CoP} in equation (3-2) is the CoP of the robot,

$$x_{CoP} = \frac{\tau_a}{mg} \tag{3-3}$$

The CoP is the point of application of the resultant ground reaction force of the robot. The CoP should stay within the convex hull of the foot support area, also called the support polygon, in order to prevent the foot from rotating. The ankle torque can thus be limited by constraining the CoP location underneath the foot in order to prevent foot rotation. Equation (3-2) shows that the CoM acceleration is proportional related to the CoP location. The CoP location, and thus the ankle torque, can be modulated in order to control the CoM acceleration and maintain balance. Placing the CoP in front of the CoM ($x_{CoP} > x_G$) results in negative CoM acceleration, placing the CoP behind the CoM ($x_{CoP} < x_G$) results in positive acceleration and pushes the CoM away. The CoP placed underneath the CoM ($x_{CoP} = x_G$) creates zero acceleration but does not necessarily stop the robot because there still might be CoM velocity. There is a point on the ground where the CoP can be placed in order to bring the robot to a stop. This point is called the ICP and is discussed in next section.

3-2-3 Instantaneous Capture Point

The ICP is the point on the ground where the CoP should instantaneously be placed and maintained in order to bring the system to a stop with the CoM above the CoP [2, 8, 32]. Once the ICP has left the support polygon the CoP cannot be placed at that position (due to the CoP constraint) unless a step will be taken or the hip-ankle strategy will be applied. The ICP can be derived by the "Linear Inverted Pendulum Orbital Energy" [35]. This is the Hamiltonian of the LIPM and consists of the total kinetic and potential energy. The kinetic energy is a function of the CoM velocity ($\dot{x}_G$),

$$\mathcal{T}_{LIPM} = \frac{1}{2} m \dot{x}_G^2 \tag{3-4}$$

As (3-2) can be viewed as a mass-spring system, the stored elastic potential energy can be found by the work done by the system,

$$\begin{aligned} \mathcal{V}_{LIPM} &= -\int F_{G_x} dx = -\int m\omega_0^2 (x_G - x_{CoP}) dx \\ &= -\frac{mg}{2z_{G_c}} (x_G - x_{CoP})^2 \end{aligned} \tag{3-5}$$

where $F_{G_x} = m\ddot{x}_G$ is the horizontal spring force and is derived from the equations of motion in equation (3-2). Note that this derivation is only valid for a constant x_{CoP} or a constant ankle torque. The total energy or Hamiltonian is given by

$$E_{LIPM} = \mathcal{T}_{LIPM} + \mathcal{V}_{LIPM} = \frac{1}{2}\dot{x}_G^2 - \frac{g}{2z_{G_c}} (x_G - x_{CoP})^2 \tag{3-6}$$

where the Hamiltonian E_{LIPM} is the orbital energy of the LIPM which is a conserved quantity and can therefore have a constant value. The orbital energy in the LIPM (E_{LIPM}) determines the behaviour of the system which is characterised by figure 3-4. If $E_{LIPM} > 0$ the CoM moves over the CoP, for $E_{LIPM} < 0$ the CoM does not reach the CoP and reverses direction. For $E_{LIPM} = 0$ the system has two eigenvalues, a stable and an unstable one. The eigenvalue for $E_{LIPM} = 0$ which brings the CoM to a stop over the CoP is of interest, this location is called the ICP. In equation (3-6) the CoP should be placed at such a location that the orbital energy becomes zero and the CoM comes to a stop over the CoP. In equation (3-6) the CoP can be placed at the ICP ($x_{CoP} = x_{ICP}$), which will result in zero orbital energy,

$$\frac{1}{2}\dot{x}_G^2 - \frac{g}{2z_{G_c}} (x_G - x_{ICP})^2 = 0 \tag{3-7}$$

with x_{ICP} the ICP location in x-direction. Solving equation (3-7) results in two solutions, as indicated by the saddle point in figure 3-4. The ICP is the solution for which the CoM moves towards the CoP,

$$x_{ICP} = x_G + \dot{x}_G \sqrt{\frac{z_{G_c}}{g}} \tag{3-8}$$

which can also be written as,

$$x_{ICP} = x_G + \frac{\dot{x}_G}{\omega_0} \tag{3-9}$$

The ICP is thus a function of the CoM position and velocity as depicted by figure 3-5. It defines where the CoP should be placed in order to come to a stop.

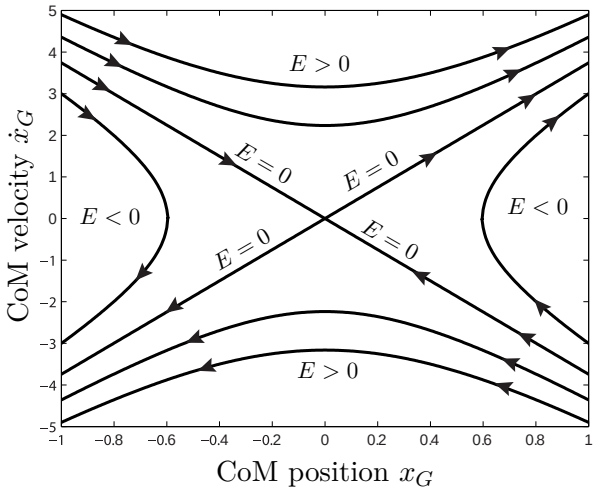

Figure 3-4: Phase portrait for the CoM of the Linear Inverted Pendulum Model. The CoP location is positioned at $(0, 0)$. For $E_{LIPM} > 0$, the CoM moves over the CoP. For $E_{LIPM} < 0$ moves to the CoM but moves back before it reaches the CoP. For $E_{LIPM} = 0$ the CoM comes to a stop over the CoP.

This knowledge can be used in order to maintain balance on the robot. Placing the CoP in front of the ICP ($x_{CoP} > x_{ICP}$) will push the ICP backward, placing the CoP behind the ICP ($x_{CoP} < x_{ICP}$) will push the ICP forward. With this strategy the ICP can be controlled to a desired location, this will be of later use in the application of the balancing control algorithm. The desired location of the ICP is for this research defined in the middle of the support polygon as this location implies best robustness against disturbances for all directions.

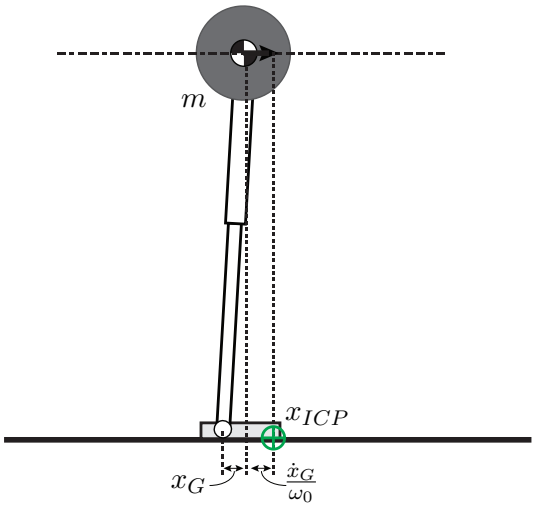

Figure 3-5: The location of the ICP x_{ICP} (in green) is calculated by the sum of the CoM projection on the ground and the CoM velocity $\dot{x}_G$ divided by ω_0.

3-3 Conclusion

A humanoid robot can use the hip-ankle strategy in case the ankle strategy is not sufficient in maintaining balance when subjected to a large disturbance. An important point on the ground that can be used to maintain balance on a humanoid robot is the Instantaneous Capture Point (ICP). The Linear Inverted Pendulum Model (LIPM) can be used to analytically derive the ICP for a humanoid robot. The ICP is composed of the CoM position and velocity of the robot and predicts how close the system is to a fall. The ICP is closely related to the Centre of Pressure (CoP), which is also a point projected on the ground. The CoP location indicates the amount of ankle torque applied and can be modulated to control the ICP to a desired location.

Now all preliminaries are introduced, a measure for the applied disturbance is selected in next chapter.

Chapter 4

Disturbance quantification

The goal of this thesis is to provide experimental evidence that the humanoid robot can maintain balance for larger disturbances using the hip-ankle strategy than using the ankle strategy. It is therefore of major importance to define what kind of disturbance will be applied to the robot and how this disturbance is quantified. The goal of this chapter is to *select a measure for the disturbance applied to the robot in order to quantify the performance of the balance controller*. The selected measure will determine how the ankle strategy and the hip-ankle strategy will be compared in simulation and experiments throughout this thesis.

In order to derive a measure for the disturbance, the requirements for this measure are presented first in section 4-1. A thorough evaluation on existing disturbances supplemented with possible other disturbance measures is then presented in section 4-2. A comparison between the obtained measures is then given in section 4-2-3. The comparison leads to the selection of the preferred measure. Later chapters will use this measure to compare the ankle and the hip-ankle strategy controllers in simulation and by physical experiments.

4-1 Disturbance measure requirements

The first step in selecting a measure for the disturbance is the definition of the requirements. Three requirements were defined to compare between different types of disturbances:

1. The main goal of this thesis is to provide experimental evidence that the hip-ankle strategy outperforms the ankle strategy. The disturbance measure should therefore be *practically measurable* during experiments; it should be easy to apply and measure the disturbance without the need of complicated equipment. Furthermore, it should be possible to analyse the measure in theory and in simulation.

2. In order to perform statistics the disturbance should be applied for multiple times and the disturbance measure should therefore give *repeatable* results. A minimum amount of uncertainty should be present in the disturbance measure.

3. The applied disturbance should be *independent of the location* on the robot it is applied to. This will allow for comparison with other robots.

The main goal of this thesis is to provide experimental evidence that the hip-ankle strategy outperforms the ankle strategy on a humanoid robot. It is therefore most important that the disturbance measure is of practical use during experiments. A weight factor 2x is therefore used for the first two requirements and a weight factor 1x for the third requirement.

The requirements are used to select a disturbance measure in this chapter. Next section introduces several measures for which will be investigated if these measures satisfy the requirements. In a table in section 4-2-3 an overview of all the disturbance measures is given.

4-2 Disturbance measures in push recovery research

In humanoid push recovery research, the performance of a balance controller is often expressed in terms of the largest allowable disturbance. This is the largest disturbance applied to the system in which a fall can still be prevented, any larger disturbance will make a fall inevitable. The largest allowable disturbance can be obtained experimentally by requiring that the robot is not allowed to take a step and gradually increasing the applied disturbance until the robot falls. Disturbances can thereby divided into two groups:

1. *Disturbance space*: The absolute magnitude of a disturbance applied to the robot that is expressed in terms which are totally independent of the robot parameters. For the disturbance space the following disturbance measures where found in push recovery research:
   - Applied impulse [8, 11, 17, 18, 20, 36–38]
   - Applied energy [7]
2. *State space*: This describes the effect of a disturbance on the state of the robot. These measures are always expressed in terms of the state of the robot. The measure can be obtained by the difference in state before and after the disturbance. The following disturbances were found in push recovery literature that are expressed in state space:
   - Velocity change [30, 39, 40]
   - Initial state placement [16, 41]

   Additionally, in chapter 3 we defined the Instantaneous Capture Point (ICP) as a point that predicts how close the system is to a fall. It could therefore also be used to describe the effect of the disturbance on the state of the robot. Although the use of ICP as a measure for disturbance was not found in literature, this measure is also added to the list:
   - Instantaneous Capture Point change

The introduced measures for disturbance will be elaborated in sections 4-2-1 and 4-2-2. A comparison between the disturbance measures is given in section 4-2-3.

4-2-1 Disturbance space

This group of disturbances are expressed in parameters independent of the robot parameters and are externally applied. The measures introduced in this section are the applied impulse and applied disturbance.

Impulse

Many roboticists [8, 11, 17, 18, 20, 36–38] use the applied impulse as a measure for their disturbance. Impulse, $\vec{I}$ (units $kg \cdot m/s$ or Ns), is equal to the applied force over time,

$$\vec{I} = \int_{t_1}^{t_2} \vec{F} dt \tag{4-1}$$

where $\vec{F}$ is the applied force in a certain direction between time t_1 and t_2. A stick [8] equipped with a force sensor can be used to push a robot on a certain location and measure the applied force over time. The maximum allowable impulse untill a fall occurs is then a measure for performance. When applying the push stick by hand, it is difficult to carry ourepeatablele experiments. However simple setups could be used which should allow for repeatable measurements.

The first drawback of this measure is that the effect of the disturbance on the robot is dependent on the location at the robot where it is applied. For a disturbance applied at a higher location it will have a larger angular momentum around the ankles of the robot.

Moreover, preferably we would like to be able to compare our controller to that of other researchers. However, the effect of the applied impulse is dependent on the properties of the platform to which it is applied. A push of certain magnitude applied to the Sarcos Primus humanoid robot [11] will have a totally different effect than the same push applied to the humanoid robot TUlip. This is due to differences in robot configuration such as the mass and foot size.

The properties of applied impulse as a measure for the disturbance are summarised in table 4-1. The ✓ sign indicates that the disturbance measure satisfies the requirement, the × sign indicates that the measure does not satisfy the requirement.

Table 4-1: Applied impulse as a measure for the disturbance.

	Practically measurable?	Repeatable?	Location independent?
Impulse	✓	✓	×

Externally applied energy

Ott et al. [7] use an approach similar to the applied impulse, they use total applied energy as a measure for disturbance. A ball with a certain weight at the end of a pendulum is used to

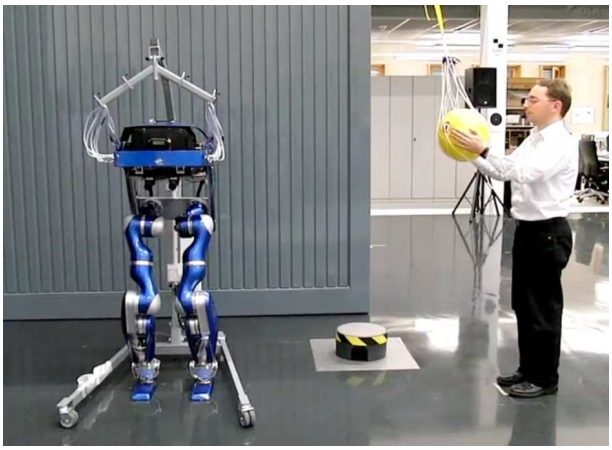

Figure 4-1: A disturbance is applied by using a ball at the end of a pendulum and swinging is from a certain height. The energy of the ball at impact can then be calculated. This energy is used as the measure for disturbance. Figure taken from [42].

define the energy applied to the robot at impact as shown in figure 4-1. In its initial position, the potential energy $\mathcal{V}$ in the ball can easily be calculated,

$$\mathcal{V} = mg\Delta h \tag{4-2}$$

with m the mass of the ball and Δh the difference in height between initial position and impact. This simple method is practically applicable and can result in repeatable measurements. However, the energy in the ball at impact is not the same as the energy transferred to the robot. This is dependent on the coefficient of restitution of ball and robot which represents the ratio between the velocity before and after impact. Additionally, the effect of this measure on the robot is also dependent on the location where the energy is applied.

The properties of the applied energy as a measure are summarised in table 4-2.

Table 4-2: Applied energy as a measure for the disturbance.

	Practically measurable?	Repeatable?	Location independent?
Applied energy	✓	✓	×

4-2-2 State space

This group of parameters express the disturbance in terms of the state parameters of the robot. The introduced disturbance measures in this section are velocity change, intitial state placement and ICP change.

Velocity change

The velocity change as a measure for disturbance is mainly used by biomechanical researchers [30, 39, 40]. In the majority of this research a support surface is used on which the human

Table 4-3: Velocity change as a measure for the disturbance.

	Practically measurable?	Repeatable?	Location independent?
Velocity change	×	✓	×

subject is standing and which can be moved in forward and backward direction by a certain velocity profile. A velocity change located at the feet will create a disturbance of the feet relative to the CoM of the subject. This velocity difference before and after the disturbance can then used as a measure for disturbance.

This method could be used to disturb the robot and the CoM velocity on the robot can then be obtained. Because the CoM velocity is measured on the robot, the measurement data has a higher uncertainty and measurements will be less repeatable compared to disturbance measures in disturbance space. The application of a velocity change at the feet also requires a unnecessary complicated and expensive setup which makes it objectionable for physical experiments. However, a setup with proper actuation be able to give repeatable results.

An overview on the properties of the velocity change as a measure for the disturbance is given in table 4-3.

Initial state placement

Another method to measure the disturbance is placing the Centre of Mass (CoM) of the robot (or human) in a certain initial state. This could be an initial state of the robot with the CoM projection on the ground outside the support polygon [16, 41]. This ensures the ankle strategy is insufficient to maintain balance so the robot is forced to use the hip-ankle strategy. A disadvantage of this method is that, for a robot with multiple Degree of Freedom (DoF), a certain location in state space can be reached in multiple ways. The same CoM location could for example be reached by bending the upper body forward or backward.

If a proper setup is used, where the robot is able to lean against a plate which is then pulled away, this experiments can be repeatable. However it is difficult to bring the physical robot to that same situation where it should lean to a plate and suddenly try to maintain its balance. As this disturbance is not applied to a certain location on the robot but involves the state of the whole robot, it is independent of the applied location.

An overview on the properties of initial state placement as a measure for the disturbance is given in table 4-4.

Table 4-4: Initial state placement as a measure for the disturbance.

	Practically measurable?	Repeatable?	Location independent?
State placement	×	✓	✓

Instantaneous Capture Point change

As introduced in chapter 3, an important variable in humanoid robot balance maintenance is the ICP as it consist of CoM position and velocity. The ICP is a point on the ground plane which indicates how close the robot is to a fall. The ICP continuously changes, if a push would be given to the back of the robot, the ICP will move forward. The ICP change due to a disturbance can be used as a measure for the disturbance. This then summarises the effect of the disturbance on the state of the robot.

As CoM position and velocity can easily be measured, the ICP is also easily be measured without the requirement of any extra devices. However, as the ICP is internally measured, errors will be larger compared to the measurement of an externally applied disturbance. Moreover, the ICP change is a method to measure the disturbance, it should be combined with another method to repeatably disturb the robot.

Table 4-5 summarises the properties of the ICP change as a measure for the disturbance.

Table 4-5: ICP change as a measure for the disturbance.

	Practically measurable?	Repeatable?	Location independent?
ICP change	✓	×	✓

4-2-3 Comparison

The disturbance measures introduced in this chapter are summarised in table 4-6. The four columns represent the requirements to the disturbance measure as introduced in section 4-1. Weight factors are given to these requirements. Because the location dependency can easily be solved by always applying the disturbance at the same location it weights half of the other requirements. The ✓ sign indicates the disturbance measure satisfies the requirement where the × sign indicates the measure does satisfy the requirement.

Table 4-6: Comparison of the disturbance measures.

	Practically measurable?	Repeatable?	Location independent?
Weight factor	2x	2x	1x
Applied impulse	✓	✓	×
Applied energy	✓	✓	×
Velocity change	×	✓	×
State placement	×	✓	✓
ICP change	✓	×	✓

From the table can be concluded that applied impulse and energy can best be used as a quantification of the disturbance applied to the robot in this research. Ideally, we are not interested in how the disturbance is applied but what the effect of this disturbance is on the

state of the robot. In practice, in this research, we want to compare the ankle strategy and the hip-ankle strategy on a humanoid robot. Therefore, we want to apply the same disturbance to the robot and evaluate if the controller can maintain balance. This led to the selection of applied impulse and energy as the measure for disturbance. Although it does not say what the effect is on the state of the robot, it allows for comparison between the ankle and hip-ankle strategy and is sufficient to reach our goal.

Both applied energy and impulse can thus be used as a measure for the disturbance. Because the impulse can easily be measured during experiments with a sensor, this measure will be used in simulation and experiments. The ability to measure the applied force allows an exact force profile over time which can be used to analyse the push recovery data. The use of this measure in this research is introduced in the following section.

4-3 Mitigation of drawbacks of chosen measure: impulse

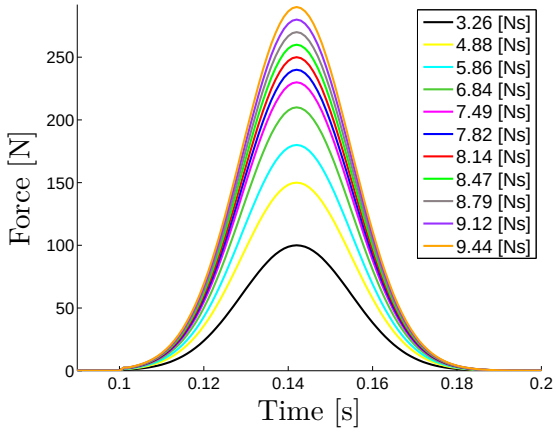

Figure 4-2: Applied disturbance profiles. The applied impulse is obtained by the integral of the applied force over time.

Although the impulse is selected as a measure, it still consists of some drawbacks. The measure impulse has the property of being dependent on the location where is is applied to. Therefore, the disturbance should always be applied at the same location of the robot in order to allow for comparison between strategies.

The second drawback is that the quantity impulse does not give an unambiguous description of the actual disturbance. The same quantity can be obtained by applying a small push over a long time span compared to a large push for a small amount of time. However, these disturbances would have a total different effect on the robot. To solve for this issue, the applied disturbances should also have the same time span and shape and can be varied in magnitude in order to come up with a fair comparison.

A Gaussian function closely approximates physical impulsive pushes and can therefore be used in order to simulate the disturbance. The Gaussian function is given by,

$$F_d(t) = ae^{\frac{-(t-c)^2}{2\sigma^2}} \tag{4-3}$$

with F_d the disturbance force, t for time, a the amplitude, c indicating the centre position of the peak and σ the width of the curve. Figure 7-3 shows an example of eleven different disturbances that are applied in simulation. The disturbance starts after 0.1 s and lasts for about 0.08 s. The impulse is calculated by integrating the disturbance force curve over time.

4-4 Conclusions

The goal of this chapter was to select a measure for the disturbance applied to the robot in order to quantify the performance of the hip-ankle strategy and ankle strategy control algorithms. Ideally, the effect of the disturbance on the state of the robot should be used as a quantification. However, measuring the effect of the disturbance on the state of the robot introduces additional errors and difficulties to obtain the measure in practice.

Although it is not ideal, the externally applied impulse will be used as a disturbance quantification. As long as the force profile over time is the same for different magnitude, it is valid to use this measure for intra-platform comparison of different strategies. The measure can easily be obtained in simulation as on a physical robot platform and can give repeatable results.

Chapter 5

Theoretical largest allowable disturbance

Before testing the benefits of the hip-ankle strategy on a real robot, in this chapter a simplified simulation model is tested. The goal of this chapter is to *define the theoretical largest allowable disturbance for the humanoid robot TUlip*. This will give an indication on the possible improvement in performance of using the hip-ankle strategy compared to the ankle strategy when applied on a real robot. Four simple models will be used which approximate the configuration of TUlip; the Linear Inverted Pendulum Model (LIPM), the (nonlinear) Inverted Pendulum Model (IPM), the Linear Inverted Pendulum plus Flywheel Model (LIPFM) and the (nonlinear) Inverted Pendulum plus Flywheel Model (IPFM). The linear models are solved analytically and used to predict the region in state space for which the CoM can be pushed back to its desired position. The nonlinear models are used evaluate if the obtained regions are realistic and obtain the largest allowable disturbance in terms of applied impulse. Section 5-1 introduces the LIPM and IPM which are used to calculate the maximum allowable disturbance for the the ankle strategy. Subsequently these models are extended in section 5-2 with a flywheel in order to obtain the theoretical maximum allowable disturbance for the hip-ankle strategy.

5-1 Analysing the ankle strategy with simple models

The LIPM, depicted in figure 5-1(a), was introduced in section 3-2-1 to analyse how to maintain balance on a humanoid. This model can be used to analytically derive the limits on the state of the CoM for which balance can be maintained in case of the ankle strategy. This can be visualised by a region in state space. The stability region can be compared with a controlled nonlinear IPM, depicted in figure 5-1(b), in order to validate if the region is realistic and to obtain the largest allowable disturbance in terms of applied impulse. The derived stability region can then later be used by the hip-ankle strategy to decide when to apply the hip-ankle strategy.

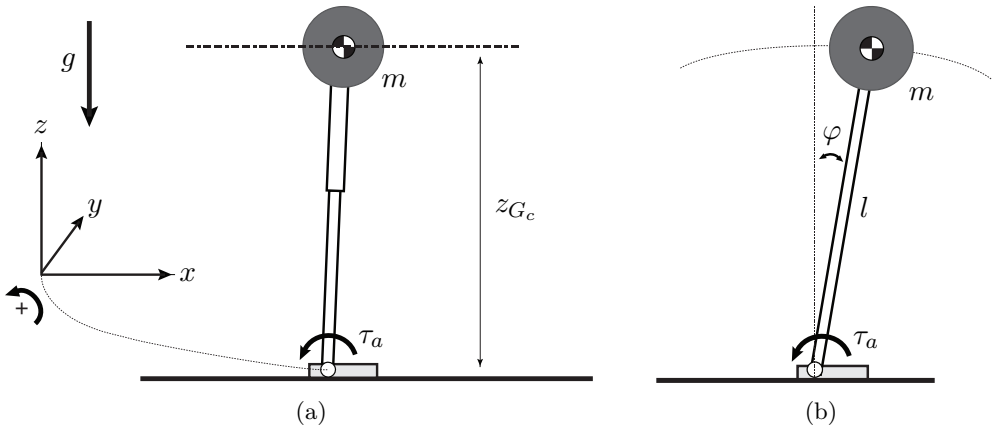

Figure 5-1: The LIPM (a) is used in this section in order to analytically derive the constraints on the CoM in state space for which the ankle strategy can be used to maintain balance. The model consists of a point mass with weight m at fixed height z_{G_c} and ankle torque τ_a can be applied. The IPM (b) is used to perform numerical simulations and obtain the largest allowable disturbance for the ankle strategy in terms of impulse. It consists of a point mass with weight m, a pendulum with length l and ankle torque τ_a can be applied.

5-1-1 Analytical solution for the Linear Inverted Pendulum Model with ankle torque

The analytical solution of the LIPM can be derived from its equation of motion. The equation of motion for the model was derived in section 3-2-1,

$$\ddot{x}_G = \omega_0^2 x_G - \frac{\tau_a}{m z_{G_c}} \tag{5-1}$$

with m is the total mass of the robot, τ_a the applied ankle torque, $\omega_0 = \sqrt{\frac{g}{z_{G_c}}}$ the reciprocal of the time constant of a single pendulum where z_{G_c} is the constant height and g the gravitational constant. This second order linear differential equation can be solved, resulting in

$$x_G(t) = c_1 e^{\omega_0 t} + c_2 e^{-\omega_0 t} + \frac{\tau_a}{mg} \tag{5-2}$$

with c_1 and c_2 constants. The initial conditions for this problem can be given by $x_G(0) = x_{G_0}$ and $\dot{x}_G(0) = \dot{x}_{G_0}$ with x_{G_0} and $\dot{x}_{G_0}$ the initial CoM location and velocity. This can be used to derive a solution for the constants,

$$c_1 = \frac{1}{2}\left(x_{G_0} + \frac{\dot{x}_{G_0}}{\omega} - \frac{\tau_a}{mg}\right) \tag{5-3a}$$

$$c_2 = \frac{1}{2}\left(x_{G_0} - \frac{\dot{x}_{G_0}}{\omega} - \frac{\tau_a}{mg}\right) \tag{5-3b}$$

Substituting these constants back in (5-2) gives the full solution for the LIPM with ankle torque,

$$x_G(t) = \frac{1}{2}\left(x_{G_0} + \frac{\dot{x}_{G_0}}{\omega_0} - \frac{\tau_a}{mg}\right) e^{\omega_0 t} + \frac{1}{2}\left(x_{G_0} - \frac{\dot{x}_{G_0}}{\omega_0} - \frac{\tau_a}{mg}\right) e^{-\omega_0 t} + \frac{\tau_a}{mg} \tag{5-4}$$

The system has two eigenvalues, a stable negative eigenvalue ω_0 and an eigenvalue causing instability in the system $-\omega_0$. The system will be stable if the coefficient of the positive eigenvalue is zero,

$$x_{G_0} + \frac{\dot{x}_{G_0}}{\omega_0} - \frac{\tau_a}{mg} = 0 \tag{5-5}$$

As explained in section 3-2-2 the term $\frac{\tau_a}{mg}$ in equation (5-5) is called the Centre of Pressure (CoP). If an ankle torque is applied that places the CoP outside of the foot, rotation of this foot will occur. Foot rotation is therefore prevented by constraining the CoP, and thus the ankle torque to remain inside the foot. This constraint is written as follows,

$$l_r < \frac{\tau_a}{mg} < l_f \tag{5-6}$$

which indicates that the CoP should stay within the rear edge of the foot l_r and the front edge of the foot l_f. The goal is to find the constraint on the state space location of the CoM such that the ankle strategy can still maintain balance. The CoP constraint can therefore be combined with equation (5-5),

$$l_r < x_{G_0} + \frac{\dot{x}_{G_0}}{\omega_0} < l_f \tag{5-7}$$

In equation (5-7) the constraints on the ankle strategy is given. If the term $x_{G_0} + \frac{\dot{x}_{G_0}}{\omega_0}$ crosses the foot edge, the ankle strategy is insufficient in preventing a fall. Note that this is equal to the constraint given on the Instantaneous Capture Point (ICP); in section 3-2-3 was stated that the ICP should stay within the foot in order to maintain balance. If the ICP is outside the foot, another strategy is required to maintain balance.

The constraints of equation (5-7) can be represented by a region in state space, figure 5-2 shows this region for the constants based on TUlip. The parameters used for this plot are given in table 5-1. The stable region is represented by the green band, the width of this band is defined by the foot edge constraints where the height of the CoM z_{G_c} defines the angle of this band.

Table 5-1: Simulation parameters for the LIPM.

Model parameter	Symbol	Value
LIPM height	z_{G_c}	0.7 [m]
Body mass	m	17.94 [kg]
Foot edge front	l_f	0.138 [m]
Foot edge rear	l_r	-0.048 [m]

If the state space location of the robot falls within the green region of figure 5-2, the ankle strategy can maintain balance. If it leaves the region, another strategy such as the hip-ankle strategy should be applied. This surface is also indicated by Stephens (2007) [1] as the decision surface, it can be used in order to decide which strategy to use.

5-1-2 Controlled Inverted Pendulum Model

The nonlinear IPM is depicted in figure 5-1(b). In order to compare the stability region of the IPM with the earlier derived stability region for the LIPM, numerical simulations are

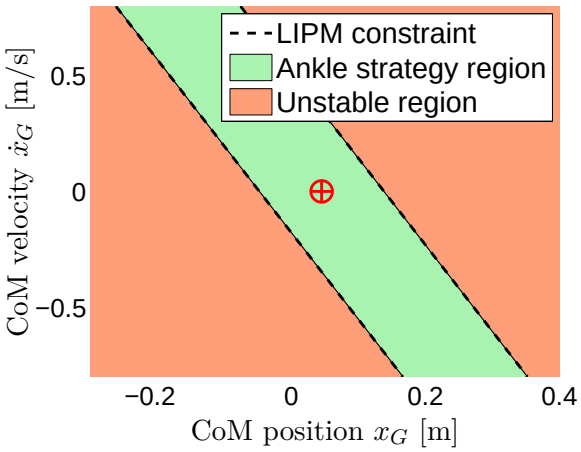

Figure 5-2: Stability region for the ankle strategy obtained by the LIPM. The green area defines the state space location for the CoM where the ankle strategy can be used to prevent a fall. The dashed lines are the constraints on the ankle strategy, given by the foot edges l_r and l_f. In the red region the ankle strategy is not capable of preventing a fall. The red cross is the desired ICP in the middle of the foot.

performed using the IPM. A controller is therefore designed which controls the ICP of the model to a desired position. This is obtained by the follwing control law,

$$x_{CoP}^{des} = x_{ICP} - K_{p,ICP}(x_{ICP}^{des} - x_{ICP}) \tag{5-8}$$

with $K_{p,ICP}$ the propertional gain, x_{CoP}^{des} the desired CoP, x_{ICP} the ICP location and x_{ICP}^{des} the desired ICP location. This controller places the CoP in front of the ICP ($x_{CoP} > x_{ICP}$) to push the ICP backward to its desired position or places the CoP behind the ICP ($x_{CoP} < x_{ICP}$) to push the ICP forward to its desired position. The ankle torque τ_a required to place the CoP at the desired location can then be calculated,

$$\tau_a = mgx_{CoP}^{des} \tag{5-9}$$

The ankle torque is again constrained such that the CoP stays inside the support polygon. Equation (5-6) gives,

$$\tau_a^{max,+} = mgl_f \tag{5-10a}$$
$$\tau_a^{max,-} = mgl_r \tag{5-10b}$$

with $\tau_a^{max,+}$ the maximum positive ankle torque and $\tau_a^{max,-}$ the maximum negative ankle torque.

Stability region

Numerical simulations can be run in order to compare the stability region derived by the LIPM constraints of equation (5-7) and stability region for the controlled IPM. Various initial conditions, x_{G_0} and $\dot{x}_{G_0}$, are therefore given for the IPM and the controller given in equation

5-8 will then try to maintain balance. The phase portrait for this controlled IPM is plotted together with the LIPM region and depicted in figure 5-3. The parameters used in this numerical simulation are given in table 5-2. The blue lines represent successful responses of the controlled IPM where the red lines the controlled IPM was not able to prevent a fall. The responses of the blue lines closely correspond with the analytical derived stability region which is bounded by the black dashed lines.

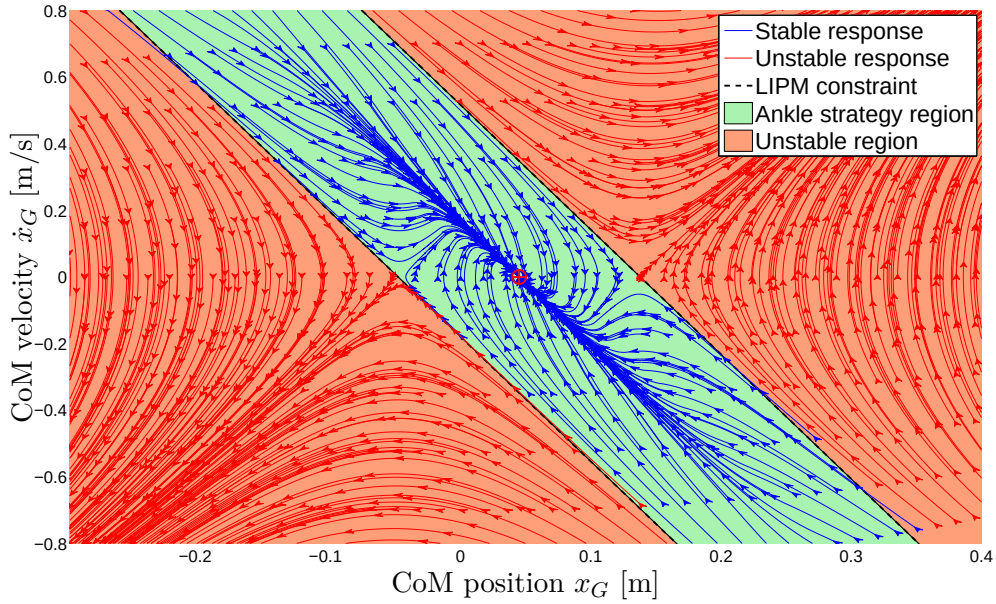

Figure 5-3: Phase portrait a controlled IPM. The dashed black lines represents the LIPM constraint of (5-7). The blue lines represent the IPM with controller responses which successfully maintained balance. For the red lines the IPM with controller was not able to maintain balance. The desired ICP is indicated by the red cross. The green stability region derived by the LIPM closely predicts the nonlinear stability region.

Table 5-2: Simulation parameters for the Inverted Pendulum Model.

Model parameter	Symbol	Value
IPM length	l	0.7 [m]
Body mass	m	17.94 [kg]
Desired ICP location	x_{ICP}^{des}	0.045 [m]
ICP control gain	$K_{p,ICP}$	3
Foot edge front	l_f	0.138 [m]
Foot edge rear	l_r	-0.048 [m]

Largest allowable disturbance

The IPM with the same controller is now used to define the largest allowable disturbance for the ankle strategy in terms of impulse. A horizontal impulse is applied at the CoM of the IPM

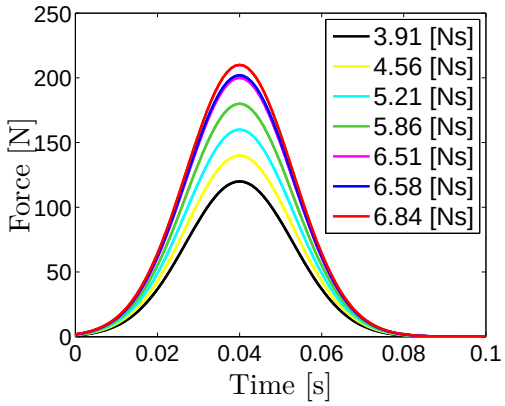

Figure 5-4: Applied disturbances for the IPM. The disturbances were applied in horizontal direction to the CoM of the model. The applied impulse is obtained by the integral of the applied force over time.

with zero initial velocity and its CoM over the desired ICP. The disturbances are depicted in figure 5-4. Figure 5-5 shows the response of the IPM with ICP controller for various disturbances. Larger disturbances bring the state-space location of the CoM closer to the edge of the green LIPM stability region. A disturbance which makes the state space location of the CoM cross this edge results in a fall. The responses show that the ankle strategy can withstand disturbances for which the ICP remains inside the support polygon. The largest allowable disturbance in terms of applied impulse is 6.58 Ns. This value corresponds with a calculation that was performed on the maximum allowable disturbance in case of locked joints, see appendix A.

5-2 Analysing the hip-ankle strategy with simple models

Now the limitations of the ankle strategy have been analysed, this section will present models to analyse the hip-ankle strategy. The point mass of the LIPM can therefore be exchanged with a flywheel at which a torque τ_f can be applied. This results in the LIPFM as depicted in figure 5-6(a). The flywheel should bring the ICP back into the ankle strategy region in case the ICP has left the foot. Ankle torque will then be sufficient to bring back the ICP to the desired position. An analytical solution for the LIPFM can be found by solving the equations of motion. Given the constraints of the model, this results in a stability region in state space which should be larger than that for the ankle strategy. The green band of figure 5-2 will therefore be increased. Again a nonlinear model is used to evaluate if the obtained linear stability regions correspond with a controlled nonlinear model. The IPFM, depicted in figure 5-6(b), will therefore be used to perform numerical simulations and obtain the largest allowable disturbance for the hip-ankle strategy.

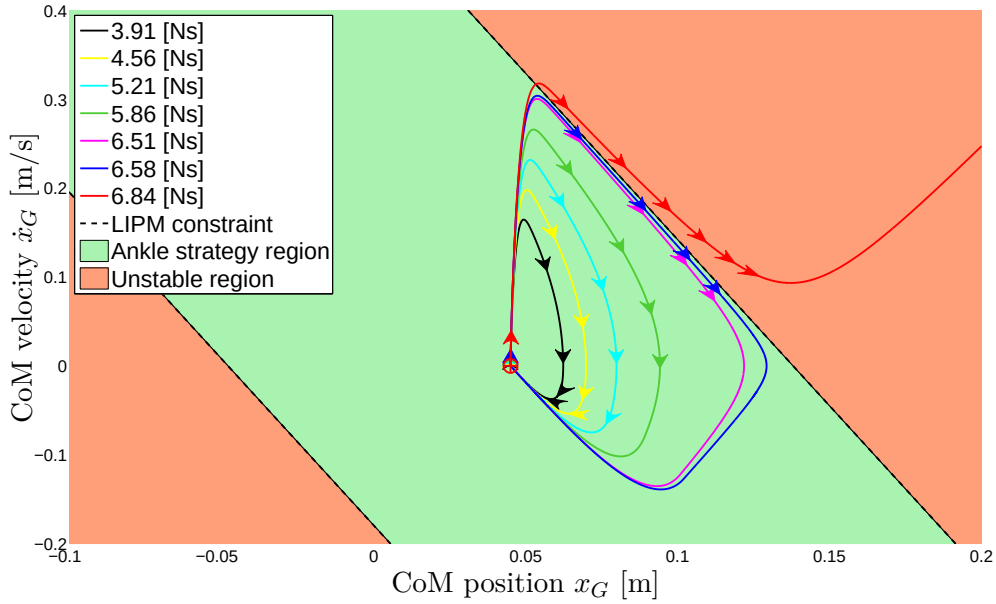

Figure 5-5: Phase portrait of the controlled nonlinear IPM subjected to impulsive disturbances. A larger disturbance brings the state space location of the CoM closer to the edge of the green LIPM stability region. The largest allowable disturbance is 6.58 Ns.

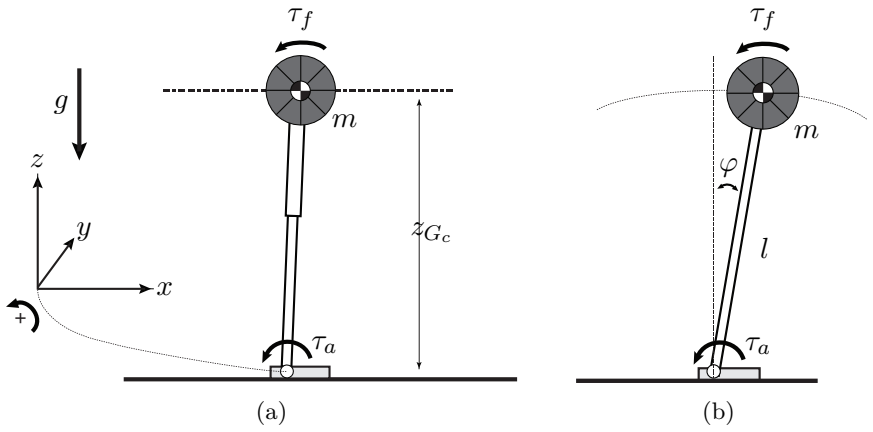

Figure 5-6: The LIPFM (a) is used to analytically derive the CoM constraints in state space for the hip-ankle strategy. The model consists of a flywheel with weight m at fixed height z_{G_c} a torque τ_f can be applied on the flwyheel and a torque τ_a can be applied at the ankle. The IPFM (b) is used to perform numerical simulations and obtain the largest allowable disturbance for the hip-ankle strategy in terms of impulse. It consists of a flywheel with weight m, flywheel torque τ_f, a pendulum with length l and ankle torque τ_a can be applied.

5-2-1 Analytical solution for the Linear Inverted Pendulum plus Flywheel Model

The equations of motion for the LIPFM are given by,

$$\tau_a = -m\ddot{x}_G z_{G_c} + mgx_G + \tau_f \tag{5-11a}$$

$$\ddot{x}_G = \omega_0^2 x_G - \frac{\tau_a}{mz_{G_c}} + \frac{\tau_f}{mz_{G_c}} \tag{5-11b}$$

In equation (5-11b) the term τ_f is the torque applied on the flywheel for which the following equation of motion is given,

$$\tau_f = I_{G_y}\ddot{\varphi}_{f_y} \tag{5-12}$$

with I_{G_y} the flywheel inertia around the CoM and $\ddot{\varphi}_{f_y}$ the acceleration of the flywheel. Equation (5-11b) shows that an increase in flywheel results in a decrease in acceleration of the CoM. This can be used to control the ICP of the robot; the maximum ICP displacement can be obtained by applying maximum torque on the flywheel and then decelerating it with maximum negative torque in order to stop it at its maximum angle. This is also denoted by bang-bang control [1, 2, 27, 37]. With bang-bang control the largest disturbance can be withstood.

An example of a bang-bang torque profile with corresponding flywheel angle φ_{f_y} and angular velocity $\dot{\varphi}_{f_y}$ is shown in figure 5-7.

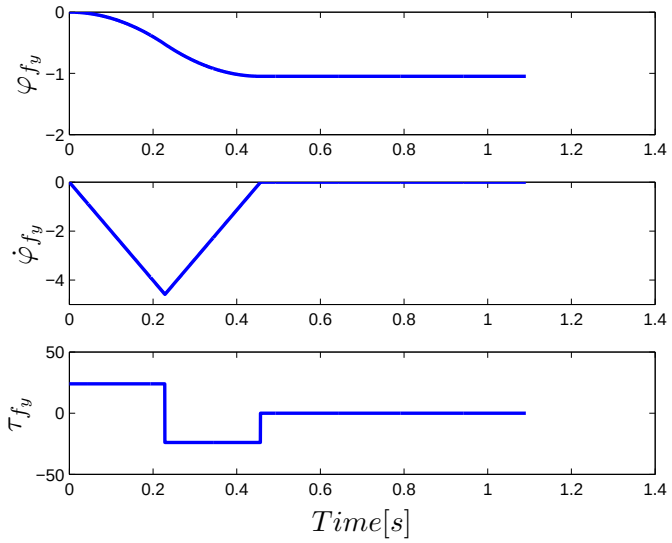

Figure 5-7: Flywheel response for a typical bang-bang hip-ankle strategy control action. The upper graph gives the flywheel angle φ_{f_y} over time, the flyhwheel velocity $\dot{\varphi}_{f_y}$ is given by the middle graph. The bang-bang torque τ_{f_y} profile is given by the lowest graph.

In mathematical terms this bang-bang torque profile is given by

$$\tau_{bb}(t) = \tau_{max}u(t) - 2\tau_{max}u(t - T_1) + \tau_{max}u(t - T_2) \tag{5-13}$$

with τ_{max} the maximum torque that can be applied on the flywheel (depending on the maximal torque the motors can apply), $u(t - T)$ is the unit step function which starts at T, at T_1 the flywheel stops accelerating and starts decelerating and at T_2 the flywheel comes to a stop [2].

The goal is to satisfy the constraint of equation (5-7) at $t = T_2$,

$$l_r < \frac{\dot{x}_G(T_2)}{\omega_0} + x_G(T_2) < l_f \tag{5-14}$$

In other words, after execution of the bang-bang control the state space location of the system should be moved within the constraints of the ankle strategy (green region in figure 5-2). The application of ankle torque can then return the ICP to its desired location. Differential equation (5-11b) can be solved analytically to find the region in state space where the hip-ankle strategy can be used to maintain balance. This results in the following constraint on the state space location of the CoM for the hip-ankle strategy [1],

$$l_r - P < \frac{\dot{x}_0}{\omega} + x_0 < l_f + P \tag{5-15}$$

where

$$P = \frac{\tau_{max}}{mg}\left[\frac{\left(e^{\omega T_{max}} - 1\right)^2}{e^{2\omega T_{max}}}\right] \tag{5-16}$$

The parameter T_{max} is the maximum time the flywheel torque can be applied in one direction. By assuming that the flywheel starts at zero angle and zero angular velocity, this term is given by,

$$T_{max} = \sqrt{\frac{I_{G_y}\theta_{max}}{\tau_{max}}} \tag{5-17}$$

where θ_{max} is the maximum flywheel angle and τ_{max} the maximum flywheel torque [11]. The benefit of applying the hip-ankle strategy is dependent on these parameters where the maximum flywheel angle is an important constraint and is 1.05 rad for TUlip. The term P in equation (5-15) indicates an extra region in state space, the green band derived for the ankle strategy is extended by this region. This region is visualised in figure 5-9, an additional grey region can be observed. This is the additional area where the CoM an be placed in state space and where the hip-ankle strategy can still maintain balance. The parameters used to obtain this plot are given in table 5-3.

Table 5-3: Simulation parameters for the LIPFM.

Model parameter	Symbol	Value
LIPM height	z_{G_c}	0.7 [m]
Body mass	m	17.94 [kg]
Foot edge front	l_f	0.138 [m]
Foot edge rear	l_r	-0.048 [m]
Maximal flywheel angle	θ_{max}	1.05 [rad]
Maximal flywheel torque	τ_{max}	24 [Nm]
Flywheel inertia	I_{G_y}	0.680 [kgm^2]

5-2-2 Controlled Inverted Pendulum plus Flywheel Model

The stability region derived with the LIPFM will now be compared with the stability of a controlled nonlinear IPFM. The IPFM is depicted in figure 5-6(b). It is similar to the IPM

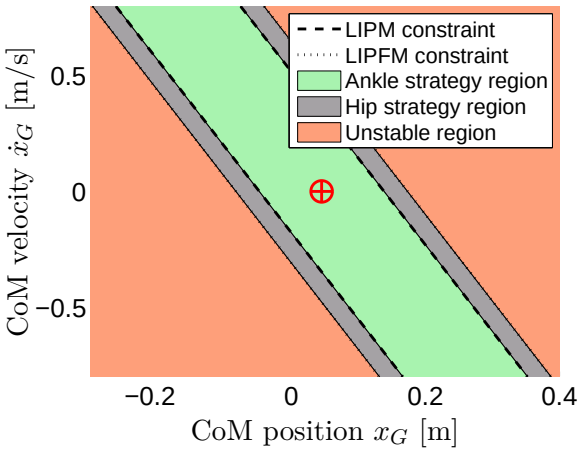

Figure 5-8: Stability region for the hip-ankle strategy obtained by the LIPFM. The green area defines the state space location for the CoM where the ankle strategy can be used to prevent a fall. The dashed lines are the constraints on the ankle strategy, given by the foot edges l_r and l_f. The grey area is defines the region where bang-bang torque on the flywheel can bring the CoM back into the green region; the hip-ankle strategy. The dotted black lines are the constraints on the hip-ankle strategy and are dependent on the maximal flywheel torque τ_{max}, maximal flywheel angle θ_{max} and inertia of the flywheel I_{G_y}. In the red region the ankle strategy is not capable of preventing a fall. The red cross is the desired ICP in the middle of the foot.

but consists of a flywheel instead of a point mass. The ankle torque of the IPFM is controlled using the same ICP control as introduced in section 5-1-2. When the CoM leaves the green region of figure 5-8 in state space (or when the ICP exceeds the foot edge) maximum torque is applied on the flywheel. Negative torque is applied in order to push the CoM of the robot in negative direction and positive torque is applied to push the CoM in positive direction. Torque in opposite direction is applied when ICP is far enough inside the foot or when the maximum torque time T_{max} is reached. The flywheel is stopped after decelerating torque is applied for the same amount of time as accelerating torque and zero torque is then applied. Numerical simulations on the controlled IPFM are performed in order to find the stability region for this model and to obtain the largest allowable disturbance in terms of impulse. The simulation parameters used for these simulations are given in table 5-4.

Table 5-4: Simulation parameters for the IPFM.

Model parameter	Symbol	Value
IPM length	l	0.7 [m]
Body mass	m	17.94 [kg]
Desired ICP location	x_{ICP}^{des}	0.045 [m]
ICP control gain	$K_{p,ICP}$	3
Foot edge front	l_f	0.138 [m]
Foot edge rear	l_r	-0.048 [m]
Maximal flywheel angle	θ_{max}	1.05 [rad]
Maximal flywheel torque	τ_{max}	24 [Nm]
Flywheel inertia	I_{G_y}	0.680 [kgm^2]

Stability region

The LIPFM is compared with the IPFM in terms of CoM locations in state space for which a fall can be prevented. A simulation is therefore performed where various initial conditions, x_{G_0} and $\dot{x}_{G_0}$, are given for the IPFM with the introduced controller. The resulting phase portrait together with the obtained stability regions with the LIPFM is depicted in figure 5-9. The blue lines represent the controller being able to maintain balance while for the red lines a fall occurs. It can clearly be observed that, for initial conditions starting in the grey hip-ankle strategy region bang-bang torque is applied and brings the CoM back into the ankle strategy region. For initial conditions starting in the red unstable area the flywheel torque cannot bring be applied long enough due to the maximum flywheel angle constraint and a fall will occur.

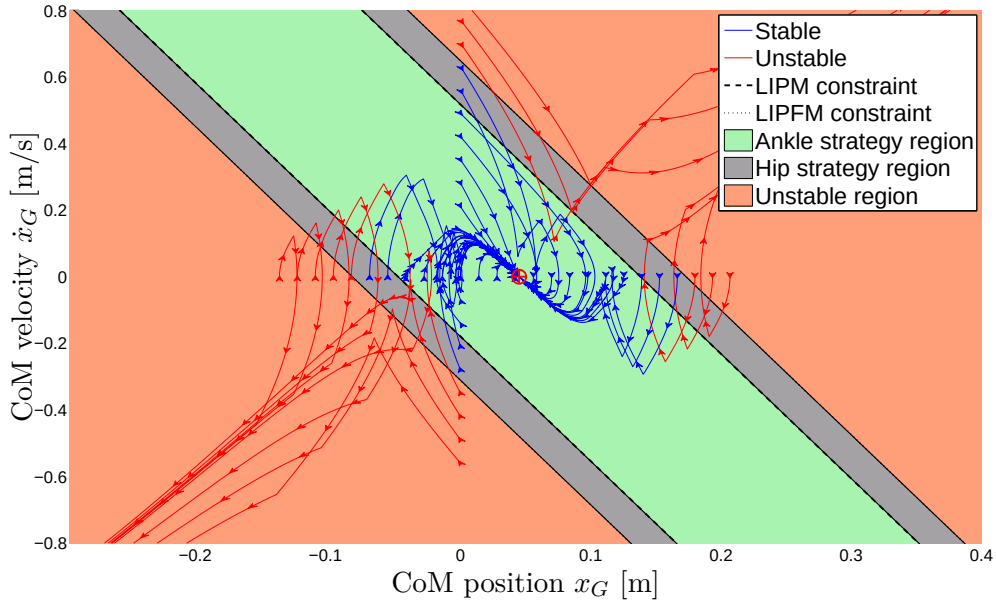

Figure 5-9: Phase portrait of the controlled IPFM for different initial positions including the regions derived analytically with the LIPFM. Initial conditions starting in the hip strategy region can still be recovered by applying bang-bang control on the flywheel. The LIPFM boundaries are a close approximation of the nonlinear IPFM control. The origin is the ankle location and the desired ICP is indicated by the red cross.

Largest allowable disturbance

In order to derive the largest allowable disturbance, the IFPM will be subjected to increasing impulsive disturbances. The disturbance profiles are shown in figure 5-10 and were applied in horizontal direction to the CoM of the model. The model has zero initial CoM velocity and its initial CoM position over the desired ICP. Figure 5-11 shows the response of the IPFM when subjected to the disturbances. Larger disturbances bring the state space location of the CoM closer to the red unstable region. The disturbances bring the CoM state space location outside the green ankle strategy region and into the grey hip-ankle strategy region but balance can

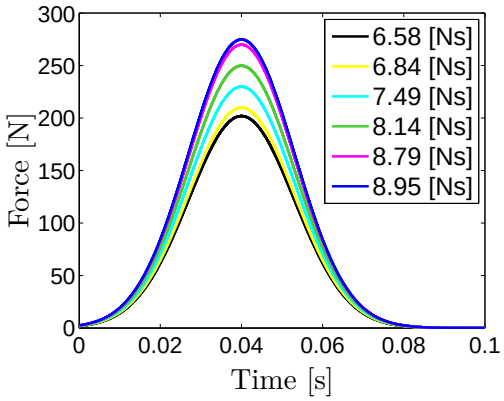

Figure 5-10: Applied disturbances for the IPFM. The disturbances were applied in horizontal direction to the CoM of the model. The applied impulse is obtained by the integral of the applied force over time.

still be maintained. From the figure can be observed that the largest allowable disturbance for the hip-ankle strategy using this model is 8.79 Ns.

The hip-ankle strategy can thus maintain balance for larger disturbances than the ankle strategy. When the ICP location has left the ankle strategy region (crossed the foot edge) flywheel torque can be applied to bring back the ICP inside the foot. The hip-ankle strategy was able to maintain balance for a maximal allowable impulsive disturbance of 8.79 Ns, 33.6% larger than the largest allowable disturbance for the ankle strategy.

5-3 Conclusions

Table 5-5: Largest allowable impulse [Ns] for ankle and hip-ankle strategy from simple model.

	Ankle strategy [Ns]	Hip-ankle strategy [Ns]	Improvement
Model	6.58	8.79	133.6%

The goal of this chapter was to find the theoretical largest allowable disturbance for the humanoid robot TUlip. The analytical solution for the Linear Inverted Pendulum Model (LIPM) defines the region in state space where the ankle strategy is sufficient in maintaining balance. For the hip-ankle strategy the Linear Inverted Pendulum plus Flywheel Model (LIPFM) was solved and showed an increased region in state space where this strategy is successful in maintaining balance. The Inverted Pendulum Model (IPM) and the Inverted Pendulum plus Flywheel Model (IPFM) with controllers were compared in simulation where impulsive disturbances were applied. For forward impulsive disturbances the hip-ankle strategy (IPFM) can maintain balance for disturbances 33.6 % larger than the ankle strategy (IPM).

Bang-bang control was used in order to derive the theoretical largest disturbance. However, the robot TUlip is not a flywheel. Therefore, the next section introduces a realistic controller.

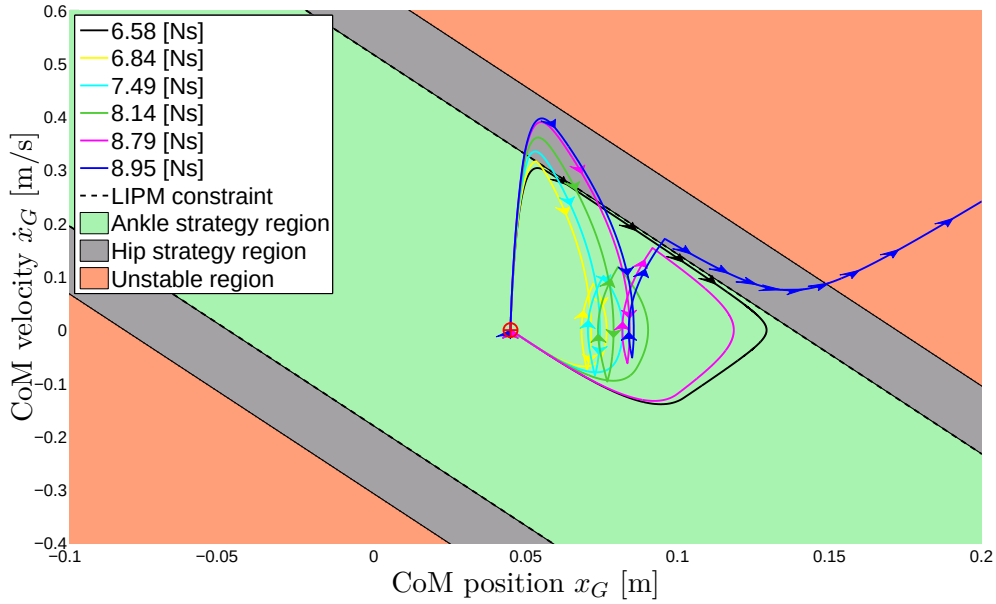

Figure 5-11: Largest allowable impulsive disturbance for the IPFM. Although the disturbance pushes the state space location of the CoM outside the ankle strategy region the system is still able to maintain balance by applying flywheel torque. The largest allowable disturbance is 8.79 Ns.

Chapter 6

Hip-ankle strategy control algorithm

In chapter 5 the Inverted Pendulum plus Flywheel Model (IPFM) was introduced to investigate the benefit of using the hip-ankle strategy over the ankle strategy. It was demonstrated that the theoretical maximum allowed disturbance for the hip-ankle strategy for the simple model based on the configuration of TUlip is 33.6% larger than using the ankle strategy. This is a fair improvement and it is therefore worth developing a hip-ankle strategy algorithm for the humanoid robot TUlip. The humanoid robot TUlip does not contain a flywheel and the application of bang-bang control is undesirable; a more sophisticated algorithm is therefore required. Therefore the goal of this section is to *present a control algorithm to maintain balance using the hip-ankle strategy that is applicable on a physical humanoid robot.* For the sake of simplicity the control algorithm in this chapter will be elaborated for the 2D case in the sagittal plane using the model introduced in figure 2-2. However, the control algorithm applies to both the forward and sideward direction.

This chapter first introduces Virtual Model Control (VMC) which is used to calculate the joint torques required to maintain balance. A general introduction on the balance control algorithm is then presented followed by an elaboration on each component of the controller.

6-1 Virtual Model Control

The hip-ankle strategy algorithm requires angular acceleration of the upper body, large enough to push the Instantaneous Capture Point (ICP) backwards into the support polygon. However, the upper body rotation should also be decelerated in order to prevent it from exceeding joint limits. For the flywheel models presented in chapter 5 the location of the CoM of the model is always fixed to the hip joint. The upper body of the physical humanoid robot is not a flywheel but the Centre of Mass (CoM) has an offset in relation to the hip joint. Simply applying maximum torque on the hip joint in one direction and then applying a torque in opposite direction for same duration (bang-bang control) will not work. The gravity working on the CoM of the upper body is now dependent on the joint angle. One could use a PD-controller to apply a torque on the hip joint to create acceleration of the upper body and

then decelerate the body with another PD-controller. This requires two controllers with four gains to be tuned, this tuning is a delicate process and gains should be tuned such that both controllers cooperate. Moreover, the gains might be dependent on the size of the disturbance. The control algorithm presented in this chapter has a more comprehensive approach. It applies virtual forces on the upper body and calculates the required joint torques by means of VMC [43].

VMC is a method to generate desired joint torques by applying virtual forces. These virtual forces will create joint torques that have the same effect as if the forces would physically be applied. The application of the virtual forces can intuitively result in the required motions for the robot to maintain balance because its effect can easily be predicted [8]. The effect of parameter changes can also be easily predicted, controller tuning will therefore not require much effort. Complex tasks that would be difficult to describe using local PD-controllers are greatly simplified by the use of VMC. This is mainly because the method does not use the inverse dynamics approach so an exact dynamical model is not required. Instead of the inverse dynamics approach it uses the Jacobian (inverse kinematics) of the robot in order to calculate the joint torques. The joint torques can be calculated by,

$$\boldsymbol{\tau} = {}^{A}_{B}\boldsymbol{J}^{T}\boldsymbol{W} \tag{6-1}$$

with $\boldsymbol{\tau}$ the joint torques, ${}^{A}_{B}\boldsymbol{J}$ the Jacobian of the robot from frame $\{A\}$ to frame $\{B\}$, and $\boldsymbol{W}$ the applied virtual forces (wrench) on the system at frame $\{B\}$. For further explanation and derivation of equation (6-1) see appendix C.

The VMC algorithm does not consider the system on joint level but controls it as a whole. The goal of the algorithm presented in this chapter is to define virtual forces on the upper body which can then be translated to joint torques by means of VMC. The virtual forces applied in the sagittal plane are depicted in figure 6-1. The three virtual forces applied on the trunk that are used by the balance control in this chapter are a virtual torque τ_{tr_y} a horizontal virtual force f_x and a vertical virtual force f_z. Together these forces are called the wrench $\boldsymbol{W}$ applied on the trunk and can be written in vector form as

$$\boldsymbol{W} = \begin{bmatrix} f_x \\ f_z \\ \tau_{tr_y} \end{bmatrix} \tag{6-2}$$

These virtual forces are applied on the trunk at all times for both the ankle strategy as the hip-ankle strategy. The virtual torque τ_{tr_y} can switch between either the ankle strategy and the hip-ankle strategy.

6-2 Balance control

For the reasons introduced above, the balance control algorithm uses VMC to apply virtual forces on the upper body. During the balance algorithm the knee joints are fully stretched and locked because this Degree of Freedom (DoF) does not have any added value in maintaining balance [39] and bent knees require unnecessary high torques. The architecture of the hip-ankle strategy control algorithm is summarised by figure 6-2. The control loop consists of the following five main components, indicated by the numbers in the figure:

1. Instantaneous Capture Point calculation
2. Instantaneous Capture Point control
3. Upper body orientation control
4. Gravity compensation
5. Joint torque calculation

Note that for the ankle strategy control algorithm the same architecture is used as depicted in 6-2. However, the upper body orientation control always locks the hip joint. The five components of the hip-ankle strategy control algorithm will be elaborated in sections 6-2-1 to 6-2-5.

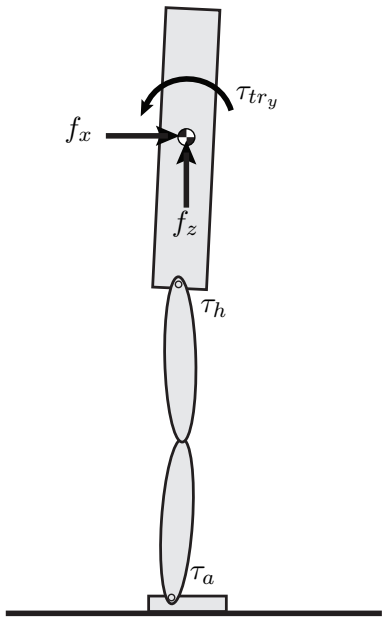

Figure 6-1: The application of the virtual forces on the trunk of the robot. The virtual forces consist of a torque τ_{tr_y} a horizontal force f_x and a virtual force f_z. The virtual forces will be translated to ankle torque τ_a and hip torque τ_h by means of VMC.

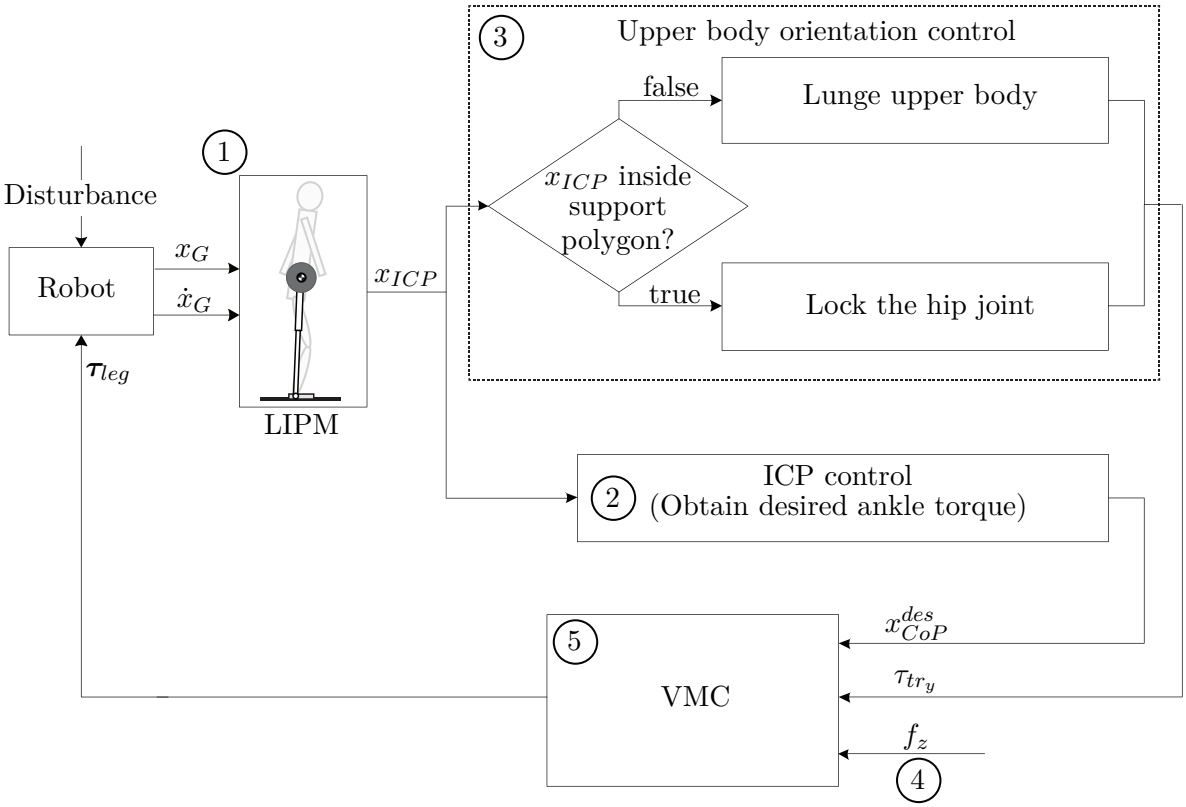

Figure 6-2: A general overview on the hip-ankle strategy balancing control scheme. (1) The position x_G and velocity $\dot{x}_G$ of the CoM of the robot are used to calculate the ICP x_{ICP} by means of the LIPM. (2) The ICP position is controlled by the ICP controller which determines where the CoP should be placed in order to push the ICP to its desired position and maintain balance. (3) Depending on the location of the ICP the upper body orientation control module switches between two modes of operation. When the ICP is inside the support polygon a stiff link between the upper body and the legs is created. For an ICP outside of the support polygon a virtual torque is applied on the trunk which creates the lunging motion of the robot. (4) The constant virtual force f_x is applied as a separate input and compensates for the gravity acting on the robot. (5) All required elements are then known to calculate the joint torques that can be sent to the robot. These joint torques are calculated by means of VMC. The ankle strategy control is the same as the hip-ankle strategy control but differs in the upper body orientation control; it always locks the hip joint.

6-2-1 Instantaneous Capture Point calculation

The first phase of the balance controller is calculation of the ICP. The location of this point determines how close the robot is to a fall and can therefore be controlled to a desired location. The CoM position x_G and velocity $\dot{x}_G$ are calculated by means of the kinematic relations of the robot. The CoM position is then projected on the horizontal ground surface by using orientation information gathered by the Inertial Measurement Unit (IMU). The ICP, x_{ICP}, is then calculated as described in section 3-2-3,

$$x_{ICP} = x_G + \frac{\dot{x}_G}{\omega_0} \tag{6-3}$$

which serves as an input for the ICP controller of next section.

6-2-2 Instantaneous Capture Point control

The core of the balance control algorithm is based on control of the ICP location. This control is carried out in parallel with the upper body orientation control which is introduced in section 6-2-3. This module tries to maintain the ICP inside the support polygon by modulating the CoP of the robot in such a way that the ICP is forced to a desired position. A desired CoP location x_{CoP}^{des} is derived based on the ICP location x_{ICP} and the desired ICP location x_{ICP}^{des}. As the CoP will push the ICP away, the CoP should be placed such that it pushes the ICP location to the desired ICP location. The desired location of the CoP is therefore obtained by the following control law,

$$x_{CoP}^{des} = x_{ICP} - K_{p,ICP}(x_{ICP}^{des} - x_{ICP}) \tag{6-4}$$

where $K_{p,ICP}$ is the proportional gain [8]. The desired ICP, is defined at the centroid of the support polygon as this entails maximum robustness against unknown disturbances in all directions. As illustrated by figure 6-3, equation (6-4) places the desired CoP in line with the ICP and desired ICP and on the opposite side of the ICP. This will push the ICP in the direction of the desired ICP and thereby maintain balance for the robot. The CoP cannot leave the support polygon by definition, if the desired CoP in equation (6-4) lies outside the foot it is projected to the edge of the support polygon.

The presented ICP controller only has a proportional gain but can be considered as a PD-controller as the ICP consist of both CoM position and velocity. The gain for this controller is set the same for both strategies, this ensures that one strategy will not have an advantage over the other in the application of ankle torque.

The virtual horizontal force f_x required to place the CoP at the desired location can be calculated, this is presented in section 6-2-5. From this horizontal virtual force the ankle torque can be calculated which controls the ICP to its desired location.

6-2-3 Upper body orientation control

The upper body orientation control regulates the pitch angle of the trunk by applying a virtual torque τ_{tr_y}. This control module is applied in parallel with the ICP control. It

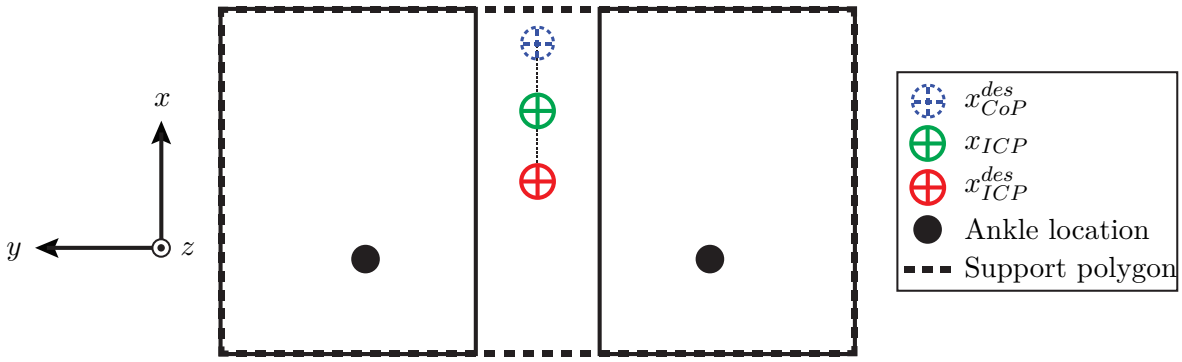

Figure 6-3: Top view of the two feet of the robot with its front facing in positive x-direction. The goal is to control the ICP x_{ICP} to its desired position x_{ICP}^{des} by modulating the desired CoP x_{CoP}^{des}. The desired CoP is therefore placed in line with the desired ICP and the ICP. The ICP should thereby lie between the CoP and the desired CoP. In this way, as the ICP is pushed away from the desired CoP, it pushes the ICP to its desired location.

switches between two modes of operation, depending on the location of the ICP. If the ICP is inside the support polygon it "locks" the hip joint at a desired angle of zero with a PD-controller. In case of large disturbances, the ICP moves out of the support polygon and a virtual torque on the upper body is applied which creates an acceleration of the upper body in the direction of the disturbance; the lunging motion. Both operation modes will be discussed below.

Locking the hip joint

This module has the objective of maintaining a desired pitch angle of the trunk relative to the legs. This creates a stiff joint between the upper body and the leg and also prevents any undesired dynamics introduced by rotation of the upper body relative to the legs. This objective is implemented by a PD-controller,

$$\tau_{tr_y} = K_{p_a}(\varphi_h^{des} - \varphi_h) + K_{d_a}(\dot{\varphi}_h^{des} - \dot{\varphi}_h) \tag{6-5}$$

where K_{p_a} is the proportional gain, K_{d_a} is the derivative gain, φ_h^{des} is the desired angle of the trunk relative to the legs (which is zero) and φ_h is the angle of the trunk relative to the legs.

Lunging upper body

In case of a larger disturbance, the ICP leaves the support polygon. As explained in section 6-2-2, the ICP controller then places the desired CoP on the edge of the support polygon and maximal ankle torque is thus applied. This ankle torque is not sufficient to bring back the ICP to its desired position. Therefore the upper body orientation controller switches to this control module. Additional to the applied ankle torque by the ICP controller a large torque is now applied on the upper body which creates rotational acceleration in the direction of

the ICP. This torque results in a lunging motion and pushes back the ICP into the support polygon. The further the ICP outside of the support polygon, the larger the required torque on the upper body. This behaviour is obtained by a P-controller on the distance of the ICP relative to its desired location,

$$\tau_{tr_y} = K_{p_h}(x_{ICP}^{des} - x_{ICP}) \tag{6-6}$$

where K_{p_h} is the proportional gain of the lunging controller, τ_{tr_y} is the applied torque on the upper body, x_{ICP} is the ICP and x_{ICP}^{des} is the desired location of the ICP.

If the ICP leaves the support polygon at the front, a large forward virtual torque is applied on the trunk in order to push the ICP back. The difference between the desired ICP and measured ICP then decreases and the virtual torque applied on the trunk therefore also decreases. A threshold is set which determines if the ICP is far enough inside the support polygon, if this threshold is reached the controller switches back to the ankle strategy. This threshold is required to prevent the controller from getting stuck at the edge of the support polygon where it would be continuously alternating between the two modes of operation.

The virtual force f_z compensates for the gravity acting on the robot. It decelerates rotation of the upper body in case the lunge is applied and it brings it to a stop. A linear transition is then made back to the controller which locks the hip joint. This brings the trunk back to an upright position.

6-2-4 Gravity compensation

The virtual vertical force f_z is always applied to compensate for the gravity acting on the CoM of the robot. This force is set equal to the mass of the robot times the gravitational constant,

$$f_z = mg \tag{6-7}$$

with m the total mass of the robot. When a lunge is applied it has the useful effect that it decelerates the upper body rotation. This virtual force has a larger arm to the hip joint for rotation of the upper body and therefore has a larger moment. This compensates the torque applied on the hip joint and stops the rotation at a certain angle.

The virtual torque τ_{tr_y} together with the virtual force in x-direction f_x and z-direction f_z on the upper body determine the total behaviour of the robot and are used to calculate the joint torques. These virtual forces are depicted in figure 6-1. Next section introduces the virtual force f_x.

6-2-5 Joint torque calculation

We now know the desired CoP, the virtual vertical force f_z and the virtual torque τ_{tr_y} on the upper body. A virtual horizontal force f_x can now be calculated such that it meets the requirements of these components and places the CoP at the desired location. All components for the VMC algorithm are then known in order to calculate the joint torques.

The calculation of the virtual force f_x given the desired CoP, the virtual vertical force and the torque is performed by the application of Virtual Toe Points (VTPs) [29]. These VTPs

represent the point on the foot about which no torque is applied in the horizontal plane, see figure 6-4. The VTP is not an existing joint on the physical robot but provides a way to calculate f_x. In our case the VTP is placed at the position of the desired CoP, the rotation of its angle φ_{vtp} is set to zero and the location changes in time with the desired CoP [8]. To calculate the virtual force f_x the relation between the virtual forces applied on the trunk in frame $\{B\}$ and the joints between frame $\{A\}$ and $\{B\}$ is required. This relation is given by the Jacobian between frame $\{A\}$ and $\{B\}$. This Jacobian is calculated by the forward kinematics between the two frames,

$$ {}^{A}_{B}\boldsymbol{X} = \begin{bmatrix} x \\ z \\ \varphi \end{bmatrix} = \begin{bmatrix} -l_{vtp}\cos\varphi_{vtp} - l_1\sin(\varphi_{vtp}+\varphi_a) - l_2\sin(\varphi_{vtp}+\varphi_a+\varphi_h) \\ -l_{vtp}\sin\varphi_{vtp} + l_1\cos(\varphi_{vtp}+\varphi_a) + l_2\cos(\varphi_{vtp}+\varphi_a+\varphi_h) \\ \varphi_{vtp}+\varphi_a+\varphi_h \end{bmatrix} \tag{6-8} $$

where x, z and φ are the location and orientation of frame $\{B\}$ with respect to frame $\{A\}$. The location of the VTP with respect to the ankle joint is indicated by l_{vtp}, l_1 is the combined length of the legs and l_2 is the length between the hip joint and frame $\{B\}$. The ankle angle is indicated by φ_a and the hip angle by φ_h. The Jacobian ${}^{A}_{B}\boldsymbol{J}$ can then be obtained by partial differentiation of (6-8) with respect to the joint angles $\vec{\varphi} = [\varphi_{vtp}\ \varphi_a\ \varphi_h]^T$,

$$ {}^{A}_{B}\boldsymbol{J} = \begin{bmatrix} J_{1,1} & J_{1,2} & J_{1,3} \\ J_{2,1} & J_{2,2} & J_{2,3} \\ 1 & 1 & 1 \end{bmatrix} \tag{6-9} $$

with

$$ \begin{aligned} J_{1,1} &= l_{vtp}\sin\varphi_{vtp} - l_1\cos(\varphi_{vtp}+\varphi_a) - l_2\cos(\varphi_{vtp}+\varphi_a+\varphi_h) \\ J_{1,2} &= -l_1\cos(\varphi_{vtp}+\varphi_a) - l_2\cos(\varphi_{vtp}+\varphi_a+\varphi_h) \\ J_{1,3} &= -l_2\cos(\varphi_{vtp}+\varphi_a+\varphi_h) \\ J_{2,1} &= -l_{vtp}\cos\varphi_{vtp} - l_1\sin(\varphi_{vtp}+\varphi_a) - l_2\sin(\varphi_{vtp}+\varphi_a+\varphi_h) \\ J_{2,2} &= -l_1\sin(\varphi_{vtp}+\varphi_a) - l_2\sin(\varphi_{vtp}+\varphi_a+\varphi_h) \\ J_{2,3} &= -l_2\sin(\varphi_{vtp}+\varphi_a+\varphi_h) \end{aligned} $$

where the VTP is placed at the desired CoP, $l_{vtp} = x^{des}_{CoP}$.

As introduced in section 6-1, the relation between the virtual forces and the joint torques is given by the Jacobian,

$$ \boldsymbol{\tau} = {}^{A}_{B}\boldsymbol{J}^T\boldsymbol{W} \tag{6-10} $$

where $\boldsymbol{\tau} = [\tau_{vtp}\ \tau_a\ \tau_h]^T$ the joint torques and $\boldsymbol{W} = [f_x\ f_z\ \tau_{tr_y}]^T$ the wrench including the virtual forces applied to the trunk (figure 6-1). The VTP is the point about which no torque is applied which gives $\tau_{vtp} = 0$. Substituting all components in (6-10) gives,

$$ \begin{bmatrix} 0 \\ \tau_a \\ \tau_h \end{bmatrix} = \begin{bmatrix} J_{1,1} & J_{2,1} & 1 \\ J_{1,2} & J_{2,2} & 1 \\ J_{1,3} & J_{2,3} & 1 \end{bmatrix} \begin{bmatrix} f_x \\ f_z \\ \tau_{tr_y} \end{bmatrix} \tag{6-11} $$

The upper row of equation (6-11) can be used to calculate the virtual horizontal force which places the CoP at the desired location, given the virtual vertical force and the virtual torque.

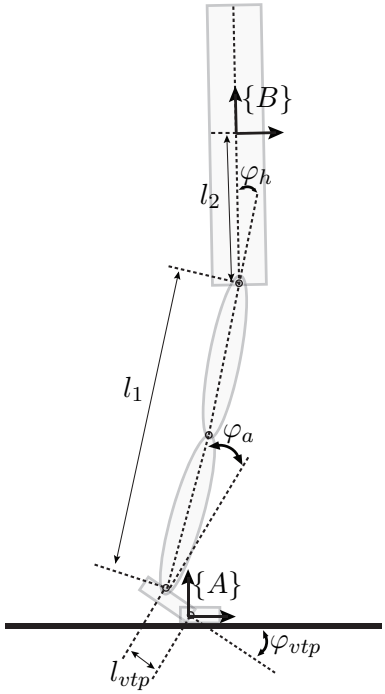

Figure 6-4: Implementation of VTPs on humanoid robot TUlip. The VTP is placed at the position of the desired CoP. The kinematic relations between the VTP (frame $\{A\}$) and the upper body (frame $\{B\}$) can be obtained in terms of the VTP angle φ_{vtp}, the ankle angle φ_a, the hip angle φ_h and length l_{vtp}, l_1, l_2. These kinematic relations provide a simple way to compute the virtual force f_x required to have zero torque at the position of the VTP and thus place the CoP at that location. Note that the virtual toe joint does not exist on the physical robot.

The virtual horizontal force is given by,

$$f_x = -\begin{bmatrix} \frac{J_{2,1}}{J_{1,1}} & \frac{1}{J_{1,1}} \end{bmatrix} \begin{bmatrix} f_z \\ \tau_{tr_y} \end{bmatrix} \tag{6-12}$$

Which calculates the horizontal force f_x given the vertical force f_z and the torque τ_{tr_y}. The virtual force f_x can be substituted back into (6-11) where the two bottom rows can be used to obtain the ankle torque τ_a and hip torque τ_h,

$$\boldsymbol{\tau}_{leg} = \begin{bmatrix} \tau_a \\ \tau_h \end{bmatrix} = \begin{bmatrix} J_{1,2} & J_{2,2} & 1 \\ J_{1,3} & J_{2,3} & 1 \end{bmatrix} \begin{bmatrix} f_x \\ f_z \\ \tau_{tr_y} \end{bmatrix} \tag{6-13}$$

6-2-6 Control scheme summary

The hip-ankle strategy control scheme including all the control components is summarised in figure 6-5. Note that for the ankle strategy the same control is applied but the hip joint is locked at all times.

6-3 Discussion

One could argue that the same behaviour could be obtained by using local PD-controllers on the ankle and hip joints and applying a large torque on the hip joint in case the ICP leaves the support polygon. However, the approach presented in this chapter is used because

- Accelerating and decelerating the upper body with the required torque, without exceeding the maximal hip joint angle, is a delicate process. Especially when disturbances of varying size are applied. With VMC the virtual components can be applied in an intuitive manner because it is not required to consider the robot in joint space. The effect of applying general virtual forces on one point of robot can easily be interpreted because they will have the same effect as if real forces would be applied.

- VMC is a simple method in the sense that a total robot can be controlled with relatively little components and therefore little parameters that have to be tuned.

- The control algorithm introduced in this section is more a more general and versatile approach. A humanoid robot is not a planar double inverted pendulum but has two legs that can be placed in many positions. Equation (6-9) can easily be adapted for the 3D case. Each leg will have his own Jacobian and the VTPs are then useful in order to distribute the joint torques over the two legs and also maintain balance in sideward direction [8, 29]. When the feet are positioned in another configuration, the support polygon will change in size and shape. Nevertheless, all methods introduced in this chapter can then still work. The implementation of the hip-ankle strategy in this way also allows to easily combine this strategy with other behaviour such as walking.

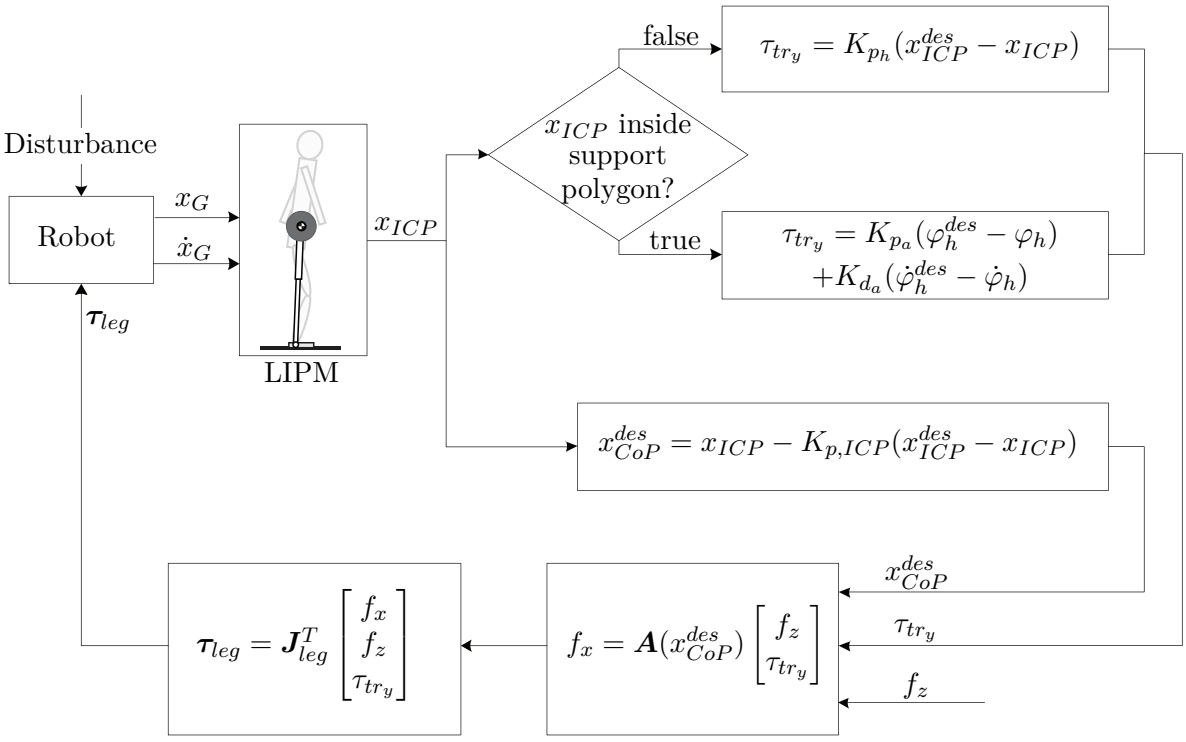

Figure 6-5: Hip-ankle strategy balancing control scheme. The position x_G and velocity $\dot{x}_G$ of the CoM of the robot are used to calculate the ICP x_{ICP} by means of the LIPM. The ICP position is controlled to its desired position x_{ICP}^{des} by modulating the desired CoP x_{CoP}^{des}. A constant virtual upward force f_z regulates the height of the CoM. In case the ICP is inside the support polygon, a virtual torque τ_{tr_y} locks the hip joint at an angle of zero using PD-control. In case the ICP is outside of the support polygon, the virtual torque τ_{tr_y} suddenly increases in the direction of the ICP. This large torque creates the lunging behaviour of the robot and pushes back the ICP inside the support polygon. The required horizontal virtual force f_x required to maintain balance is then calculated from the desired CoP x_{CoP}^{des}, the virtual torque on the trunk τ_{tr_y} and the virtual force f_z. Are required components are then available to calculate the joint torques τ_{leg} by means of VMC.

6-4 Conclusion

The hip-ankle strategy control algorithm introduced in this chapter uses VMC to apply virtual forces on the trunk in order to maintain balance. At all times, the ICP is controlled to its desired position through the desired CoP, which is a commanded quantity. If the CoP is sufficient to keep the ICP within the support polygon the control algorithm will create a stiff hip joint. In case the ICP leaves the support polygon, the hip-ankle strategy applies a virtual torque on the upper body in the direction of the ICP. This torque pushes the ICP back into the support polygon.

The next chapter will investigate if it is physically possible for the robot to maintain balance using the introduced hip-ankle strategy controller.

Chapter 7

Hip-ankle strategy simulation

In chapter 5 simple models confirmed that using the hip-ankle strategy a 33.6% larger disturbance can be withstand than solely using the ankle strategy. Chapter 6 introduced the control algorithm which can be used to apply this hip-ankle strategy on the real robot. Before this algorithm is implemented on the humanoid robot TUlip it is of crucial importance to examine whether it is physically possible for the robot to maintain balance using this algorithm. Key factors in the functioning of the algorithm on the robot are motor saturation and range of motion of the hip-ankle joint. As large accelerations are needed for the algorithm, the electric motors of the robot should be able to deliver the required torque. The hip-ankle strategy also requires a large rotation of the hip joint, if this rotation exceeds the range of motion of the robot it can possibly result in large damage of the robot.

The hip-ankle strategy algorithm will therefore first be implemented in Matlab on a Double Inverted Pendulum Model (DIPM) with mass distribution, dimensions and torque limits based on the humanoid robot TUlip. A disturbance will be be applied which brings the ICP outside the support polygon and thus enforces the model to use the hip-ankle strategy to prevent a fall. Given the configuration and constraints of the robot the model can then be used to *evaluate if the humanoid robot TUlip will be able to maintain balance using the hip-ankle strategy and result in better balance maintenance performance.*

7-1 The double pendulum as a model for the robot

In the balance algorithms on the physical humanoid the knees of will be locked by applying a large torque. This allows to model the robot as a DIPM as shown in figure 7-1. The model consist of two rods with uniformly distributed mass m_1 and m_2. The lower rod has length l_1 which is equal to the upper and lower leg as shown in figure 6-4 and a CoM position at (x_1, z_1). The upper rod has length l_2 with a CoM position at (x_2, z_2) and models the trunk of the robot. The mass of each limb, the inertia around the CoM of each limb and dimensions of the limbs are based on that of the physical humanoid and shown in table 7-1.

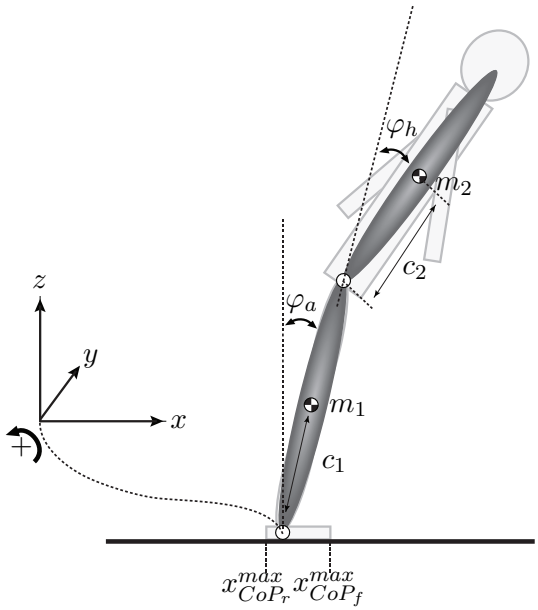

Figure 7-1: The Double Inverted Pendulum Model (DIPM) as a model for the humanoid robot TUlip. Two rods with uniformly distributed mass (m_1 and m_2) and length l_1 and l_2 are connected through the hip joint with angle φ_h. Ankle rotation is indicated by φ_a, the ankle joint is connected to the ground and simulates the contact of the foot with the ground. The ankle joint torque is limited to keep the CoP under the foot and prevent the foot from rotating, $x^{max}_{CoP_r} < X_{CoP} < x^{max}_{CoP_f}$. The hip joint torque is limited to the maximal torque .

Table 7-1: Model parameters for the Double Inverted Pendulum Model.

Body	Length l_i [m]	Mass m_i [kg]	CoM offset c_i [m]	Inertia I_{yy} $[kgm^2]$
1	0.595	6.48	0.298	0.10186
2	0.499	11.46	0.250	0.20518

The DIPM is only valid in case no foot rotation occurs, this means the CoP should remain within the area underneath the foot. The ankle torque is therefore limited as follows,

$$x_{CoP_r}^{max} < x_{CoP} < x_{CoP_f}^{max} \tag{7-1}$$

with x_{CoP} the CoP position, $x_{CoP_f}^{max}$ the maximum CoP position at the front of the foot and $x_{CoP_r}^{max}$ the maximum CoP position at the rear of the foot. This results in the maximal ankle torques,

$$\tau_a^{max,+} = x_{CoP_f}^{max} F_{GRF_z} \tag{7-2a}$$

$$\tau_a^{max,-} = x_{CoP_r}^{max} F_{GRF_z} \tag{7-2b}$$

In equation (7-2) the maximum allowable ankle torque in positive direction is given by $\tau_a^{max,+}$ and the maximum allowable ankle torque in negative direction is given by $\tau_a^{max,-}$. The ground reaction force in z-direction is given by $F_{GRF_z} = mg$.

In order to simulate saturation of the electric motors on the robot the joint torques are clipped. The maximum joint torques are set to 24 Nm for both the ankle torque and the hip torque given by the specifications of the robot.

7-1-1 Equations of motion

The equations of motion for the double pendulum can be obtained using the Lagrange equations with the generalised coordinates $\boldsymbol{q} = (\varphi_a \ \varphi_h)^T$. With φ_a the ankle joint angle and φ_h the hip joint angle. The kinematic relations of the double pendulum can be expressed in terms of the generalised coordinates,

$$x_1 = -\frac{1}{2} l_1 \sin\varphi_a \tag{7-3a}$$

$$z_1 = \frac{1}{2} l_1 \cos\varphi_a \tag{7-3b}$$

$$x_2 = -l_1 \sin\varphi_a - \frac{1}{2} l_2 \sin(\varphi_a + \varphi_h) \tag{7-3c}$$

$$z_2 = l_1 \cos\varphi_a + \frac{1}{2} l_2 \cos(\varphi_a + \varphi_h) \tag{7-3d}$$

The equations of motion can now be obtained by using the Euler-Lagrange equation,

$$\frac{d}{dt}\left(\frac{\partial \mathcal{T}}{\partial \dot{q}_j}\right) - \frac{\partial \mathcal{T}}{\partial q_j} + \frac{\partial \mathcal{V}}{\partial q_j} = Q_j \qquad j = 1, 2 \tag{7-4}$$

with $\mathcal{T}$ the total kinetic energy of the system, $\mathcal{V}$ the total potential energy, Q_j the external applied forces on the system and j the degree of freedom. Dynamics introduced by viscous and Coulomb friction are neglected in this simulation. The kinetic energy is required by (7-4) and is given by

$$\mathcal{T} = \frac{1}{2}\left[m_1(\dot{x}_1^2 + \dot{z}_1^2) + m_2(\dot{x}_2^2 + \dot{z}_2^2) + I_1\dot{\varphi}_a^2 + I_2(\dot{\varphi}_a + \dot{\varphi}_h)^2\right] \tag{7-5}$$

where $\dot{x}_1$, $\dot{x}_2$, $\dot{z}_1$, and $\dot{z}_2$ can be found by differentiating equation (7-3). The potential energy is obtained by

$$\mathcal{V} = m_1 g z_1 + m_2 g z_2 \tag{7-6}$$

Substituting the kinetic and potential energy in equation (7-4) gives the equations of motion for the DIPM,

$$\ddot{\boldsymbol{q}} = \boldsymbol{M}^{-1}\left(\boldsymbol{Q} - \boldsymbol{C}(\boldsymbol{q}, \dot{\boldsymbol{q}}) - \boldsymbol{F}_g(\boldsymbol{q})\right) \tag{7-7}$$

with $\boldsymbol{M}$ the mass matrix, $\boldsymbol{C}$ the vector of Coriolis and centrifugal terms and $\boldsymbol{F}_g$ the vector with gravitational forces. Full derivation of the equations of motion can be found in appendix B. The acceleration terms obtained in equation (7-7) are numerically integrated by means of a 4^{th} order Runge-Kutta integration in Matlab in order to obtain the corresponding joint velocities and positions.

The hip-ankle strategy control control algorithm of chapter 6 is implemented in the simulation to control the joint torques as shown in figure 7-2. The joint torques are substitute in equation (7-7) by $\boldsymbol{Q} = [\tau_a \ \tau_h]^T$. The disturances should also be simulated and is the topic of next section.

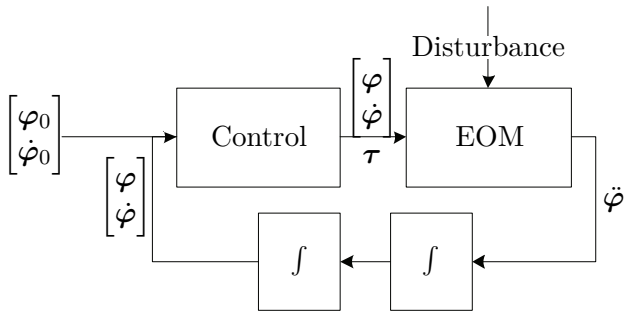

Figure 7-2: Overview of the hip-ankle strategy simulation. Initial angles and angular velocities are set. The control algorithm calculates the required ankle and hip torques to maintain balance. These joint torques together with the joint angles, angular velocities and disturbance force are used to calculate the joint accelerations by the equations of motion. The joint accelerations are then numerically integrated by means of a 4^{th} order Runge-Kutta integration.

Table 7-2: Simulation parameters for the Double Inverted Pendulum Model.

Model parameter	Symbol	Value
Upper body stiffness gain	K_{p_a}	40
Upper body damping gain	K_{d_a}	10
Desired hip angle	φ_h^{des}	0
Desired hip angular velocity	$\dot{\varphi}_h^{des}$	0
Lunging gain	K_{p_h}	150
ICP control gain	$K_{p,ICP}$	3
Desired ICP	x_{ICP}^{des}	0.045 [m]
Start lunging threshold		0.138 [m]
Stop lunging threshold		0.100 [m]

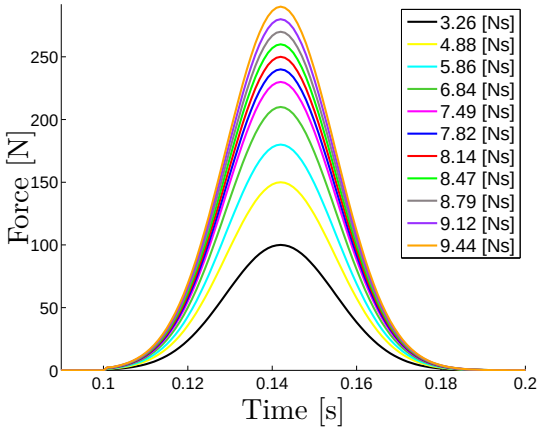

Figure 7-3: Disturbances applied in this simulation. The disturbances are applied to the CoM of the upper pendulum. The disturbance are generated by a Gaussian function and have the same time span and shape but vary in peak force. The applied impulse is calculated by the integral of the applied force over time and used as a measure for the disturbance.

7-2 Disturbance

Horizontal impulses are applied to the CoM of the upper pendulum. As explained in chapter 4 the applied disturbances should have the same time span and shape but higher magnitude in order to come up with a fair comparison. A Gaussian function is used to simulate physical pushes applied to the robot. Figure 7-3 shows the eleven disturbances that are applied in this simulation. The impulse is then calculated by integrating the disturbance force curve.

7-3 Results

In order to evaluate the hip-ankle strategy controller, simulations are run for increasing disturbances. The largest disturbance for which the controller is able to recover is the largest allowable disturbance. The hip-ankle strategy controller is compared with the ankle strategy controller with the algorithms as presented in chapter 6. Both controllers use the same gains for the desired Centre of Pressure (CoP) controller but differ in their upper body torque controller. The simulation parameters that were used are given in table 7-2.

7-3-1 Largest allowable disturbance

The resulting motion of the DIPM with hip-ankle strategy controller subjected to the largest allowable disturbance (9.12 Ns) is shown in figure 7-4. From this figure a forward lunging motion can clearly be observed. At $t = 2.0s$ the ICP has approximately returned to its desired location, the response in figure 7-4 is therefore a successful push recovery.

Figure 7-5 shows the response of the ICP (x_{ICP}), the CoM (x_{CoM}), the COP (x_{CoP}) and the desired CoP (x_{CoP}^{des}) position relative to the ankle position for both strategies in case of the the largest allowable disturbances. The desired ICP position is positioned in the middle of

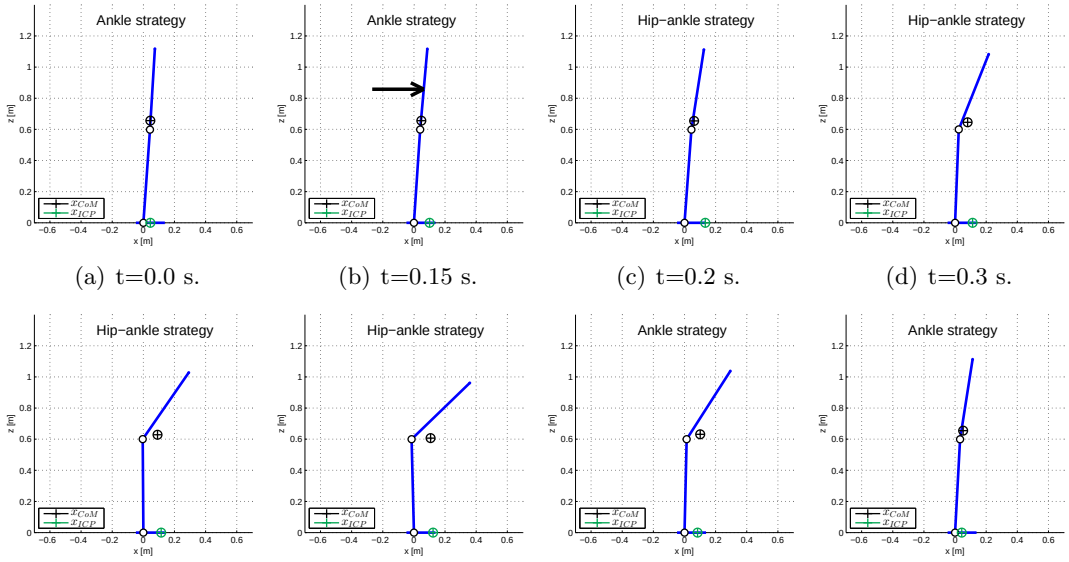

(a) t=0.0 s. (b) t=0.15 s. (c) t=0.2 s. (d) t=0.3 s.

(e) t=0.4 s. (f) t=0.6 s. (g) t=1.4 s. (h) t=2.0 s.

Figure 7-4: Humanoid robot TUlip recovering from a large horizontal disturbance of 9.12 Ns using the hip-ankle strategy. The disturbance profile starts at $t = 0.1$ s. The hip-ankle strategy is engaged when the ICP leaves the support polygon (in this case the area under the feet). The strategy results in a large rotation of the hip joint. When the ICP is well inside the feet the controller switches to the ankle strategy and the posture is recovered.

the foot, $x_{ICP}^{des} = 0.045$ m. In case of the hip-ankle strategy, when the ICP leaves the support polygon it is quickly pushed back by a large torque on the trunk. It does therefore not cross the edge by a large value. It is also clear that the CoP is constrained as the CoP does not cross the foot edge line. Figure 7-6 shows the CoM position x_{CoM} and velocity $\dot{x}_{CoM}$. A large increase in CoM velocity can be observed which is caused by the disturbance.

The joint torques for the largest allowable disturbance for both strategies are shown in figure 7-7. The CoP constraint has implications on the ankle torque, it can be observed that it is clipped. The hip torque profiles are interesting in the comparison between the ankle and the hip-ankle strategy. For the ankle strategy the disturbance force is counteracted by a torque on the hip which works in opposite direction of the disturbance. The hip-ankle strategy controller first applies the same strategy but as soon as the ICP leaves the support polygon the hip joint is released which creates an acceleration of the upper body in the direction of the force. This behaviour is caused by the virtual torque τ_{tr_y} that is applied on the system. The torque profile of this virtual force for both strategies is depicted in figure 7-8. In case of the ankle strategy the disturbance force is counteracted by the virtual force on the trunk. For the hip-ankle strategy, when the ICP leaves the support polygon a large virtual torque is applied on the trunk which causes the acceleration of the upper body. The system moves to a new equilibrium where the virtual force in z-direction, f_x, decelerates the upper body. The application of the virtual torque on the trunk in case of the hip-ankle strategy creates a forward angular acceleration of the trunk, this is shown in figure 7-9.

The ankle and hip joint angles, φ_a and φ_h, are presented in figure 7-10. From this figure

a large rotation of the upper body can be observed in case of the hip-ankle strategy. This rotation does not violate the maximum allowable angle constraint of 1.05 rad.

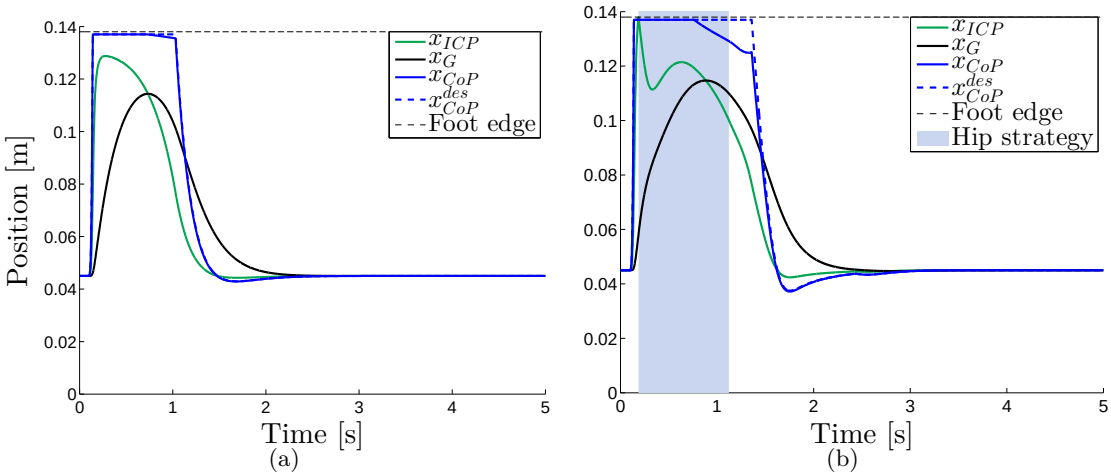

Figure 7-5: Response of the ICP x_{ICP}, the CoM x_{CoM}, the COP x_{CoP} and the desired CoP x_{CoP}^{des} position relative to the ankle position in x-direction over time. Figure (a) gives the response for the maximum allowable disturbance (7.82 Ns) in case of the ankle strategy. Figure (b) shows the response for the largest allowable disturbance in case of the hip-ankle strategy (9.12 Ns). The ICP quickly reaches the edge of the support polygon for both strategies. In case of the hip-ankle strategy the ICP is pushed back by a lunging motion when the ICP crosses the support polygon edge.

7-3-2 Comparison

Figure 7-11 shows the phase portraits for both strategies for increasing impulse. The figure shows that the largest allowable disturbance for the ankle strategy is 7.82 Ns where the hip-ankle strategy was able to maintain balance for a disturbance of 9.12 Ns, an improvement of 16.6%. The edge of the support polygon is indicated by the black dashed lines in these phase planes. The ankle strategy is not sufficient to maintain balance when that edge is reached while the hip-ankle strategy can still maintain balance. The hip-ankle strategy successfully counteracts the impulsive disturbance and pushes the ICP back into the ankle strategy region.

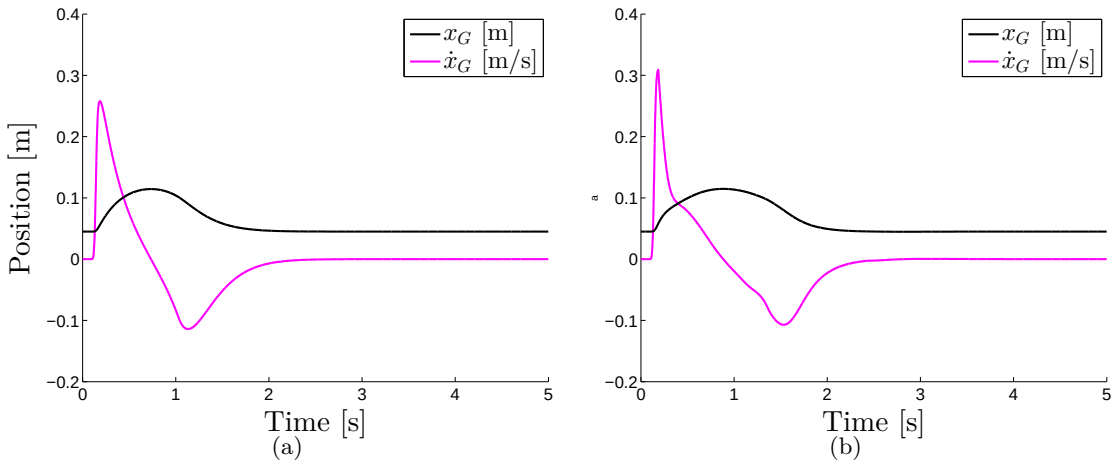

Figure 7-6: CoM position x_{CoM} and velocity $\dot{x}_{CoM}$ for the ankle strategy (a) and the hip-ankle strategy (b). A large increase of CoM velocity is caused by the impulsive disturbance.

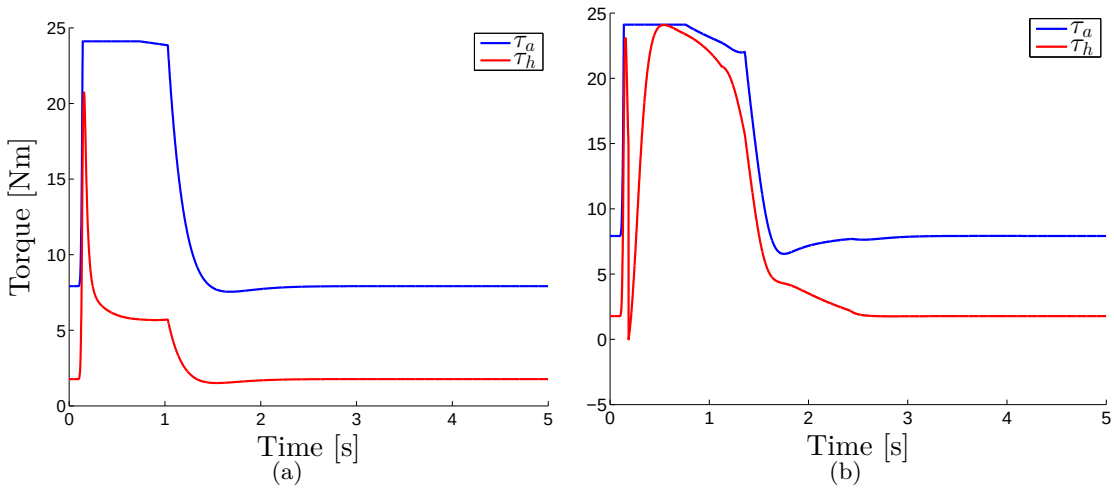

Figure 7-7: Ankle τ_a and hip torque τ_h for the ankle strategy (a) with a disturbance of 7.82 Ns and the hip-ankle strategy (b) with a disturbance of 9.12 Ns. The torques are clipped at certain periods due to the CoP constraints or the motor saturation constraint. A large drop in hip torque can be observed when the hip-ankle strategy is engaged, this creates the forward lunge of the upper body.

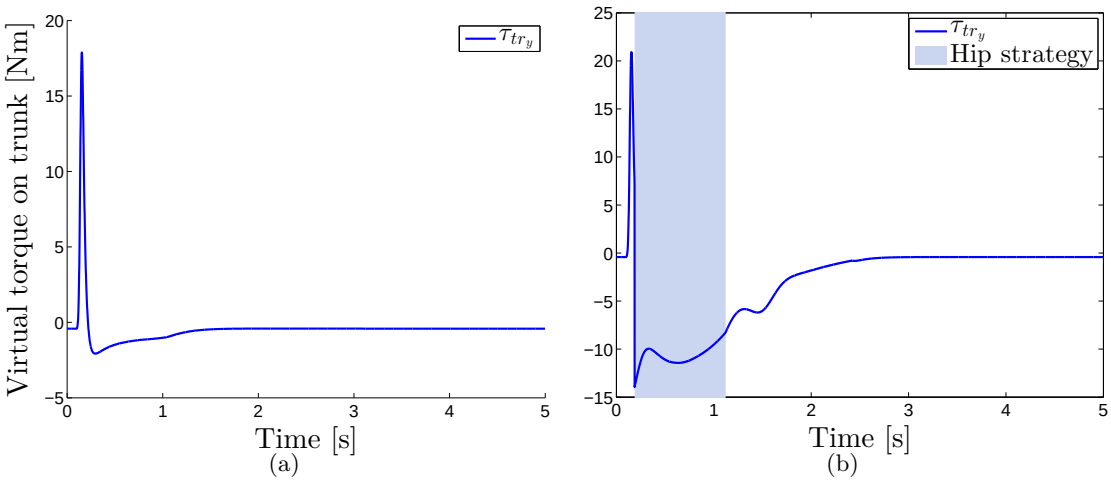

Figure 7-8: Virtual torque applied on the trunk τtr_y for the ankle strategy (a) and the hip-ankle strategy (b). In the ICP leaves the support polygon a large forward virtual torque is applied which is shown in (b) where the virtual torque changes from negative to positive.

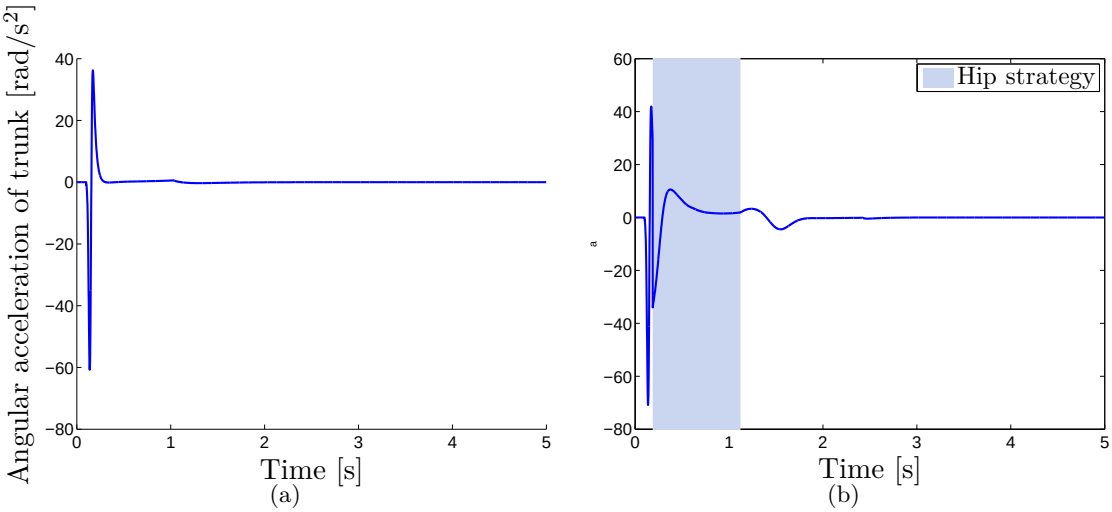

Figure 7-9: Angular acceleration of the trunk in global coordinates for the ankle strategy (a) and the hip-ankle strategy (b). In case of the hip-ankle strategy a forward acceleration of the trunk is observed, this pushes the ICP back into the support polygon.

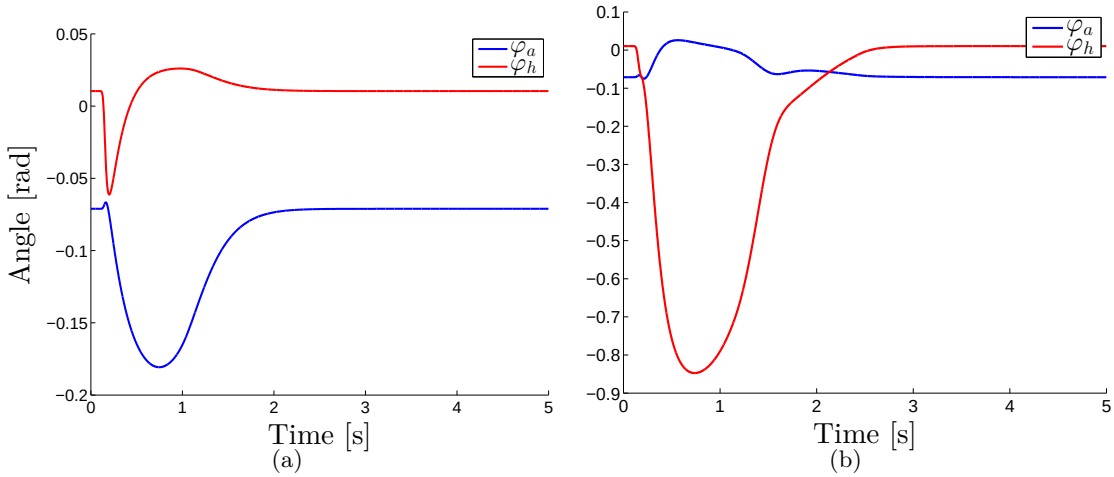

Figure 7-10: Ankle joint angle φ_a and hip joint angle φ_h for the ankle strategy (a) with a disturbance of 7.82 Ns and the hip-ankle strategy (b) with a disturbance of 9.12 Ns. For the hip-ankle strategy, the hip joint angle does not exceed the maximum allowable angle of 1.05 rad.

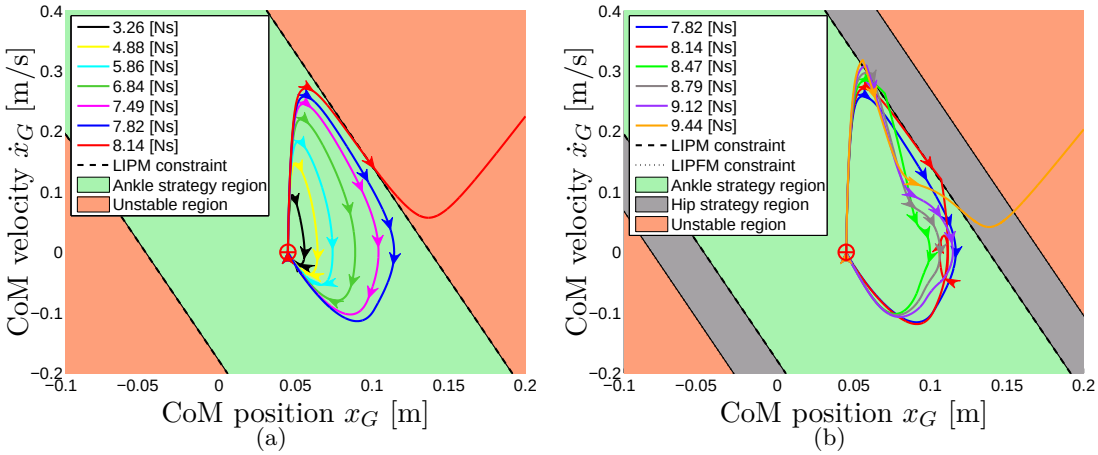

Figure 7-11: Simulation results in phase plane for the ankle strategy (a) and the hip-ankle strategy (b). When the ankle strategy reaches the edge of the support polygon (dashed black line, LIPM constraint) it is not able to maintain balance. In case of the hip-ankle strategy, the edge of the support polygon is crossed and a fall is still prevented. The maximum allowable disturbance for the ankle strategy is is 7.82 Ns the hip-ankle strategy can recover from a push of 9.12 Ns.

7-4 Conclusions

From the results presented in this chapter can be concluded that it is theoretically possible to maintain balance using the hip-ankle strategy for a larger maximal allowable disturbance than solely using the ankle strategy on the humanoid robot TUlip. In the simulation the hip-ankle stategy can withstand a largest allowable disturbance of 16.6% larger than the ankle strategy. In case of the hip-ankle strategy, the ICP has crossed the support polygon border but an angular acceleration of the upper body in the direction of the disturbance was able to push the ICP back. The hip-ankle strategy did not exceed the maximum allowable hip joint angles. The hip-ankle strategy can therefore be implemented on the physical humanoid robot TUlip.

The experimental setup used to measure the performance of the hip-ankle strategy controller implemented on TUlip is introduced in the next chapter.

Table 7-3: Maximum allowable impulse [Ns] for ankle and hip-ankle strategy in simulation.

	Ankle strategy [Ns]	Hip-ankle strategy [Ns]	Improvement
Simulation	7.82	9.12	116.6%

Chapter 8

Experimental setup

As explained in chapter 7 the hip-ankle strategy outperforms the ankle strategy in simulation when subjected to impulsive disturbances to the back of the robot. The goal of this chapter is to *describe the experimental setup used to examine the hip-ankle strategy control algorithm implemented on the physical robot.* This chapter starts with an introduction on the hardware used during the experiments. Subsequently the measurement protocol will be discussed followed by a discussion on the signal processing. This chapter will end with a conclusion.

8-1 Hardware

An overview of the hardware used in the experiments is shown in figure 8-1(a). The setup consists of the humanoid robot TUlip, a "disturbance rod" equipped with a load cell and a trigger mechanism with laser.

8-1-1 The robot

The humanoid robot TUlip is the subject which will be disturbed. The hip-ankle strategy control algorithm introduced in chapter 6 is implemented on this robot. The robot is placed in double support with its feet naturally aligned. After every disturbance the feet are placed at predefined locations as shown in figure 8-1(b). In order to prevent damage in case of a fall a rope with negligible weight is used to catch the robot.

8-1-2 The disturbance rod

The actual disturbance applied to the back of the robot is performed by a rod of 2.9 kg which will from now on will be referred to as the disturbance rod. Applying pushes with this disturbance stick by hand is interesting but it is will be very difficult to repeat the same measurement for multiple times. Therefore, to increase the consistency of the measurements,

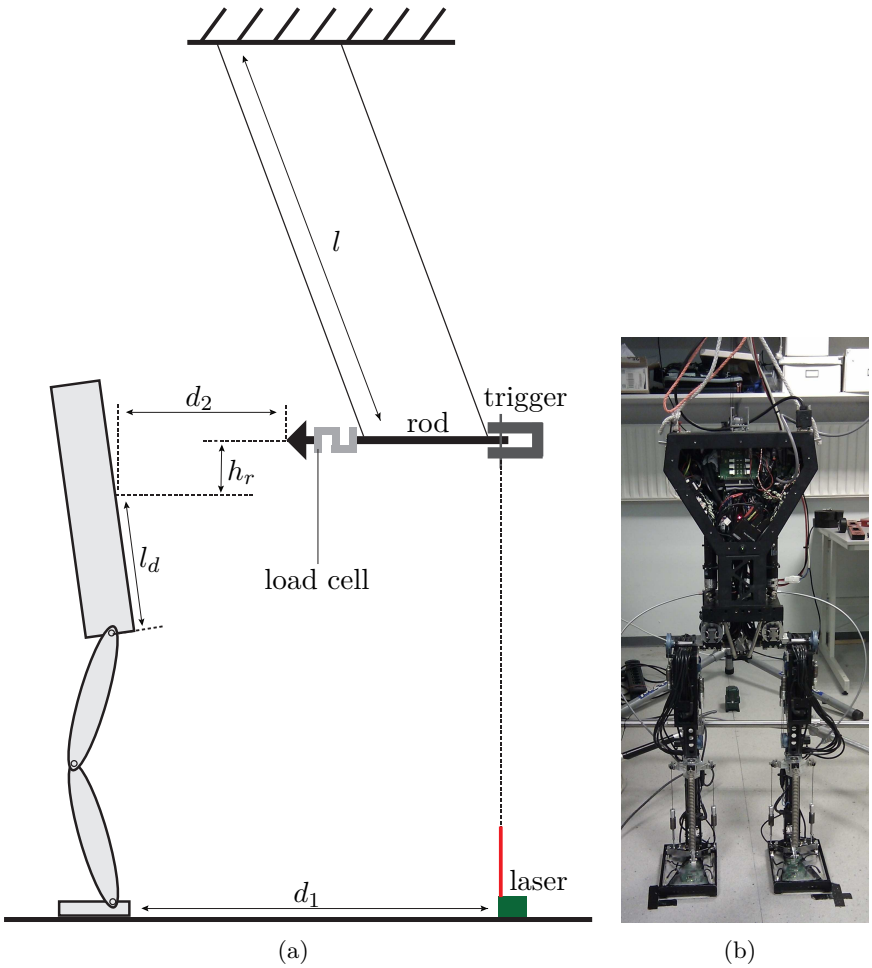

Figure 8-1: Experimental setup for the push recovery experiments. (a) shows a side view of TUlip with its feet placed in position. The disturbance rod is placed in the trigger mechanism, this trigger mechanism is positioned at a distance d_1 and alligned by using a laser. The distance between the front of the disturbance rod and the location of impact at the robot is indicated by d_2 and can be obtained from d_1. The distance d_1 is varied in order to change the potential energy of the disturbance rod and thus the magnitude of the disturbance. In figure (b) a front view of TUlip is given. Before every disturbance the feet are positioned within the predefined locations.

the disturbance rod is hung on two cables in a parallellogram mechanism and a trigger mechanism is used. The trigger mechanism is used for in order to have zero initial velocity and to accurately release the rod at a certain distance. The trigger mechanism can be placed at a specified distance d_1 from the robot. Distance d_2 can then be calculated which is the distance between the front of the disturbance rod when placed in the trigger mechanism and the front of the disturbance rod at impact. Increasing this distance results in a larger disturbance. The distance can accurately be measured by means of a laser that projects a beam on the rod and on the floor where a scale is drawn. The parallellogram mechanism is used to keep the disturbance rod horizontally at all times, cables are used to prevent any friction that will occur when using a bar mechanism. The location of impact of the disturbance rod on TUlip is at a distance $l_d = 0.365$m from the hip joint (see figure 8-1(a)).

Theoretical applied impulse

An estimation can be made on the theoretical impulse applied by the disturbance rod to the robot. This will be of later use to verify the measured impulse. The theoretical applied impulse can be calculated by the potential energy of the disturbance rod which is dependent on its height h_r.

The potential energy in the stick can be calculated as follows

$$\mathcal{V}_r = m_r g h_r \tag{8-1}$$

with m_r the mass of the disturbance rod, g the gravitational constant and h_r the initial height of the disturbance rod. The height of the disturbance rod can be calculated from the geometrical relations of the system,

$$h_r = l - \sqrt{l^2 - d_2^2} \tag{8-2}$$

with l the length of the pendulum cables as depicted in figure 8-1(a). Assuming that no energy is lost in the system between initial position of the disturbance rod and just before impact, the kinetic energy at impact is equal to the initial potential energy. This results in,

$$\mathcal{T}_r = \mathcal{V}_r \tag{8-3a}$$

$$\frac{1}{2} m_r \dot{x}_r^2 = m_r g h_r \tag{8-3b}$$

with $\dot{x}_r$ the horizontal velocity of the disturbance rod just before impact. This horizontal velocity of the rod can therefore be written as,

$$\dot{x}_r = \sqrt{2 g h_r} \tag{8-4}$$

The Momentum-Impulse Theorem states that the change in momentum of an object is equal to the impulse exerted on it,

$$\vec{I}_d = \int_{t_i}^{t_f} \vec{F}_d dt = \Delta \vec{p} = m \Delta \vec{v} \tag{8-5}$$

with $\vec{I}_d$ the applied impulse, $\vec{F}_d$ the disturbance force between initial time t_i and final time t_f during the impulse, $\Delta \vec{p}$ the change in linear momentum due to the impact, $\Delta \vec{v}$ the change

in velocity due to the impact. If we assume that the velocity of the disturbance rod is $\dot{x}_r$ just before impact and zero afterwards the theoretical applied impulse is given by,

$$\vec{I}_d = m_r \dot{x}_r \tag{8-6}$$

The relation between the initial height of the disturbance rod and the theoretical applied

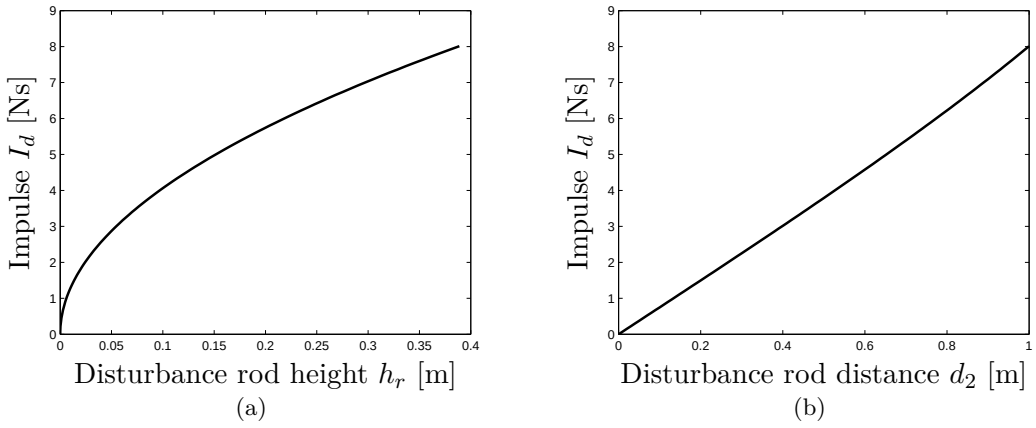

Figure 8-2: Figure (a) shows the relation between the intitial disturbance rod height h_r and the theoretical applied impulse I_d. Figure (b) shows the relation between the initial disturbance rod distance d_2 and the theoretical applied impulse I_d given this distance.

impulse is given in figure 8-2(a). Figure 8-2(b) shows the relation between the distance d_2 of the disturbance rod to the robot and the theoretical applied impulse.

This theoretical applied impulse neglects the coefficient of restitution of the disturbance rod. It assumes that the disturbance rod comes to a complete stop after the impact and all energy of the disturbance rod is transferred to the robot. In reality this is not the case, in order to measure the exact applied impulse the disturbance rod is equipped with a load cell. This also introduces the ability to log the data over time. The load cell is introduced in next section.

Load cell

An analogue S-Beam load cell (SCAIME ZFA 25 kg) was mounted at the end of a rod as shown in figure 8-1(a). The load cell has a capacity of 250 N with an output of $3 \pm 0.5\%$ mV/V and a combined error of $\pm 0.03\%$. The measured signal was fed trough an instrumentation amplifier. The amplified signal was connected to the robot in order to log the variables synchronously with the robot variables in the real time motion control loop.

8-2 Measurement protocol

The goal of the experiments is to obtain the largest allowable disturbance for the ankle strategy and the hip-ankle strategy. Therefore a measurement protocol has been set up which is equal for both strategies. The measurement protocol starts with calibrating the robot, placing both feet on the ground and starting the log. The following steps are then performed:

1. Place the robot in double support and make sure both feet are in the predefined location as shown in figure 8-1(b).
2. Place the trigger mechanism at a specified distance d_1.
3. Pull back the disturbance rod and place it in the disturbance rod.
4. Release the disturbance rod.
5. Wait for the robot to be fully recovered and go back to step 1.

This measurement cycle is repeated for ten times for the same distance d_1. The trigger mechanism is then pulled 0.025 m away from the robot and the same process is repeated. This is repeated until the robot is not able to maintain balance when subjected to the disturbance. Each measurement cycle of ten measurements is called a disturbance set. For the ankle strategy the applied disturbances range from $d_2 = 0.425$ m to $d_2 = 0.525$ m. For the hip-ankle strategy the applied disturbances range from $d_2 = 0.425$ m to $d_2 = 0.600$ m.

8-3 Signal processing

Dedicated logging software is used to log several variables which are required for later analysis of the performance of the robot. Raw measurement data of the load cell for one disturbance set is shown in figure 8-3(a). The ten disturbances are cut out and aligned at the point where the disturbance rod starts to apply a force to the robot, this results in figure 8-3(b). The impulse can now be obtained for each disturbance by taking the integral of each force curve over time. For each set (ten disturbances) the impulses are calculated and visualised in a box plot. The box plot for the applied impulses for the ankle strategy is depicted in figure 8-4(a), the box plot for the applied impulses using the hip-ankle strategy is shown in figure 8-4(b). For both figures the dashed line represents the theoretical applied disturbance as calculated in section 8-1-2. The trend observed for the measured applied impulse corresponds to the trend of the theoretical applied impulse for both strategies.

The median of the impulses of each disturbance set serves as a measure for the applied disturbance. This results in an impulse corresponding to a disturbance rod distance d_2 for both strategies which is summarised in table 8-1. The median of the set of applied impulses will be used in the presentation of the results in next section.

8-4 Summary

Eight sets of each ten of the same disturbances are applied to the robot for both the ankle as the hip-ankle strategy. The median of the applied impulse, presented in table 8-1 will serve as a measure for the disturbance.

The next chapter introduces the results obtained by the measurement protocol given in this chapter.

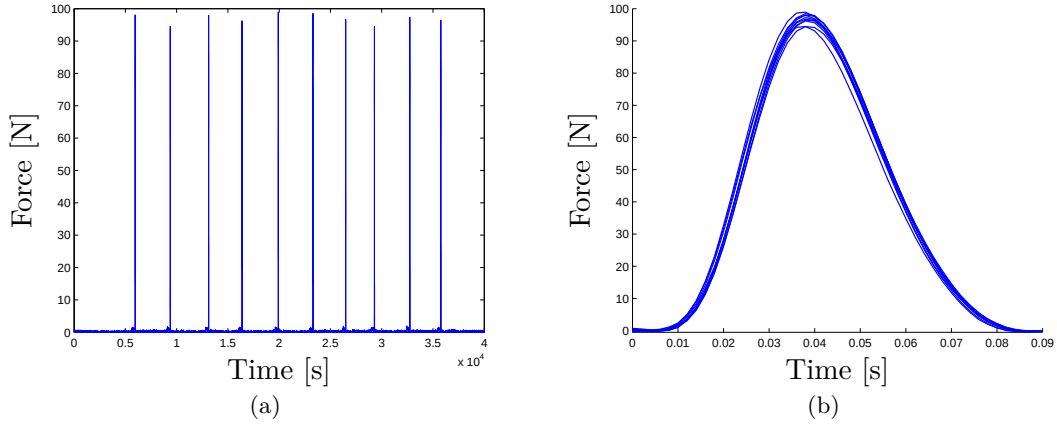

Figure 8-3: In (a) raw measurement data of the load cell is given over time. The ten cycles shown in this figure are cut out and aligned at the start of the impact. The resulting ten aligned impulses are shown in figure (b).

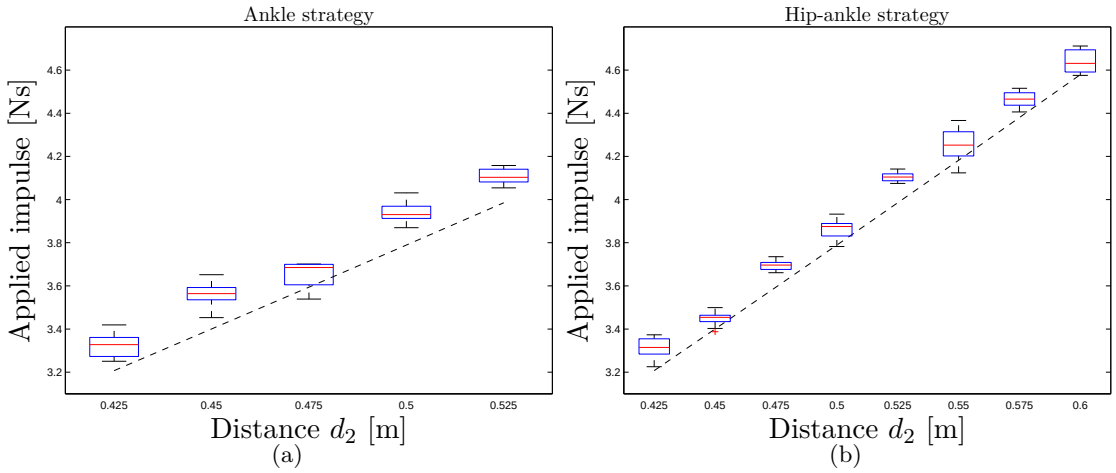

Figure 8-4: Box plot of the impulses for the eight sets of disturbances, each box represents ten impulses. An example of one disturbance set is given in figure 8-3(b). Figure (a) shows the applied disturbances for the ankle strategy where (b) shows the applied disturbances for the hip-ankle strategy. The median of these sets are used as the measure for the disturbance of each set. The dashed lines represent the theoretical applied disturbance as calculated in section 8-1-2.

Table 8-1: Quantification of the applied disturbance of the disturbance rod. For each measurement set the distance d_2 is varied. For each set ten disturbances are applied for both the ankle as the hip-ankle strategy. The median of the applied impulses of each set serves as the measure for the disturbance and are given in column three for the ankle strategy and in column four for the hip-ankle strategy.

Set	Distance d_2 $[m]$	Impulse ankle strategy $[Ns]$	Impulse hip-ankle strategy $[Ns]$
1	0.425	3.3	3.3
2	0.450	3.6	3.5
3	0.475	3.7	3.7
4	0.500	3.9	3.9
5	0.525	4.1	4.1
6	0.550	-	4.3
7	0.575	-	4.5
8	0.600	-	4.6

Chapter 9

Results

This chapter presents the results obtained by experimental evaluation of the hip-ankle strategy and the ankle strategy on the physical humanoid robot TUlip. The experimental protocol which led to these results was presented in chapter 8. Section 9-1 discusses the ankle strategy results and section 9-2 discusses the hip-ankle strategy results. Section 9-3 presents a comparison between the ankle and hip-ankle strategy. Section 9-4 draws conclusions on the obtained experimental results.

9-1 Ankle strategy

This section presents the results obtained by experimental evaluation of the ankle strategy on the humanoid robot TUlip. An ankle strategy control algorithm was implemented within the software architecture of the humanoid robot TUlip. The control algorithm for this strategy is the same as the hip-ankle strategy control algorithm presented in chapter 6 but with the hip joints always locked. The robot is thus not able to lunge the upper body. The parameters used for the controller are shown in table 9-1.

Table 9-1: Control parameters for the ankle strategy experiments.

Model parameter	Symbol	Value
Upper body stiffness gain	K_{p_a}	30
Upper body damping gain	K_{d_a}	4
Desired hip angle	φ_h^{des}	0
Desired hip angular velocity	$\dot{\varphi}_h^{des}$	0
ICP control gain	$K_{p,ICP}$	1
Desired ICP	x_{ICP}^{des}	0.045 [m]

As explained in the previous chapter, a disturbance rod is used which can be swung to the back of the upper body of the robot. Ten disturbances with the same disturbance rod distance form a set of disturbances. The distance of the disturbance rod is then increased and the

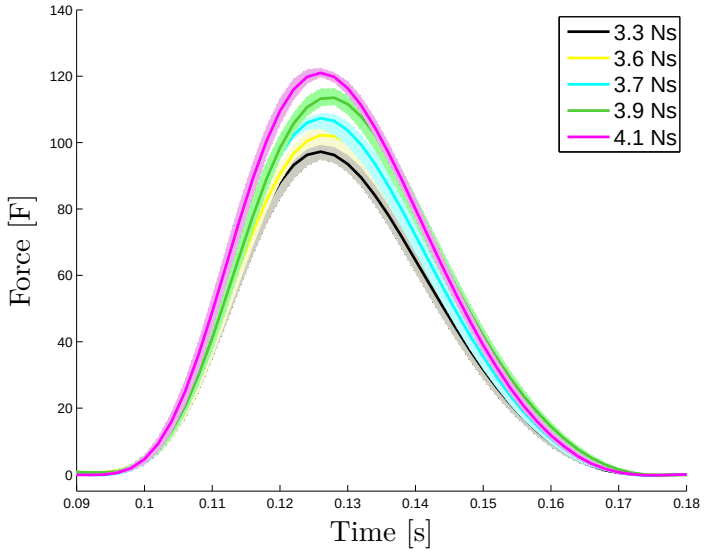

Figure 9-1: Applied disturbances for the ankle strategy. The solid lines represent the median of ten disturbances and the surrounding filled regions represent the range of the data. The applied disturbance sets range from 3.3 Ns to 4.1 Ns.

same process is repeated to form a new set. The applied disturbances in case of the ankle strategy are presented in figure 9-1. The solid lines represent the median of the disturbance and the range of each set is represented by the light coloured area surrounding this median. All disturbances have approximately the same duration but differ in their magnitude. The applied impulse is calculated by the integral of the applied force over time. The median of all applied impulses of one set represents the applied disturbance. In figure 9-1 five sets can be observed with the applied disturbance ranging from 3.3 Ns to 4.1 Ns. In total fifty disturbances are thus applied for the ankle strategy (five sets of ten disturbances).

The five disturbance sets for the ankle strategy have five sets of corresponding measured data of the response of the robot. Figure 9-2 presents the median of the five data sets for the measured data of the applied disturbance force, the Instantaneous Capture Point (ICP), the Centre of Mass (CoM) position and velocity and the Centre of Pressure (CoP) over time. All data is given in x-direction and relative to the ankle location. The applied disturbance force profile is shown in figure 9-2(a). The disturbance starts at approximately 0.1 s and lasts for 0.07 s. Figure 9-2(b) shows the ICP response to this disturbance, immediately after a disturbance is applied the ICP increases in magnitude and moves in the direction of the front of the support polygon edge (indicated by the black dashed line). For larger disturbances the ICP moves closer to the edge of the support polygon. The largest disturbance of 4.1 Ns brings the robot to a fall which is indicated by the ICP moving far outside of the support polygon. Note that the ICP does not move any further because to robot is caught by ropes in order to prevent any damage to the robot. The ICP is composed out of CoM position and velocity, the responses for these parameters are shown in figure 9-2(c) and 9-2(d). It can be observed that the disturbance causes a quick increase in CoM velocity, the peak observed in the CoM velocity measurement can also be observed in the ICP measurement. The CoM moves in the direction of the support polygon edge and a fall for the largest disturbance of 4.1 Ns can be observed. The CoP is estimated on the robot by dividing the ankle torque with

the gravitational force acting on the robot,

$$x_{CoP} = \frac{\tau_a}{mg} \tag{9-1}$$

with τ_a the ankle torque and m the total mass of the robot[1]. Measurement data for the CoP is presented in figure 9-2(e). A slower response than for the ICP can be observed here. As the CoP is dependent on the ankle torque, the limited control bandwidth of this Series Elastic Actuation (SEA) joint causes this slower response. The CoP is constraint to stay within the support polygon to prevent foot rotation. It can be observed that the CoP already slightly crosses the support polygon edge, this creates some foot rotation. A fall occurs for the disturbance of 4.1 Ns because the ankle torque cannot compensate for the applied disturbance. It is therefore not sufficient to bring the CoM back to its desired position. If a larger ankle torque would be allowed, the foot would start to rotate and a fall would still occur. The boundaries on the ankle strategy are reached, the maximum allowable disturbance for this strategy is therefore 3.9 Ns.

9-2 Hip-ankle strategy

This section introduces the results obtained by experimental evaluation of the hip-ankle strategy on the humanoid robot TUlip. The control algorithm for this strategy was introduced in chapter 6. The algorithm will apply a forward lunge in case the ICP moves out of the support polygon at the front of the robot. After application of this lunge the posture is slowly recovered by transferring from the lunging controller to the controller which controls the upper body straight up. Again, this controller was implemented within the software architecture of the robot. The parameters used in this control algorithm are shown in table 9-2.

Table 9-2: Control parameters for the hip-ankle strategy experiments.

Model parameter	Symbol	Value
Upper body stiffness gain	K_{p_a}	30
Upper body damping gain	K_{d_a}	4
Desired hip angle	φ_h^{des}	0
Desired hip angular velocity	$\dot{\varphi}_h^{des}$	0
ICP control gain	$K_{p,ICP}$	1
Desired ICP	x_{ICP}^{des}	0.045 [m]
Lunging gain	K_{p_h}	80
Start lunging threshold		0.138 [m]
Stop lunging threshold		0.100 [m]

Eight sets of ten disturbances were applied with each set a different disturbance rod distance. The plot of the disturbance force over time for this eighty disturbances is depicted in figure 9-3. The median of each disturbance set is shown with the range represented by the surrounding region. The sets range from 3.3 Ns to 4.6 Ns. Note that these sets are different than the sets presented in figure 9-1 as those were used in separate measurements on the ankle strategy.

[1]Note that this is not equal to the exact CoP which, for example, could be measured by a force plate.

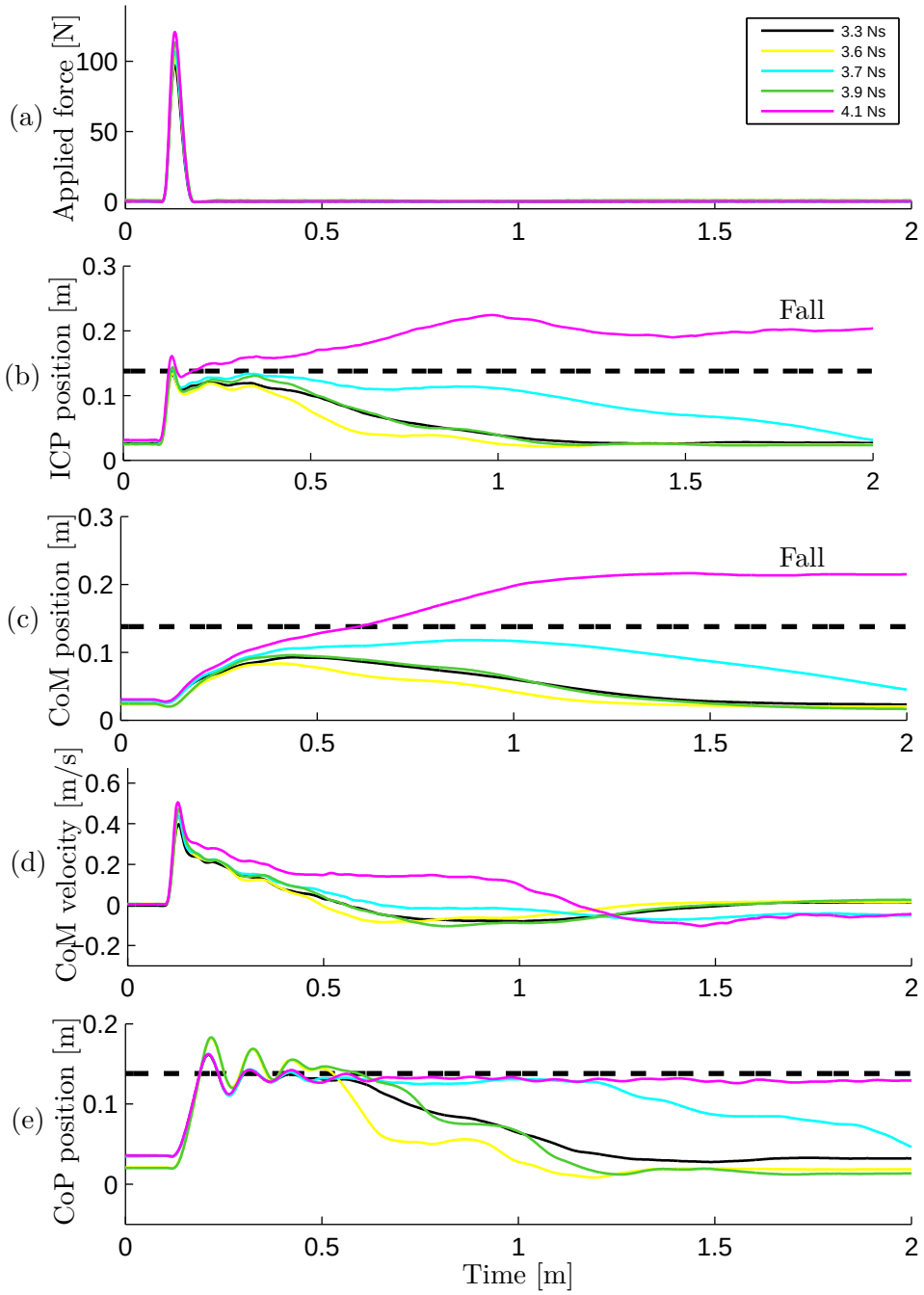

Figure 9-2: Measured data for the ankle strategy for varying disturbance magnitude over time. Each line represent the median of ten measurements. All variables are in the x-direction and relative to the ankle joint. The black dashed line represents the edge of the support polygon. (a) shows the disturbance force profile of which a closer view is shown in figure 9-1. The ICP response to this disturbance is given in (b). The ICP quickly increases in magnitude due to the disturbance. The largest disturbance of 4.1 Ns results in a fall of the robot as shown by the line crossing the support polygon edge and remaining there. Figure (c) and (d) show the CoM position and velocity. The measured CoP is shown in (e), a slow response is observed here due to the limited SEA control bandwidth. The CoP slightly moves out of the support polygon which causes some foot rotation. A fall occurs for the disturbance of 4.1 Ns because not enough ankle torque can be applied to compensate for the disturbance.

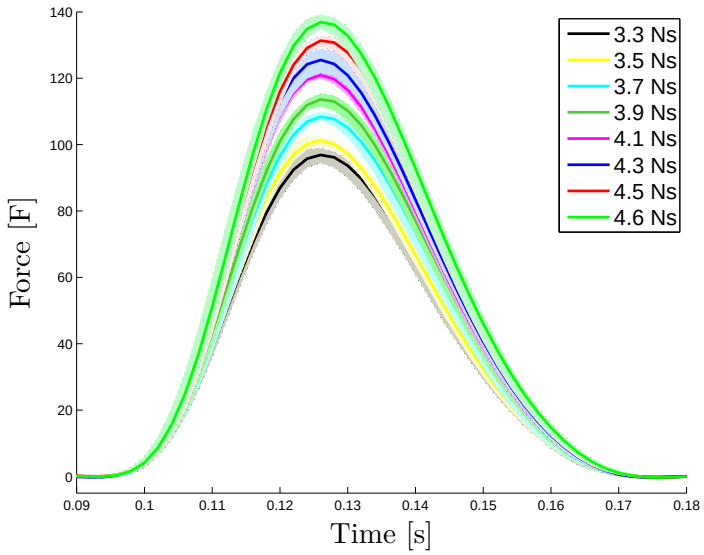

Figure 9-3: Applied disturbances for the hip-ankle strategy. The solid lines represent the median of ten disturbances and the surrounding filled regions represent the range of the data. The applied disturbance sets range from 3.3 Ns to 4.6 Ns.

Measurement data corresponding to the disturbance sets of figure 9-3 is presented in figure 9-4. The plots represent the median of the applied disturbance force, the ICP, the CoM position and velocity and the CoP over time. All data is given in x-direction and relative to the ankle location. The disturbance force over time is depicted in figure 9-4(a), see 9-3 for a closer view. The ICP plot in figure 9-4(b) shows that for all applied disturbances the ICP is returned to its desired position. From this can thus be concluded that the robot successfully maintained balance for all the applied disturbances ranging from 3.3 Ns to 4.6 Ns. It can also be observed that the ICP is moved further outside of the support polygon (indicated by the dashed black line), due to the disturbance, while a fall is still prevented. Figure 9-4(c) shows that the CoM position is maintained within the support polygon and returned to its desired position. The CoM velocity in figure 9-4(d) shows a large increase in magnitude due to the disturbance. The CoP, in figure 9-4(e), is again constrained to stay within the support polygon (dashed black line). Although it slightly crosses the support polygon edge this does not create substantial foot rotation and balance was maintained. A slow response of the CoP due to the control bandwidth limitation is also observed for the hip-ankle strategy.

Note that the data presented in figure 9-4 all represent situations for which the robot could maintain balance. Any larger disturbance than 4.6 Ns resulted in a fall of the robot. However this disturbance, for which a fall occurred, was not repeated for ten times because it also forced the robot to its maximum hip joint angle. If this would be repeated for several times it might result in damage to the robot.

In order to get more insight in the response of the robot, the measured data of the largest allowable disturbance for the hip-ankle strategy will be discussed in next section.

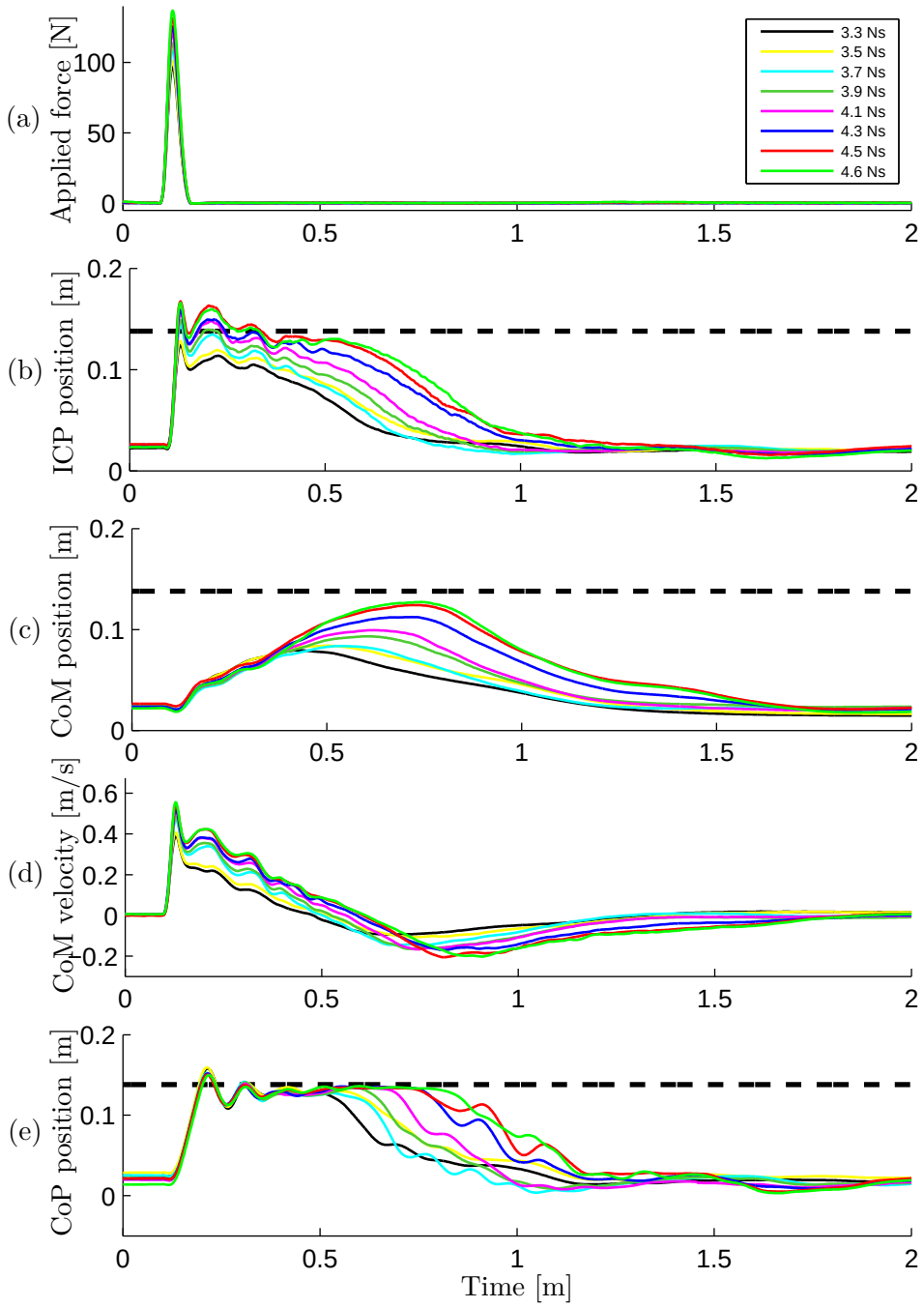

Figure 9-4: Measured data for the hip-ankle strategy for varying disturbance magnitude over time. Each line represent the median of ten measurements. All variables are in the x-direction and relative to the ankle joint. The black dashed line represents the edge of the support polygon. In (b) the ICP is forced outside of the support polygon by the impulsive disturbance shown in (a). This is due to a large increase in velocity (d). The CoM in figure (c) stays within the support polygon for all disturbances. The CoP (e) shows slow response due to the limited control bandwith. The largest allowable disturbance for the hip-ankle strategy is 4.6 Ns.

9-2-1 Largest allowable disturbance for the hip-ankle strategy

Figure 9-5 shows a sequence of images for the humanoid robot TUlip recovering from the largest allowable disturbance, 4.6 Ns. At t=0.0 s the disturbance rod approaches the robot, the image at t=0.1 s is right after impact of the disturbance rod and the ICP is rapidly forced forward. At t=0.2 s the lunge is applied in order to push back the ICP, a forward angular acceleration of the upper body is observed. At t=0.3 s the ICP is pushed back inside the support polygon and the robot slowly recovers its body posture until at t=0.9 where the ICP is near its desired position.

Responses of the CoP, the desired CoP, CoM and ICP for the largest allowable disturbance for the hip-ankle strategy are shown in figure 9-6(a). The limited control bandwidth can clearly be observed when comparing the desired CoP and the measured CoP. The desired CoP quickly increases in order to place it in front of the CoP and reaches the support polygon edge. However, the measured CoP reaches this support polygon edge approximately 0.1 s later. The light blue area indicates when the hip-ankle strategy is applied. When the ICP left the support polygon (at t=0.1 s) the upper body orientation control module switches to the lunging controller and applies a large virtual torque on the trunk. The ICP is pushed back and the controller switches back to the ankle strategy (at t=0.27 s). When the hip-ankle strategy is applied a large virtual torque is applied on the trunk in the direction of the disturbance. The application of this virtual torque results in an angular acceleration of the trunk as shown 9-6(b). This figure shows the angular acceleration of the trunk around the pitch joint and is measured by the Inertial Measurement Unit (IMU) of the robot. From the figure can be observed that the disturbance creates a large angular acceleration of the upper body. Rotational deceleration of the trunk then occurs because the hip joint is still locked. When the ICP left the support polygon the lunge is performed and a second peak is observed.

Figure 9-7 presents the joint angles and torques for the largest allowable disturbance in case of the hip-ankle strategy. The plots of the ankle torques show the low control bandwidth due to the SEA on these joints. An important constraint in the application of the hip-ankle strategy is the maximum hip pitch angle. The plots for the hip pitch angles show that the maximum hip pitch angle of -1.05 rad is not exceeded. The lowest graph on the right in figure 9-7 shows the virtual torque applied on the trunk. When the lunge is started, a sudden change in desired torque is observed, resulting in the large angular acceleration of the trunk. When the lunge is engaged almost no hip torque is to be applied. The energy added by the disturbance rod is transferred into angular acceleration of the trunk by simply “releasing” the hip joints.

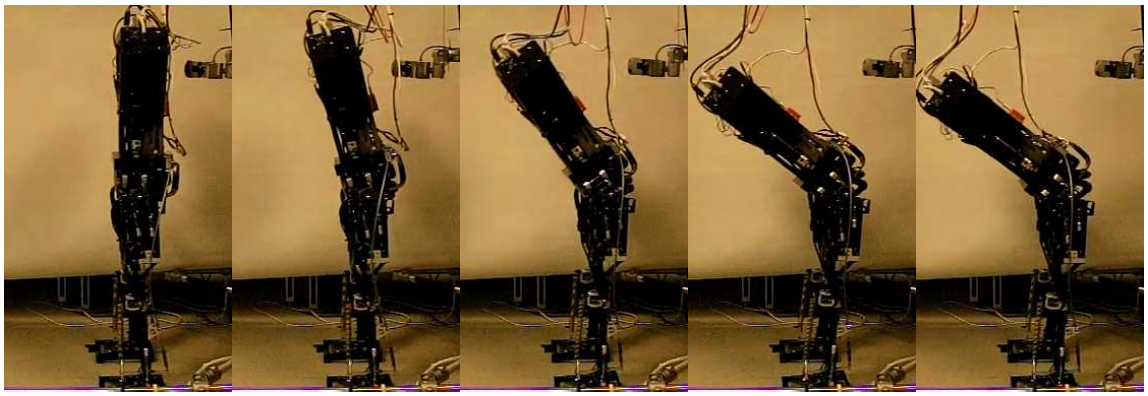

(a) t=0.0 s. (b) t=0.1 s. (c) t=0.2 s. (d) t=0.3 s. (e) t=0.4 s.

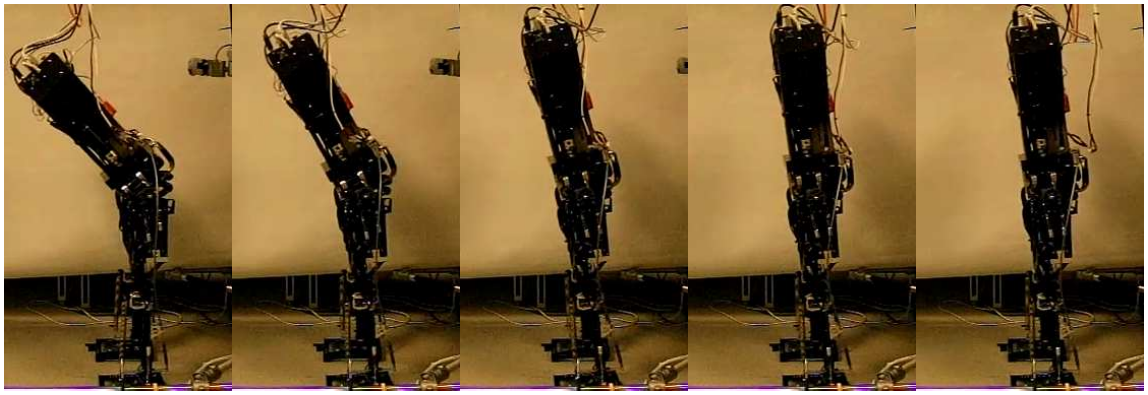

(f) t=0.5 s. (g) t=0.6 s. (h) t=0.7 s. (i) t=0.8 s. (j) t=0.9 s.

Figure 9-5: Humanoid robot TUlip recovering from a large push of 4.6 Ns using the hip-ankle strategy. At $t = 0.1$ s the disturbance is applied. The forward lunging motion can clearly be observed from $t = 0.2$ s to $t = 0.4$ s and pushes back the ICP inside the support polygon. After the lunge, the posture is recovered by gradually transferring to the controller which locks the hip joint.

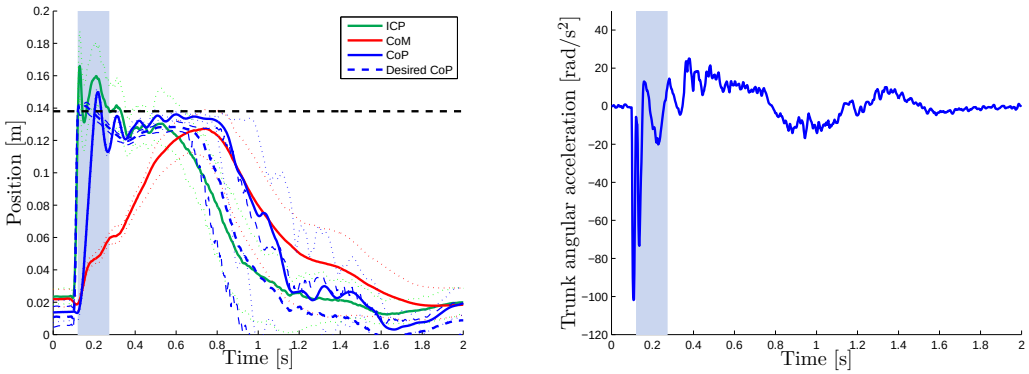

(a) (b)

Figure 9-6: Responses of the CoP, the desired CoP, CoM and ICP for the largest allowable disturbance for the hip-ankle strategy are shown in (a). The light blue area indicates when the forward lunge is applied, this starts when the ICP is outside of the support polygon. When the lunge is applied, a large virtual pitch torque is applied on the trunk and an angular acceleration of the trunk is generated. This is confirmed by (b), which shows the angular acceleration of the trunk gathered by the IMU data. A large angular acceleration is caused by the disturbance. When the lunge is applied (light blue area) another peak is be observed.

9-3 Ankle and hip-ankle strategy comparison

Figure 9-8 presents the phase portraits for both the ankle strategy 9-8(a) and the hip-ankle strategy 9-8(b) obtained by the experiments. The lines give the median of the CoM in state space for each disturbance set. The phase portrait for the ankle strategy shows four successful push recoveries and one fall, a total of fifty measurements. The largest allowable disturbance for the ankle strategy is 3.9 Ns. The phase portrait for the hip-ankle strategy shows eight successful push recoveries, a total of eighty measurements. The largest allowable disturbance for this strategy is 4.6 Ns, any larger disturbance resulted in a fall of the robot[2]. The hip-ankle strategy is able to maintain balance when subjected to a push 18% larger than the ankle strategy. The comparison between the largest allowable disturbance for the ankle and hip-ankle strategy implemented on the robot is presented by the box plot in figure 9-9.

[2]Measurements for a fall of the robot in case of the hip-ankle strategy are not presented because it was not repeated for ten times. This was because the the maximum hip angle was reached for these disturbances which might result in damage of the robot.

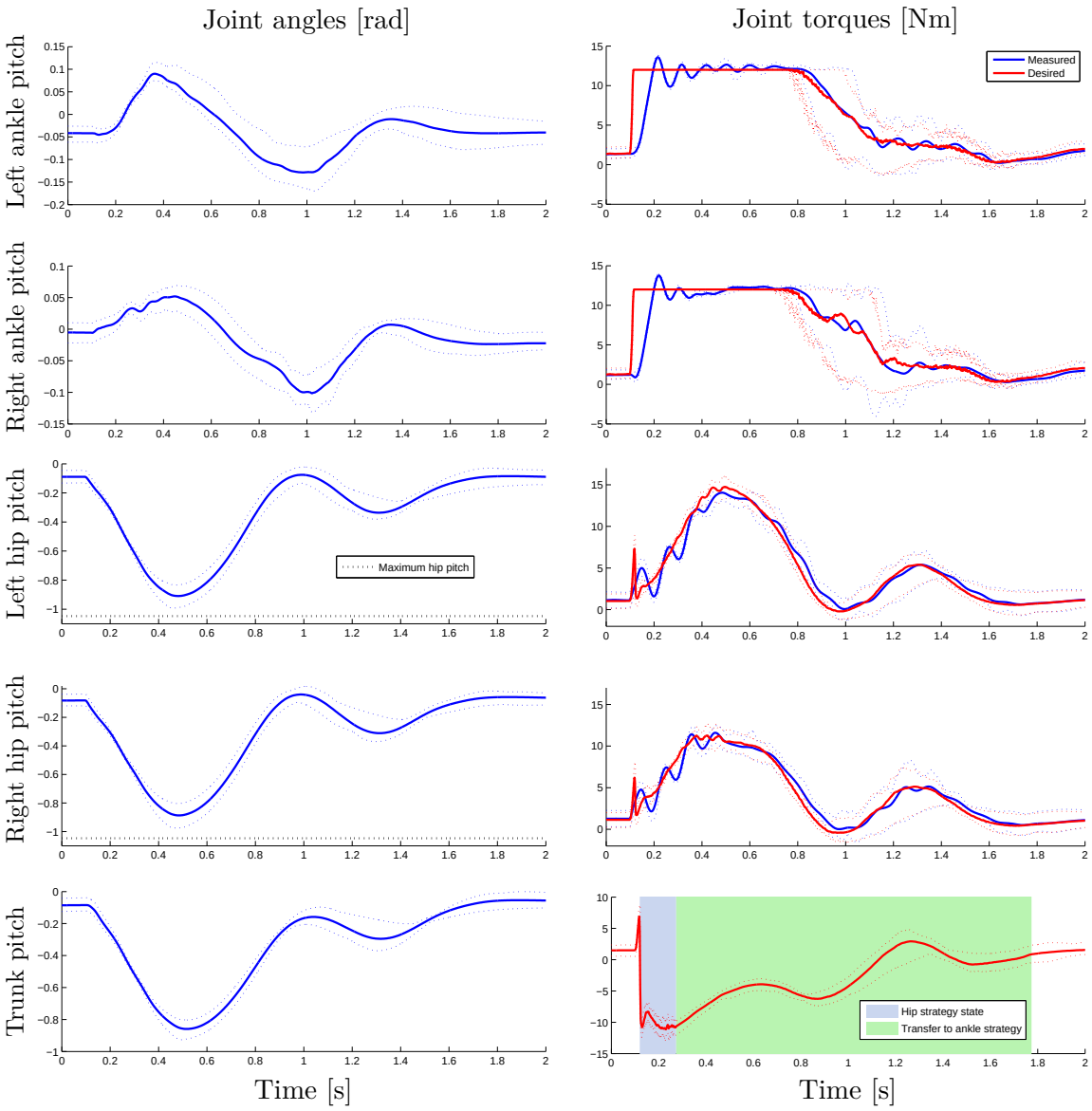

Figure 9-7: Joint angles and joint torques for the largest allowable disturbance for the hip-ankle strategy of 4.6 Ns. The hip pitch joint angles do not exceed the maximum hip pitch angle indicated by the black dotted lines an -1.05 rad. The slow response of the CoP is also observed in the ankle torques. The lower right graph shows the virtual torque applied on the trunk. When the lunge is started, a large sudden change in desired torque is observed resulting in a large angular acceleration of the trunk. When the hip-ankle strategy is engaged almost no application of hip torque is required. This is because the system uses the energy added by the disturbance rod in order to create the angular acceleration of the trunk.

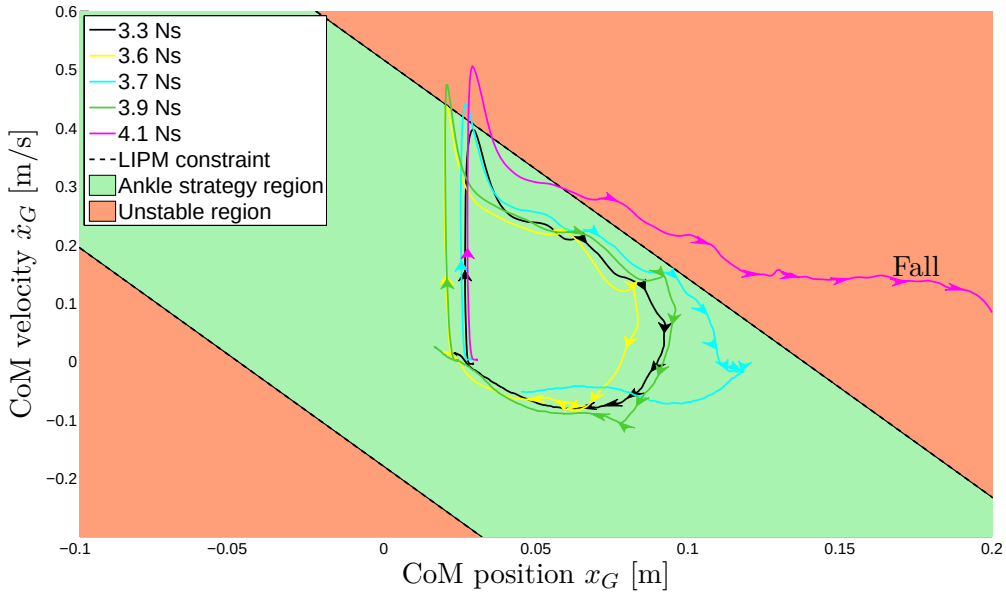

(a) Ankle strategy.

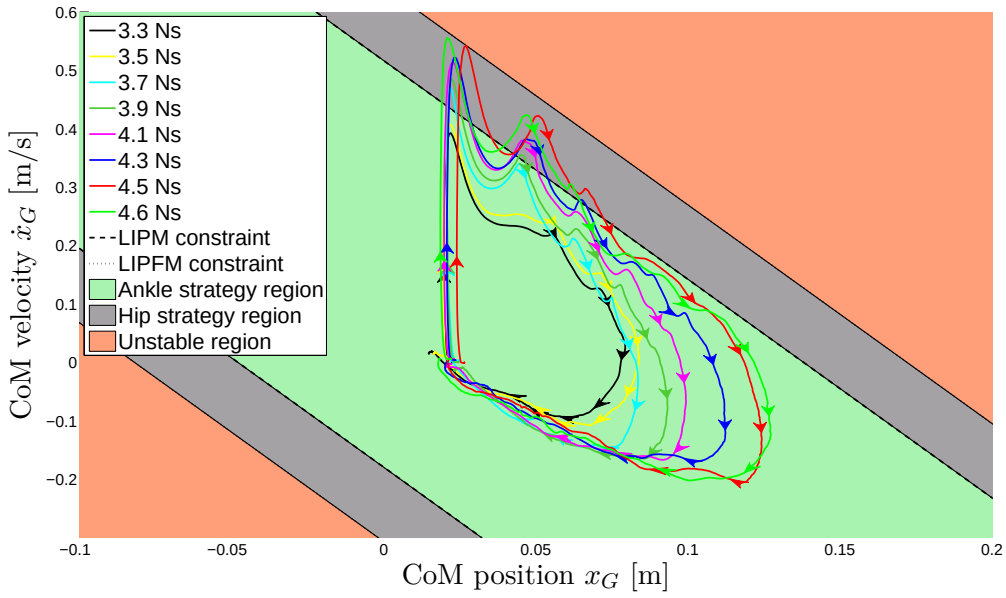

(b) Hip-ankle strategy.

Figure 9-8: Phase portraits, obtained by experiments, of the CoM of the robot for the ankle strategy (a) and the hip-ankle strategy (b). The x-axis represents the CoM position x_G while the CoM velocity $\dot{x}_G$ is presented on the y-axis. Each line represents the median of ten measurements. The green area is the theoretical stability region for the ankle strategy, analytically derived by the LIPM. The dashed black line is the edge of this region (foot edge). The grey area is the theoretical stability region for the hip-ankle strategy, analytically derived by the LIPFM. The dotted black line is the edge of this region. From (a) can be observed that the largest allowable disturbance for the humanoid robot using the ankle strategy is 3.9 Ns. A fall is shown for the larger disturbance of 4.1 Ns. Figure (b) shows that the largest allowable disturbance for the hip-ankle strategy is 4.6 Ns.

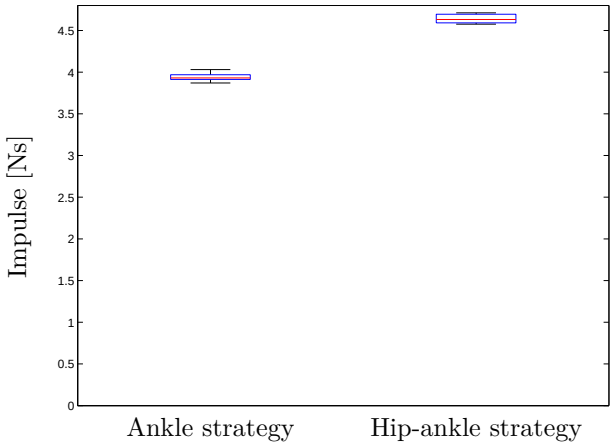

Figure 9-9: Comparison in largest allowable disturbance between the ankle strategy and the hip-ankle strategy. Each box represents ten applied disturbances. The median of the largest allowable disturbance for the ankle strategy is 3.9 Ns. For the hip-ankle strategy, the median of the largest allowable disturbance is 4.6 Ns. As the boxes do not overlap the largest allowable disturbance for the hip-ankle strategy is significantly larger than the largest allowable disturbance for the ankle strategy.

9-4 Conclusions

Table 9-3: Maximum allowable impulse for the ankle and hip-ankle strategy obtained by experimental evaluation.

	Ankle strategy [Ns]	Hip-ankle strategy [Ns]	Improvement
Experiments	3.9	4.6	118%

The hip-ankle strategy algorithm was implemented on the robot TUlip and compared with the ankle strategy algorithm. The hip-ankle strategy is able to maintain balance for impulsive disturbances 18% larger than the ankle strategy. Angular acceleration of the upper body is applied in case the ICP leaves the support polygon. This angular acceleration pushes the ICP back inside the support polygon where the ankle strategy can recover the desired upright posture.

Chapter 10

Discussion and future work

This chapter discusses the results obtained throughout the various chapters of this thesis. Section 10-1 compares the largest allowable disturbances of the ankle and hip-ankle strategy obtained simulations and experiments throughout this thesis. Section 10-2 analyses the accuracy of the measurements obtained in chapter 9. Section 10-3 discusses on the use of simple models for the control of balance on humanoids robots. Section 10-4 discusses on the generality of results, it discusses if this control method also can be applied to other robots and what the limiting factors of the algorithm are.

10-1 Comparison of model, simulation and experiments

Table 10-1 provides the results obtained on the largest allowable disturbance for the ankle strategy and the hip-ankle strategy. A simulation on the Inverted Pendulum Model (IPM) and Inverted Pendulum plus Flywheel Model (IPFM) in chapter 5 resulted in the values given in the first row of the table. A simulation was performed using the Double Inverted Pendulum Model (DIPM) in order to test the hip-ankle strategy on a more realistic model and resulted in the values in row two of table 10-1. Finally the hip-ankle strategy was experimentally evaluated and resulted in row three of the table.

From this quantitative comparison the following can be noticed:

1. In the simulation of simple models, a larger improvement in performance was obtained by using the hip-ankle strategy than observed in the simulation of the DIPM and experiments.
2. The largest allowable disturbance obtained by experiments on the robot is approximately 50% lower in comparison with the simulations for both ankle and hip-ankle strategy.
3. The largest allowable disturbance on the humanoid robot TUlip for which a fall can be prevented was improved with 18% by using the hip-ankle strategy.

These points will be discussed in sections 10-1-1 to 10-1-3.

Table 10-1: Comparison of the largest allowable disturbance for the ankle strategy and the hip-ankle strategy in case of simulation on simple models (Simple models), a simulation on the DIPM (DIPM) and experiments on the humanoid robot TUlip (experiments). The improvement defines the increase in largest allowable disturbance by using the hip-ankle strategy compared to the ankle strategy.

	Ankle strategy [Ns]	Hip-ankle strategy [Ns]	Improvement
Simple models	6.58	8.79	133.6%
DIPM	7.82	9.12	116.6%
Experiments	3.9	4.6	118%

10-1-1 Simulation on simple models versus DIPM simulation and experiments

Simulations of simple models in chapter 5 showed that the robot using the hip-ankle strategy can theoretically withstand a 33.6% larger disturbance than using the ankle strategy. For the hip-ankle strategy, the robot was thereby modelled as the IPFM. Because the robot is modelled as a flywheel its CoM location is always fixed at the hip joint. Bang-bang control on the torque input of the flywheel is used because it has the largest effect on the Instantaneous Capture Point (ICP). It can therefore withstand the theoretical largest allowable disturbance.

For the DIPM and the robot, the CoM is not positioned at the hip joint. This results in an extra torque component around the hip joint, caused by gravity acting on the trunk, in case of a rotation. It is therefore not possible to simply apply bang-bang control on the hip with maximum torque in one direction and then maximum hip torque in the opposite direction for the same amount of time. A hip joint torque input with less effect on the ICP is the result. Moreover, the inertia of the flywheel on the IPFM is modelled as the inertia of the trunk around the hip joint. As the CoM of the robot is not positioned at the hip joint and the robot also consists of legs with mass, this is a rough estimation. Lee & Goswami (2007) [44] introduced the Reaction Mass Pendulum as a better representation of the inertia of all individual limbs around the CoM of the robot. The continuous change of the inertia of the robot is characterised by a continuous change of the inertia of the Reaction Mass pendulum around the CoM. However, this model introduces unnecessary complexity and is beyond the scope of this study.

10-1-2 Experiments versus DIPM simulation

The largest effect of the reduction in performance of the physical humanoid robot compared to the simulation can be explained by the limited control bandwidth introduced by the Series Elastic Actuation (SEA). As explained in chapter 2, the maximum bandwidth of the SEA on TUlip is 5-10 Hz for torques between 5-10 Nm. This limited bandwidth is clearly visible in the ankle torque plots for the left and right ankle which are shown in the top right of figure 9-7. The rise time of the ankle torque given the step input is approximately 0.1 s, which corresponds to the a control bandwith 10 Hz. The limited control bandwith is caused by motor velocity saturation; they cannot obtain the required rotational velocity to tension the springs of the SEA fast enough. During the disturbance, the CoP should be placed in front of the ICP but in from the measurements can be observed that this is not the case. This is

shown in 9-6(a). The limited control bandwidth on TUlip is therefore a huge limitation in order to have fast responses to disturbances.

However, the limited control bandwith is not a limiting factor for the hip joint torque. The hip joints use the energy in the system caused by the disturbance. The forward motion of the CoM is transferred into forward acceleration of the upper body around the hip joints by "releasing" these joints. This phenomenom can be observed from the joint torques in figure 9-7.

10-1-3 Ankle strategy versus hip-ankle strategy in experiments

From table 10-1 can be observed that the humanoid robot TUlip can maintain balance for disturbances 18% larger than solely using the ankle strategy. The goal of this thesis is therefore clearly reached.

10-2 Consistency of the measurements

The box plots in chapter 8 (figure 8-4) presented consistend impulse values, measured by the load cells, as a result of the applied disturbance. The measured impulses by the load cell shows consistent values as presented in the box plots in chapter 8. However, the phase portraits in figure 9-8 show some dispersion in initial CoM position before the disturbance is applied. This dispersion can be explained by the robot slightly swaying when standing in rest in double support before the disturbance is applied. This swaying of the robot is visualised by figure 10-1 which shows a plot of the Centre of Mass (CoM) position and velocity of the robot in double support with its feet in the predefined positions as it is placed before the disturbance. No disturbance was applied and the CoM position and velocity was measured for a period of 60 s. The plot shows drift in the signal for both the CoM position and velocity. For the CoM position it has amplitude of approximately 0.5 cm with a relatively low frequency. The CoM velocity drift in the signal with an amplitude of 0.015 m/s can be observed. This swaying of the robot has a slight effect on the initial position and velocity of the CoM of the robot before the disturbance is applied.

The swaying effect can be explained by drift in the Inertial Measurement Unit (IMU). This IMU measures the orientation of the upper body of the robot which is then used to project the CoM on the ground plane. The IMU is placed on the upper body of the robot at a distance of approximately 1 m of the ground plane. A small drift in the orientation will therefore result in a large error on the ground plane.

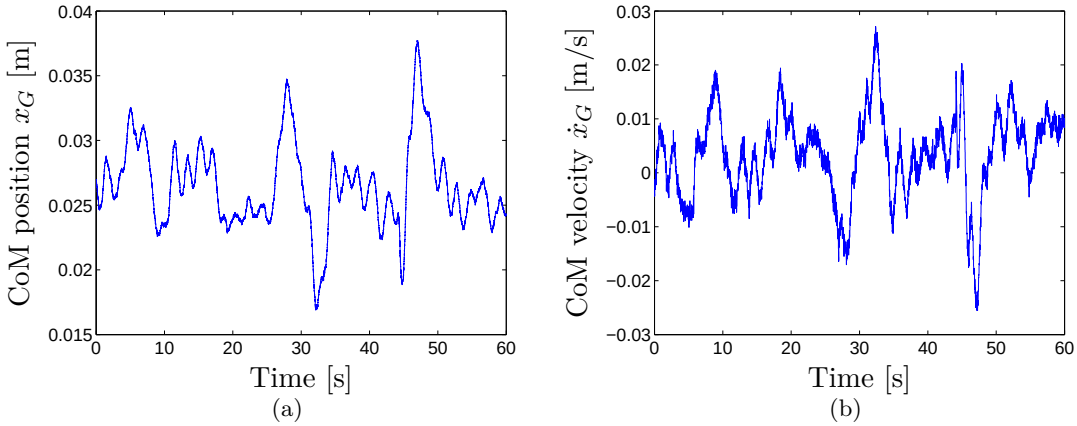

Figure 10-1: CoM position and velocity plots over time for the robot in double support. The swaying motion of the robot can be observed from the deviations shown in these plots. This sway results in dispersion of all the measurement data.

10-3 Use of the Linear Inverted Pendulum Model

The control algorithm on the humanoid robot uses the Linear Inverted Pendulum Model (LIPM) in order to calculate the ICP. For the ankle strategy and hip-ankle strategy the ICP is controlled to the centroid of the foot by applying the required ankle torques. For the hip-ankle strategy the ICP location is also used in order to decide when to apply the virtual torque on the trunk and the size of this virtual torque is based on the ICP location.

The LIPM simplifies the twelve Degree of Freedom (DoF) robot to a point mass moving at a fixed height. The model can be used because of the relative small angles in the ankles and therefore negligible height difference for the CoM. These are the key parameters in the balance maintenance of a robot. For the LIPM, the accuracy of the CoM state estimation is of major importance. In chapter 3 was explained that when the ICP crosses the edge of the support polygon the robot will fall. However measurements on the robot (figure 9-2(b)) show that the ICP leaves the foot while a fall was still prevented. It is suspected that this is an error in the ICP estimation on the robot. The major component of the ICP at the moment it crosses the edge of the foot is CoM velocity it is therefore expected that there is an error in estimation of this parameter.

10-4 Generality of results

The hip-ankle strategy introduced in this thesis was designed in a comprehensive and simplistic way. Simplicity is pursued in order to make the algorithm work on the robot. And so that it can be easily implemented on other robots. If each joint would have a local controller which has to be tuned separately one might lose the total overview which can result in the controller not working at all. The controller is comprehensive in a way that it does not just work for a specific case. The ICP relative to the stance leg should always be measurable and even when the support polygon changes in size, the control rules are still valid. The hip-ankle

strategy could also easily be combined with, for example, walking. Instead of using the support polygon as a reference in order to decide when to apply the strategy, the application of capture regions could be used [27, 32].

10-4-1 Limitations of the hip-ankle strategy on a humanoid robot

The hip-ankle strategy applied on a humanoid robot is dependent on the configuration of the platform. A major limitation for the effectiveness of the application of this method is the maximum hip joint angle. After a large rotational acceleration of the upper body, deceleration is required in order to prevent from exceeding this constraint. The rotational acceleration that can be obtained by the robot platform is dependent on the maximum torque the hip joint can deliver. The effect of the acceleration of the upper body on the ICP is dependent on the total weight distribution of the robot. The hip-ankle strategy is highly effective when the inertia of the upper body around the hip joint is high relative to the inertia of the legs.

Next to these parameters, the bandwidth of the torque controllers on the joints is of major importance in the overal performance of the control algorithm. In case of a small bandwidth, the required torque to counteract the disturbance cannot be applied in time.

10-5 Future work

This research demonstrated the hip-ankle strategy for a humanoid robot in the double support stance phase and focused on the sagittal plane. Experiments demonstrated that the hip-ankle strategy can withstand pushes 18% larger than solely using the ankle strategy. This percentage may seem small but it can be of great value to improve the balance control of a robot in many situations. Because the algorithm is implemented in the VMC framework it can easily be combined with other tasks.

10-5-1 Lunging in other directions

Now the evidence is provided that the algorithm can be used to improve the balance control in forward direction, it can also be used to improve the balance in the other directions (backward, left and right). This will improve robustness against disturbances in all directions. For disturbances in sideward directions the robot should stand in single stance in order to apply the hip-ankle strategy.

10-5-2 Stepping

Subsequently, the hip-ankle strategy can be combined with stepping. Based on the regions defined in chapter 5, the statemachine of the robot can decide which strategy to apply. By lunging, balance can be maintained for situations that require a cross step. This can drastically improve the lateral stability of the robot and prevent a fall in many cases.

10-5-3 Walking

Improving the balance while making a step also improves the walking performance of a robot. Fast corrections of the ICP location in lateral direction can be obtained by an acceleration of the upper body in that direction. A corrective step in lateral direction is then not required. Also forward motion of the CoM can easily be controlled while making a step by lunging. The application of the hip-ankle strategy could also be of great value for walking on rough terrain.

10-5-4 Complex tasks

The hip-ankle strategy could also be used to perform more complex tasks. The hip-ankle strategy can outperform the ankle strategy even more when the support polygon is decreased by for example placing a robot on a wedge or letting it walk on a balance beam. In case of the ankle strategy, the ability to control the ICP by applying ankle torque decreases when the support polygon decreases. However, by using the hip-ankle strategy balance could still be maintained.

10-5-5 Improving the controller

The algorithm presented in this thesis was designed to be able to work on a humanoid robot and provide experimental evidence that it can outperform the ankle strategy. A more optimal controller with even better performance might exist. An online optimisation algorithm could be performed on the robot that takes into account the CoP constraints, disturbance size and current state of the robot in order to maximally push the ICP back into the support polygon. However, it should be taken into account that the algorithm should be able to work in real-time on a robot with limited computational power. The algorithm also might require models of the dynamics of the robot, which can be difficult to determine given the series elastic actuation on the robot.

The hardware of TUlip could also be improved in order to improve the overall balancing performance of the robot. By improving the bandwidth of the torque control faster responses can be obtained for the ankle strategy and hip-ankle strategy. Moreover, improving the CoM estimation will improve the prediction when to lunge and the ICP control.

Chapter 11

Conclusions

The goal of this thesis was to *provide experimental evidence that a humanoid robot can maintain balance for larger disturbances by using the hip-ankle strategy than solely using the ankle strategy.* Therefore, the theoretical largest allowable disturbance was investigated for the hip-ankle strategy. Subsequently, a hip-ankle strategy control algorithm was designed and simulated on a more realistic model for the humanoid robot TUlip. Finally, this control algorithm was experimentally evaluated and compared with the ankle strategy.

The theoretical largest allowable disturbance was obtained by simulating the Inverted Pendulum Model (IPM) as a model for the ankle strategy and the Inverted Pendulum plus Flywheel Model (IPFM) as a model for the hip-ankle strategy. An impulse applied in horizontal direction to the CoM of the robot served as the disturbance. The IPM could only apply ankle torque to compensate for the disturbance in which the ankle torque was constrained by the Centre of Pressure (CoP) to stay inside the support polygon. As soon as the Instantaneous Capture Point (ICP) crossed the edge of the support polygon, a fall occurred. The IPFM consisted of an additional flywheel to which bang-bang control torque was applied if the ICP left the support polygon. The hip-ankle strategy was able to maintain balance for disturbances 33.6% larger than the ankle strategy for model parameters based on TUlip.

A control algorithm for the humanoid robot TUlip was designed which uses Virtual Model Control (VMC) to calculate joint torques for given virtual forces and torques on the upper body of the robot. The ankle strategy control algorithm for the humanoid robot TUlip always locks the hip joint and applies ankle torque to compensate for disturbances. The hip-ankle strategy control algorithm locks the hip joint and applies ankle torque in the same way as the ankle strategy if the ICP stays inside the support polygon. When the ICP crosses the edge of the support polygon, a large virtual torque is applied on the upper body. This creates rotational acceleration of the upper body in the direction of the ICP and pushes the ICP back into the support polygon.

A simulation of the hip-ankle strategy algorithm, using the Double Inverted Pendulum Model (DIPM), showed that it is physically possible for the humanoid robot TUlip to maintain balance using this algorithm. Additionally, the simulation showed that the hip-ankle strategy is able to maintain balance for disturbances 16.6% larger than solely using the ankle strategy.

Finally, the hip-ankle strategy was implemented on the humanoid robot TUlip and compared with the ankle strategy. Experimental evaluation showed that the robot is able to maintain balance for disturbances that are 18% larger using the hip-ankle strategy than solely using the ankle strategy. The hip-ankle strategy was compared with the ankle strategy subjected to the largest allowable disturbance. The ankle strategy applied maximum ankle torque to compensate for this disturbance, any larger ankle torque would result in foot rotation which causes the robot to fall.

The results in this thesis provided the first experimental evidence ever that a humanoid robot using the hip strategy in addition to the ankle strategy can maintain balance for larger disturbances than solely using the ankle strategy.

Appendix A

Maximum allowable disturbance for the ankle strategy with locked joints

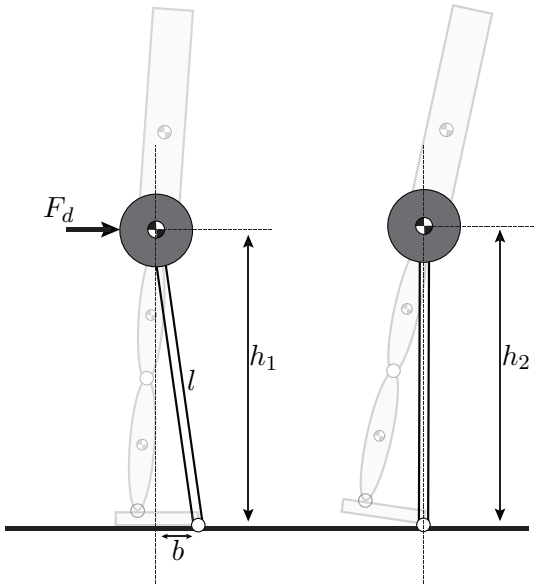

Figure A-1: Illustration of a push with locked joints. Energy is required to push the CoM of the robot over the edge of the foot.

Figure A-1 shows a simple model for the robot with locked joints in the sagittal plane. The robot will fall if the CoM is pushed over the tip of the foot. The amount of impulse required for this push can be evaluated with an energy based analysis. An elevation of $h_d = h_2 - h_1$ of the CoM is required to place it on the foot edge,

$$h_d = \sqrt{b^2 + h_1^2} - h_1 \tag{A-1}$$

with h_1 the initial CoM height, b the distance from the initial CoM position to the tip of the foot and h_2 the final CoM height. The amount of energy required to force the CoM on top of the foot edge is then,

$$\mathcal{V}_d = mgh_d \tag{A-2}$$

with m the mass of the robot and g the gravitational constant. The elevation of the pendulum can thus be reached by giving the pendulum an initial velocity of

$$mgh_d = \frac{1}{2}mv_d^2 \tag{A-3a}$$

$$v_d = \sqrt{2gh_d} \tag{A-3b}$$

with v_d the initial tangential velocity. It is assumed that a push can give the pendulum this velocity without displacing the CoM. The Momentum-Impulse Theorem can than be used to calculate the impulse required push the CoM over the ankles and let it fall. This theorem states that the change in momentum of an object is equal to the impulse exerted on it,

$$\vec{I}_d = \int_{t_i}^{t_f} \vec{F}_d dt = m\Delta\vec{v} = \Delta\vec{p} \tag{A-4}$$

with $\Delta\vec{p}$ the change in linear momentum, $\Delta\vec{v}$ the change in velocity and $\vec{I}_d$ the impulse. With zero initial velocity the required change in velocity due to the push is $\Delta\vec{v} = v_d$, which gives,

$$I_d^{max} = mv_d \tag{A-5}$$

If the difference in direction of the applied disturbance and the tangential pendulum velocity is neglected the maximal allowable disturbance for a humanoid robot with locked joints can be estimated with,

$$I_d^{max} = m\sqrt{2gh_d} = m\sqrt{2g(\sqrt{b^2 + h_1^2} - h_1)} \tag{A-6}$$

which gives 6.23 Ns for a CoM height of 0.7 m and an initial position of the CoM in the centre of the foot ($b = 0.093$).

Appendix B

Double pendulum equations of motion

The double pendulum is expressed in terms of generalised coordinates $\boldsymbol{q} = (\varphi_a \ \varphi_h)^T$. The kinematic relations can be expressed as

$$x_1 = -\frac{1}{2} l_1 \sin\varphi_a \tag{B-1a}$$

$$z_1 = \frac{1}{2} l_1 \cos\varphi_a \tag{B-1b}$$

$$x_2 = -l_1 \sin\varphi_a - \frac{1}{2} l_2 \sin(\varphi_a + \varphi_h) \tag{B-1c}$$

$$z_2 = l_1 \cos\varphi_a + \frac{1}{2} l_2 \cos(\varphi_a + \varphi_h) \tag{B-1d}$$

which can be differentiated to

$$\dot{x}_1 = -\frac{1}{2} l_1 \dot{\varphi}_a \cos\varphi_a \tag{B-2a}$$

$$\dot{z}_1 = -\frac{1}{2} l_1 \dot{\varphi}_a \sin\varphi_a \tag{B-2b}$$

$$\dot{x}_2 = -l_1 \dot{\varphi}_a \cos\varphi_a - \frac{1}{2} l_2 \dot{\varphi}_a \cos(\varphi_a + \varphi_h) - \frac{1}{2} l_2 \dot{\varphi}_h \cos(\varphi_a + \varphi_h) \tag{B-2c}$$

$$\dot{z}_2 = -l_1 \dot{\varphi}_a \sin\varphi_a - \frac{1}{2} l_2 \dot{\varphi}_a \sin(\varphi_a + \varphi_h) - \frac{1}{2} l_2 \dot{\varphi}_h \sin(\varphi_a + \varphi_h) \tag{B-2d}$$

These equations can be inserted in the potential and kinetic energy equations

$$\mathcal{T} = \frac{1}{2}\left[m_1(\dot{x}_1^2 + \dot{z}_1^2) + m_2(\dot{x}_2^2 + \dot{z}_2^2) + I_1\dot{\varphi}_a^2 + I_2(\dot{\varphi}_a + \dot{\varphi}_h)^2\right] \tag{B-3a}$$

$$\mathcal{V} = m_1 g z_1 + m_2 g z_2 \tag{B-3b}$$

With the potential and kinetic energy the Euler-Lagrange equation can be solved giving the equations of motion for the double inverted pendulum. The Lagrange equations are given by,

$$\frac{d}{dt}\left(\frac{\partial \mathcal{T}}{\partial \dot{q}_j}\right) - \frac{\partial \mathcal{T}}{\partial q_j} + \frac{\partial \mathcal{V}}{\partial q_j} = Q_j \qquad j = 1, 2 \tag{B-4}$$

which results in equations of the following form

$$\boldsymbol{M}\ddot{\boldsymbol{q}} + \boldsymbol{C}(\boldsymbol{q}, \dot{\boldsymbol{q}}) + \boldsymbol{F}_g(\boldsymbol{q}) = \boldsymbol{Q} \tag{B-5}$$

Equation (B-5) can be solved for the joint accelerations,

$$\ddot{\boldsymbol{q}} = \boldsymbol{M}^{-1}\left(\boldsymbol{Q} - \boldsymbol{C}(\boldsymbol{q}, \dot{\boldsymbol{q}}) - \boldsymbol{F}_g(\boldsymbol{q})\right) \tag{B-6}$$

with

$$\boldsymbol{M} = \begin{bmatrix} \frac{1}{4}l_1^2 m_1 + l_1^2 m_2 + \frac{1}{4}l_2^2 m_2 + l_1 l_2 m_2 \cos\varphi_h + I_1 + I_2 & \frac{1}{4}m_2 l_2^2 + \frac{1}{2}l_1 l_2 m_2 \cos\varphi_h + I_2 \\ \frac{1}{4}m_2 l_2^2 + \frac{1}{2}l_1 l_2 m_2 \cos\varphi_h + I_2 & \frac{1}{4}m_2 l_2^2 + I_2 \end{bmatrix} \tag{B-7a}$$

$$\boldsymbol{C} = \begin{bmatrix} -\frac{1}{2}l_1 l_2 m_2 \sin(\phi_h)\dot{\phi}_h^2 - l_1 l_2 m_2 \dot{\phi}_a \dot{\phi}_h \sin\phi_h \\ \frac{1}{2}l_1 \dot{\phi}_a^2 \sin\phi_h \end{bmatrix} \tag{B-7b}$$

$$\boldsymbol{F}_g = \begin{bmatrix} -\frac{1}{2}g l_2 m_2 \sin(\phi_a + \phi_h) - \frac{1}{2}g l_1 m_1 \sin\phi_a + g l_1 m_2 \sin\phi_a \\ -\frac{1}{2}l_2 m_2 g \sin(\phi_a + \phi_h) \end{bmatrix} \tag{B-7c}$$

$$\boldsymbol{Q} = \begin{bmatrix} \tau_a - P l_1 \cos\phi_a \\ \tau_h - \frac{1}{2}P l_2 \cos(\phi_a + \phi_h) \end{bmatrix} \tag{B-7d}$$

In equation (B-7d) P is the applied disturbance force.

Appendix C

Jacobians in robotic systems

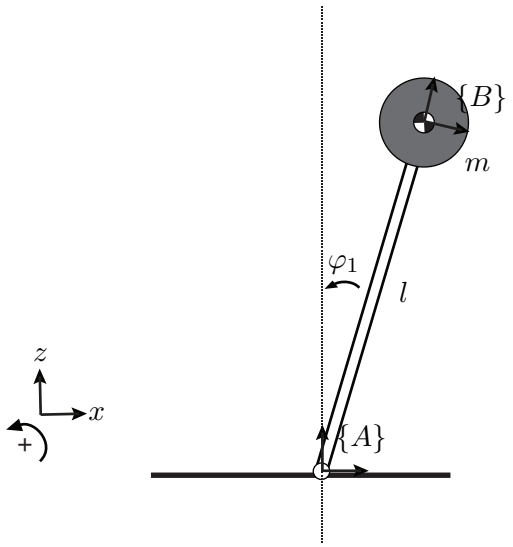

Figure C-1: An inverted pendulum model with angle φ_1 and a point mass with weight m.

The Virtual Model Control (VMC) control algorithm makes use of the Jacobian of the system in order to express the joint torques in terms of virtual forces. This appendix first explains a more traditional way of using the systems Jacobian in section C-1 which introduces the Jacobian as a relation between the end effector velocity and the joint velocities. Section C-2 then introduces how to use the Jacobian to obtain the joint torques given end effector forces.

C-1 Relation between end effector velocity and joint velocities

Traditionally the Jacobian is used to obtain the relation between the end effector velocity in frame $\{B\}$ relative to frame $\{A\}$ and the joint velocities [29],

$$ {}^A_B\dot{\boldsymbol{X}} = {}^A_B\boldsymbol{J}\dot{\boldsymbol{\varphi}} \tag{C-1} $$

with ${}^A_B\dot{\boldsymbol{X}}$ the velocity of frame $\{B\}$ relative to frame $\{A\}$, ${}^A_B\boldsymbol{J}$ the Jacobian from frame $\{A\}$ to frame $\{B\}$ and $\dot{\boldsymbol{\varphi}}$ the joint velocities. For the one Degree of Freedom (DoF) example in figure C-1 the Jacobian can be calculated from the kinematic relations between frame $\{A\}$ and $\{B\}$, where frame $\{A\}$ is the fixed reference frame and frame $\{B\}$ the end effector. The forward kinematics is given by

$$ {}^A_B\boldsymbol{X} = \begin{bmatrix} x \\ z \\ \varphi \end{bmatrix} = \begin{bmatrix} -l\sin(\varphi_1) \\ l\cos(\varphi_1) \\ \varphi_1 \end{bmatrix} \tag{C-2} $$

with l the length of the pendulum, and φ_1 the angle. The Jacobian can be obtained by the partial derivative of equation (C-2) with respect to the generalised coordinate φ_1,

$$ {}^A_B\boldsymbol{J} = \begin{bmatrix} \frac{\partial x}{\partial \varphi_1} \\ \frac{\partial z}{\partial \varphi_1} \\ \frac{\partial \varphi}{\partial \varphi_1} \end{bmatrix} = \begin{bmatrix} -l\cos(\varphi_1) \\ -l\sin(\varphi_1) \\ 1 \end{bmatrix} \tag{C-3} $$

Equation (C-3) can be substituted in equation (C-1) and gives

$$ {}^A_B\dot{\boldsymbol{X}} = \begin{bmatrix} -l\cos(\varphi_1)\dot{\varphi}_1 \\ -l\sin(\varphi_1)\dot{\varphi}_1 \\ \dot{\varphi}_1 \end{bmatrix} \tag{C-4} $$

This gives us the velocity of frame $\{B\}$ relative to frame $\{A\}$ and could also easily be calculated by hand for this one DoF system. However, for increasing DoFs of the system this approach provides the tool to systematically solve the problem.

C-2 Relation between end effector force and joint torques

Next to the relation between end effector velocity and joint velocities, the Jacobian can also be used to express the end effector forces and torques in terms of joint torques. This relation can be found be applying the principle of virtual work [45]. Virtual displacements of frame $\{B\}$ relative to frame $\{A\}$ are related by to virtual joint displacements the Jacobian,

$$ \delta^A_B\boldsymbol{X} = {}^A_B\boldsymbol{J}\delta\boldsymbol{\varphi} \tag{C-5} $$

with $\delta^A_B\boldsymbol{X}$ the virtual displacement of the end effector of frame $\{B\}$ relative to frame $\{A\}$, ${}^A_B\boldsymbol{J}$ the Jacobian between frame $\{A\}$ and $\{B\}$ and $\delta\boldsymbol{\varphi}$ the virtual joint displacements. The principle of virtual work states that, for a system in static equilibrium, the virtual work of the forces in the system is zero for all virtual displacements.

$$ \delta w = \sum_{i=1}^{m} \boldsymbol{F}_i \delta \boldsymbol{X}_i \tag{C-6} $$

with δw the virtual work, $\boldsymbol{F}_i$ force i in the system and $\delta \boldsymbol{X}_i$ the virtual displacement cause by force i. Let $\boldsymbol{\tau}$ denote the vector of joint torques and $\boldsymbol{W}$ the forces applied on the end effector. The principle of virtual work then gives,

$$\delta w = \boldsymbol{W}^T \delta {}^A_B \boldsymbol{X} - \boldsymbol{\tau}^T \delta \boldsymbol{\varphi} \tag{C-7}$$

with $\boldsymbol{W}^T \delta {}^A_B \boldsymbol{X}$ the external applied virtual work and $\boldsymbol{\tau}^T \delta \boldsymbol{\varphi}$ the internal virtual work. This can be combined with equation (C-5) and gives

$$\delta w = (\boldsymbol{W}^T {}^A_B \boldsymbol{J} - \boldsymbol{\tau}^T) \delta \boldsymbol{\varphi} \tag{C-8}$$

where the virtual work of the total system should be zero ($\delta w = 0$) for any $\delta \boldsymbol{\varphi}$. This is the case for $\boldsymbol{W}^T {}^A_B \boldsymbol{J} - \boldsymbol{\tau}^T = 0$, which gives,

$$\boldsymbol{\tau} =^A_B \boldsymbol{J}^T \boldsymbol{W} \tag{C-9}$$

Equation (C-9) shows the relation between the joint torques and the forces applied on the end effector given that the whole system should be in static equilibrium. Using this equation the joint torques $\boldsymbol{\tau}$ can be calculated for given virtual forces $\boldsymbol{W}$. The system will then apply joint torques as if these forces were applied.

For the example in figure C-1 the joint torque τ_1 around the joint in frame $\{A\}$ can be obtained by the Jacobian of the system and the virtual forces applied on frame $\{B\}$. The applied virtual forces $\boldsymbol{W}$ on the system at frame $\{B\}$ cab in this case be a virtual horizontal force f_x, the virtual vertical force f_z and a torque $\tau_{B,y}$. The joint torque in figure C-1 can then be written as,

$$\tau_1 =^A_B \boldsymbol{J}^T \boldsymbol{W} = -l \cos(\varphi_1) f_x - l \sin(\varphi_1) f_z + \tau_{B,y} \tag{C-10}$$

with τ_1 the torque around the joint at frame $\{A\}$. If, for example, only a virtual vertical force f_z would be applied which equals the gravity acting on the mass ($f_x = 0$, $f_z = mg$ and $\tau_{B,y}$) the system will be statically balanced.

Bibliography

[1] B. Stephens, "Humanoid push recovery," in *Proc. 7th IEEE-RAS Int Humanoid Robots Conf*, pp. 589–595, 2007.

[2] J. Pratt, J. Carff, S. Drakunov, and A. Goswami, "Capture point: A step toward humanoid push recovery," in *Proc. 6th IEEE-RAS Int Humanoid Robots Conf*, pp. 200–207, 2006.

[3] M. Vukobratovic, A. A. Frank, and D. Juricic, "On the stability of biped locomotion," *Biomedical Engineering, IEEE Transactions on*, vol. BME-17, pp. 25 –36, jan. 1970.

[4] S. Kajita, F. Kanehiro, K. Kaneko, K. Yokoi, and H. Hirukawa, "The 3d linear inverted pendulum mode: a simple modeling for a biped walking pattern generation," in *Proc. IEEE/RSJ Int Intelligent Robots and Systems Conf*, vol. 1, pp. 239–246, 2001.

[5] S. Kajita, K. Yokoi, M. Saigo, and K. Tanie, "Balancing a humanoid robot using backdrive concerned torque control and direct angular momentum feedback," in *Proc. ICRA Robotics and Automation IEEE Int. Conf*, vol. 4, pp. 3376–3382, 2001.

[6] S.-H. Hyon and G. Cheng, "Disturbance rejection for biped humanoids," in *Robotics and Automation, 2007 IEEE International Conference on*, pp. 2668 –2675, april 2007.

[7] C. Ott, M. Roa, and G. Hirzinger, "Posture and balance control for biped robots based on contact force optimization," in *Humanoid Robots (Humanoids), 2011 11th IEEE-RAS International Conference on*, pp. 26 –33, oct. 2011.

[8] J. Pratt, T. Koolen, T. De Boer, J. Rebula, S. Cotton, J. Carff, M. Johnson, and P. Neuhaus, "Capturability-based analysis and control of legged locomotion , part 2: Application to m2v2 , a lower body humanoid," *International Journal of Robotics Research*, Submitted, 2012, Under review.

[9] M. Popovic, A. Englehart, and H. Herr, "Angular momentum primitives for human walking: Biomechanics and control," in *Proc. of the IEEE/RSJ International Conference on Intelligent Robots and Systems*, pp. 1685–1691, 2004.

[10] H. Herr and M. Popovic, "Angular momentum in human walking," *The Journal of Experimental Biology*, vol. 211, no. 4, pp. 467–481, 2008.

[11] B. Stephens, *Push Recovery Control for Force-Controlled Humanoid Robots*. PhD thesis, Robotics Institute, Carnegie Mellon University, Pittsburgh, PA, May 2011.

[12] Y.-C. Pai and J. Patton, "Center of mass velocity-position predictions for balance control," *Journal of Biomechanics*, vol. 30, no. 4, pp. 347 – 354, 1997.

[13] C. Runge, C. Shupert, F. Horak, and F. Zajac, "Ankle and hip postural strategies defined by joint torques," *Gait & Posture*, vol. 10, no. 2, pp. 161 – 170, 1999.

[14] Y. Abe, M. da Silva, and J. Popović, "Multiobjective control with frictional contacts," in *Proceedings of the 2007 ACM SIGGRAPH/Eurographics symposium on Computer animation*, SCA '07, (Aire-la-Ville, Switzerland, Switzerland), pp. 249–258, Eurographics Association, 2007.

[15] A. Macchietto, V. Zordan, and C. R. Shelton, "Momentum control for balance," *ACM Trans. Graph*, no. 28, 2009.

[16] A. Hofmann, M. Popovic, and H. Herr, "Exploiting angular momentum to enhance bipedal center-of-mass control," in *Proc. IEEE Int. Conf. Robotics and Automation ICRA '09*, pp. 4423–4429, 2009.

[17] M. Abdallah and A. Goswami, "A biomechanically motivated two-phase strategy for biped upright balance control," in *Proc. IEEE Int. Conf. Robotics and Automation ICRA 2005*, pp. 1996–2001, 2005.

[18] S.-H. Lee and A. Goswami, "Ground reaction force control at each foot: A momentum-based humanoid balance controller for non-level and non-stationary ground," 2010.

[19] D. n. Nenchev and A. Nishio, "Ankle and hip strategies for balance recovery of a biped subjected to an impact," *Robotica*, vol. 26, pp. 643–653, September 2008.

[20] B. Jalgha and D. Asmar, "A simple momentum controller for humanoid push recovery," in *Advances in Robotics*, vol. 5744 of *Lecture Notes in Computer Science*, pp. 95–102, Springer Berlin / Heidelberg, 2009.

[21] S. Kajita, F. Kanehiro, K. Kaneko, K. Fujiwara, K. Harada, K. Yokoi, and H. Hirukawa, "Resolved momentum control: humanoid motion planning based on the linear and angular momentum," *Intelligent Robots and Systems, 2003. (IROS 2003). Proceedings. 2003 IEEE/RSJ International Conference on*, vol. 2, pp. 1644 – 1650 vol.2, oct. 2003.

[22] E. C. Whitman and B. J. Stephens, "Torso rotation for push recovery using simple change of variables," 2011.

[23] B. Stephens and C. Atkeson, "Dynamic balance force control for compliant humanoid robots," in *Intelligent Robots and Systems (IROS), 2010 IEEE/RSJ International Conference on*, pp. 1248 –1255, oct. 2010.

[24] D. Hobbelen, T. de Boer, and M. Wisse, "System overview of bipedal robots flame and tulip: Tailor-made for limit cycle walking," in *Intelligent Robots and Systems, 2008. IROS 2008. IEEE/RSJ International Conference on*, pp. 2486 –2491, sept. 2008.

[25] D. Hobbelen, *Limit Cycle Walking*. PhD thesis, Delft University of Technology, 2008.

[26] T. D. Boer, *Foot placement in robotic bipedal locomotion*. PhD thesis, Delft University of Technology, 2012.

[27] T. Koolen, T. De Boer, J. Rebula, A. Goswami, and J. Pratt, "Capturability-based analysis and control of legged locomotion, part 1: Theory and application to three simple gait models," *International Journal of Robotics Research*, Submitted, 2012, Under Review.

[28] G. Pratt and M. Williamson, "Series elastic actuators," in *Intelligent Robots and Systems 95. 'Human Robot Interaction and Cooperative Robots', Proceedings. 1995 IEEE/RSJ International Conference on*, vol. 1, pp. 399 –406 vol.1, aug 1995.

[29] J. Pratt and G. Pratt, "Intuitive control of a planar bipedal walking robot," in *Robotics and Automation, 1998. Proceedings. 1998 IEEE International Conference on*, vol. 3, pp. 2014 –2021 vol.3, may 1998.

[30] F. B. Horak and L. M. Nashner, "Central programming of postural movements: adaptation to altered support-surface configurations," *Journal of Neurophysiology*, vol. 55, no. 6, pp. 1369–1381, 1986.

[31] J. Pratt, *Exploiting inherent robustness and natural dynamics in the control of bipedal walking robots*. PhD thesis, MIT, 2000.

[32] J. Pratt and R. Tedrake, "Velocity-based stability margins for fast bipedal walking," in *Fast Motions in Biomechanics and Robotics* (M. Diehl and K. Mombaur, eds.), vol. 340 of *Lecture Notes in Control and Information Sciences*, pp. 299–324, Springer Berlin Heidelberg, 2006.

[33] T. Komura, A. Nagano, H. Leung, and Y. Shinagawa, "Simulating pathological gait using the enhanced linear inverted pendulum model," vol. 52, no. 9, pp. 1502–1513, 2005.

[34] M. Popovic, A. Goswami, and H. Herr, "Ground reference points in legged locomotion: Definitions, biological trajectories and control implications," *The International Journal of Robotics Research*, vol. 24(12), no. 24, pp. 1013–1032, 2005.

[35] S. Kajita, K. Tani, and A. Kobayashi, "Dynamic walk control of a biped robot along the potential energy conserving orbit," in *Intelligent Robots and Systems '90. 'Towards a New Frontier of Applications', Proceedings. IROS '90. IEEE International Workshop on*, pp. 789 –794 vol.2, jul 1990.

[36] S.-H. Hyon, R. Osu, and Y. Otaka, "Integration of multi-level postural balancing on humanoid robots," in *Robotics and Automation, 2009. ICRA '09. IEEE International Conference on*, pp. 1549 –1556, may 2009.

[37] B. Jalgha, D. Asmar, and I. Elhajj, "A hybrid ankle/hip preemptive falling scheme for humanoid robots," in *Robotics and Automation (ICRA), 2011 IEEE International Conference on*, pp. 1256 –1262, may 2011.

[38] C. Atkeson and B. Stephens, "Multiple balance strategies from one optimization criterion," in *Humanoid Robots, 2007 7th IEEE-RAS International Conference on*, pp. 57 –64, 29 2007-dec. 1 2007.

[39] C. Runge, C. Shupert, F. Horak, and F. Zajac, "Ankle and hip postural strategies defined by joint torques," *Gait & Posture*, vol. 10, no. 2, pp. 161 – 170, 1999.

[40] H. Hemami, K. Barin, and Y.-C. Pai, "Quantitative analysis of the ankle strategy under translational platform disturbance," *Neural Systems and Rehabilitation Engineering, IEEE Transactions on*, vol. 14, pp. 470 –480, dec. 2006.

[41] L. A. Wojcik, D. G. Thelen, A. B. Schultz, J. A. Ashton-Miller, and N. B. Alexander, "Age and gender differences in peak lower extremity joint torques and ranges of motion used during single-step balance recovery from a forward fall.," (Department of Mechanical Engineering and Applied Mechanics, University of Michigan, Ann Arbor 48109-2125, USA. wojcik@vt.edu FAU - Wojcik, L A), pp. –, 2000.

[42] "Ieee spectrum." `http://spectrum.ieee.org/robotics/humanoids`, Accessed March 2012.

[43] J. Pratt, C.-M. Chew, A. Torres, P. Dilworth, and G. Pratt, "Virtual model control: An intuitive approach for bipedal locomotion," *The International Journal of Robotics Research*, vol. 20, no. 2, pp. 129–143, 2001.

[44] S.-H. Lee and A. Goswami, "Reaction mass pendulum (rmp): An explicit model for centroidal angular momentum of humanoid robots," in *Proc. IEEE Int Robotics and Automation Conf*, pp. 4667–4672, 2007.

[45] M. Spong, S. Hutchinson, and M. Vidyasagar, *Robot Dynamics and Control*. 2nd ed., 2004.

Index